



**Asociación Argentina de Astronomía
Book series**

From the First Structures to the Universe Today

AAABS N° 4

Edited by

**María Emilia De Rossi
Susana Pedrosa
Leonardo J. Pellizza**



ISBN 978-987-24948-1-0

From the First Structures to the Universe Today

AAABS N° 4

Buenos Aires, 2013

**ASOCIACIÓN ARGENTINA DE ASTRONOMÍA
BOOK SERIES**

VOLUME 4

ASOCIACIÓN ARGENTINA DE ASTRONOMÍA

FROM THE FIRST STRUCTURES TO THE UNIVERSE TODAY

Edited by
María Emilia De Rossi
IAFE (CONICET/UBA)
derossi@iafe.uba.ar

Susana Pedrosa
IAFE (CONICET/UBA)
supe@iafe.uba.ar

Leonardo J. Pellizza
IAFE (CONICET/UBA)
pellizza@iafe.uba.ar

<p>De Rossi, María Emilia From the first structures to the Universe Today / María Emilia De Rossi, Susana Pedrosa, Leonardo J. Pellizza Buenos Aires: Asociación Argentina de Astronomía, 2013 250p.;</p> <p>ISBN 978-987-24948-1-0</p> <p>1. Astrofísica. I. Pedrosa, Susana. II. Pellizza, Leonardo J. III. Título CDD 523.01</p>

Fecha de catalogación: 06/06/2013

BUENOS AIRES
2013

Contents

Preface	vii
Lectures	1
The first stars and galaxies – Basic principles <i>V. Bromm</i>	3
Galaxy evolution throughout the cosmic epochs: an observational perspective <i>R. Maiolino</i>	23
Invited talks	47
State of the art of semi-analytic models <i>S.A. Cora</i>	49
Gas and metal distributions within simulated disk galaxies <i>B.K. Gibson, S. Courty, D. Cunnama, M. Mollá</i>	57
Structure and galaxy evolution from clustering or environment measurements <i>N. Padilla</i>	65
Contributed talks	73
Synthetic high-mass X-ray binary populations in a cosmological frame <i>M.C. Artale, L.J. Pellizza, P.B. Tissera, I.F. Mirabel</i>	75
Towards a panchromatic picture of galaxy evolution during the reionization epoch <i>J.E. Forero-Romero, G. Yepes, S. Gottlöber, F. Prada</i>	79
On the mass assembly of sub-Milky-Way galaxies <i>A. González-Samaniego, V. Avila-Reese</i>	83
On the size evolution of early type galaxies <i>G.L. Granato, C. Ragone-Figueroa, M.G. Abadi</i>	87
PEGAS: Hydrodynamical code for numerical simulation of the gas components of interacting galaxies <i>I. Kulikov</i>	91
Dark matter halo properties at low and high redshift <i>J.C. Muñoz-Cuartas, V. Müller, S. Gottlöber</i>	96
	iii

Modelling Ly α emitters in a hierarchical Universe: a hybrid approach <i>A. Orsi, C.G. Lacey, C.M. Baugh</i>	100
Cosmic voids as a tool to constrain cosmology <i>S.G. Patiri</i>	104
Angular momentum conservation in Λ CDM simulations <i>S. Pedrosa, M.E. De Rossi</i>	108
The distribution of young stars and metals in simulated cosmological disk galaxies <i>K. Pilkington, B.K. Gibson, D.H. Jones</i>	112
The contribution of starbursts and normal galaxies to IR luminosity functions and the molecular gas content of the Universe at $z < 2$ <i>M.T. Sargent, E. Daddi, M. Béthermin, D. Elbaz</i>	116
A first look at galaxy flyby interactions: characterizing the frequency of flybys in a cosmological context <i>M. Sinha, K. Holley-Bockelmann</i>	120
Infant mortality in the hierarchical merging scenario <i>R. Smith, M. Fellhauer, S. Goodwin</i>	124
The effect of supernovae on galaxy chemical evolution <i>O.N. Snaith, P.B. Tissera, S. Pedrosa, M.E. de Rossi, J.M. Vílchez</i>	129
Massive galaxies in most dense environments at $z \sim 1.4$ <i>V. Strazzullo, P. Rosati, M. Pannella, R. Gobat, J. Santos</i>	133
Contributed posters	137
Counter-rotating bar in a simulation of a disk galaxy <i>D.G. Algorry, M.G. Abadi</i>	139
Determination of the Galactic star formation rate by means of dynamical simulations of open clusters <i>L.A. Bignone, L.J. Pellizza, A.E. Piatti, T.E. Tecce</i>	140
Ultra compact dwarf galaxies in the Antlia cluster <i>J.P. Caso, L. Bassino, T. Richtler, A. Smith Castelli</i>	141
The Tully-Fisher relation and the formation histories of galaxies <i>M.E. De Rossi, S.E. Pedrosa</i>	142
Extragalactic globular clusters in the Milky Way? <i>B. Dias, B. Barbuy, I. Saviane, E. Held, S. Ortolani, G. Da Costa, M. Gulieuszik, L. Rizzi, Y. Momany, D. Katz</i>	143
Differential CCD photometry of globular clusters <i>R. Figuera Jaimes, A. Arellano Ferro, D.M. Bramich, S. Giridhar</i>	144
Revisiting the colour-magnitude relation of early-type galaxies in the Virgo cluster <i>N. González, A. Smith Castelli, F. Faifer, J.C. Forte</i>	145

Kinematics and morphological properties of southern interacting galaxies: the minor merger AM 1219-430	147
<i>J.A. Hernandez-Jimenez, M. Pastoriza, I. Rodrigues, A. Krabbe, C. Winge, C. Bonatto</i>	
Simulations of galaxy cluster mergers: the dynamics of Abell 3376	148
<i>R.E.G. Machado & G.B. Lima Neto</i>	
Characterizing the magnetic field in the intracluster medium	149
<i>M.S. Nakwacki, E.M. de Gouveia Dal Pino, G. Kowal, R. Santos de Lima</i>	
Survival of galaxy disks in a Λ CDM cosmology	150
<i>L.F. Quiroga, J.C. Muñoz-Cuartas, S. Sanes, J.E. Forero-Romero, S. Gottlöber, J. Zuluaga</i>	
Effects of baryon mass loss on profiles of large galactic dark matter halos	151
<i>C. Ragone-Figueroa, G.L. Granato, M.G. Abadi</i>	
A photometric and spectroscopic study of the Hickson Compact Group 44	152
<i>A. Smith Castelli, F. Faifer, C. Escudero, J.M. Gomes, L. Vega Neme, N. González</i>	
Environment and properties of obscured and unobscured active galactic nuclei	153
<i>M. Taormina, C. Bornancini</i>	
Formation of first structures in a Λ CDM Universe	154
<i>C. Villalón and M. Domínguez Romero</i>	

Preface

Our knowledge of how cosmic structures formed and evolved has improved in the last decades as new and more precise observations are being achieved. Moreover, the development of more sophisticated theoretical models and the advent of high-resolution numerical simulations have contributed a great deal to the comprehension of the physical universe. Therefore, the confrontation of observations and theoretical models is crucial to improve our understanding of galaxy formation within the hierarchical clustering scenario. In November 2011, the 'Second Workshop on Numerical and Observational Astrophysics: From the First Structures to the Universe Today' was held in the Institute for Astronomy and Space Physics (IAFE), Ciudad Autónoma de Buenos Aires, Argentina. This international workshop brought together about seventy active scientists working in both areas to discuss about new results and future challenges.

Stimulating discussions were fostered among participants in a friendly atmosphere to obtain new insight into different open issues which include:

- The physical processes which might regulate the star formation activity over Hubble time.
- The role of metals in galaxy formation.
- The interplay between environmental effects and internal processes to shape a galaxy.
- The impact of galaxy formation on the properties of the intergalactic and intracluster media.

The meeting also included extended talks focused on providing students and researchers with new knowledge on the very high-redshift universe and on challenges posed by current state-of-arts numerical models. This is an exciting and promising field of research for the next years given the development of new observational instruments which will yield unprecedented results about the first stages of structure formation.

This book contains the proceedings arising from this fruitful meeting. In order to improve the scientific content and editorial quality, all published manuscripts were subject to a referee process by experts in the different fields. The Editorial Committee is very grateful to all the colleagues who contributed by reviewing these proceedings.

Finally, we would like to deeply thank all participants for making this meeting such a success and especially, our invited lecturers and speakers whose presentations were excellent. This success was also possible thanks to our Scientific

Organizing Committee composed by leading expert in the field and the enthusiastic work of the Local Organizing Committee. We would also like to express our gratitude to our colleagues at IAFE and Facultad de Ciencias Exactas y Naturales (Universidad de Buenos Aires) for providing a friendly atmosphere during the meeting and also helping us with some organization tasks. Likewise we are grateful to our sponsors that partially supported this meeting

The Editorial Committee

M.E. De Rossi, S. Pedrosa and L.J. Pellizza

From the first structures to the Universe today

Scientific Organising Committee

Avila-Reese, Vladimir
Baugh, Carlton
Borgani, Stefano
García Lambas, Diego
Helmi, Amina
Jing, Yi-Peng
Mirabel, I. Félix
Navarro, Julio
Padilla, Nelson
Sodré, Laerte
Springel, Volker
Thomas, Peter
Tissera, Patricia (chair)

Local Organising Committee

Artale, María Celeste
De Rossi, María Emilia (chair)
Pedrosa, Susana
Pellizza, Leonardo J.
Pérez, María Josefa
Tecce, Tomás
Tissera, Patricia (co-chair)

Sponsors

CONICET



Consejo Nacional de Investigaciones Científicas y Técnicas, Argentina

AGENCIA
NACIONAL DE PROMOCION
CIENTIFICA Y TECNOLOGICA



Agencia Nacional de Promoción Científica y Tecnológica, Argentina



CosmoComp Network



LACEGAL Network



Advanced Micro Devices, Inc.



Participants' photo.

Lectures

The first stars and galaxies – Basic principles

V. Bromm

University of Texas, Department of Astronomy, Austin, U.S.A.

Abstract. Understanding the formation of the first stars and galaxies is a key problem in modern cosmology. In these lecture notes, we will derive some of the basic physical principles underlying this emerging field. We will consider the basic cosmological context, the cooling and chemistry of primordial gas, the physics of gravitational instability, and the main properties of the first stars. We will conclude with a discussion of the observational signature of the first sources of light, to be probed with future telescopes, such as the *James Webb Space Telescope*.

1. Introduction

The first sources of light fundamentally transformed the early Universe, from the simple initial state of the cosmic dark ages into one of ever-increasing complexity (for comprehensive reviews, see Barkana & Loeb 2001; Bromm et al. 2009; Loeb 2010; Whalen et al. 2010). This process began with the formation of the first stars, the so-called Population III (Pop III), at redshifts $z \sim 20 - 30$. These stars are predicted to form in dark matter minihalos, comprising total masses of $\sim 10^6 M_\odot$. Current models suggest that Pop III stars were typically massive, or even very massive, with $M_* \sim 10 - 100 M_\odot$; these models also predict that the first stars formed in small groups, including binaries or higher-order multiples. First star formation has been reviewed in Bromm & Larson (2004) and Glover (2005). There, you will find a survey of the key papers up to 2005. For the most recent developments, I recommend to consult the specialized literature (e.g., Turk et al. 2009; Stacy et al. 2010; Clark et al. 2011, Greif et al. 2011).

Once the first stars had formed, feedback processes began to modify the surrounding intergalactic medium (IGM). It is useful to classify them into three categories (see Ciardi & Ferrara 2005): radiative, mechanical, and chemical. The first feedback consists of the hydrogen-ionizing photons emitted by Pop III stars, as well as the less energetic, molecule-dissociating radiation in the Lyman-Werner (LW) bands. Once the first stars die, after their short life of a few million years, they will explode as a supernova (SN), or directly collapse into massive black holes (MBHs). In the SN case, mechanical and chemical feedback come into play. The SN blastwave exerts a direct, possibly very disruptive, feedback on its host system, whereas the chemical feedback acts in a more indirect way, as follows: The first stars, forming out of metal-free, primordial gas, are predicted to be characterized by a top-heavy initial mass function (IMF). Once the gas had been enriched to a threshold level, termed “critical metallicity” (Z_{crit}), the mode of star formation would revert to a more normal IMF, which is dominated by lower mass stars (see Frebel et al. 2007). Chemical feedback refers to this transition in star

formation mode, implying that less massive stars have a less disruptive impact on their surroundings. The complex physics of pre-galactic metal enrichment, and the nucleosynthesis in Pop III SNe, are reviewed in Karlsson et al. (2012).

The first, Pop III stars are thus predicted to form in small groups, in minihalos with shallow gravitational potential wells. As they were typically very massive, they would quickly exert a strong negative feedback on their host systems. Numerical simulations indicate that this feedback completely destroys the host, in the sense of heating and evacuating all remaining gas. There would therefore be no opportunity for a second burst of star formation in a minihalo. Furthermore, since all (most?) Pop III stars are massive enough to quickly die, there would be no long-lived system of low-mass stars left behind. The Pop III forming minihalos, therefore, are *not* galaxies, if a bona-fide galaxy is meant to imply a long-lived stellar system, embedded in a dark matter halo. The question: *What is a galaxy, and, more specifically, what is a first galaxy?*, however, is a matter of ongoing debate (see Bromm et al. 2009). And as we have seen, this question is intimately tied up with the feedback from the first stars, which in turn is governed by the Pop III IMF (top-heavy or normal).

Theorists are currently exploring the hypothesis that “atomic cooling halos” are viable hosts for the true first galaxies (Oh & Haiman 2002). These halos have deeper potential wells, compared to the minihalos mentioned above; indeed, they have ‘virial temperatures’ of $T_{\text{vir}} \simeq 10^4$ K, enabling the primordial gas to cool via efficient line emission from atomic hydrogen. We will further clarify these concepts below. It is useful to keep in mind that observers and theorists often employ different definitions. As a theorist, you wish to identify the first, i.e., lowest-mass, dark matter halos that satisfy the conditions for a galaxy. Observers, on the other hand, usually aim at detecting truly metal-free, primordial systems. Recent simulation results, however, suggest that such metal-free galaxies do not exist. The reason being that rapid SN enrichment from Pop III stars, formed in the galaxy’s minihalo progenitors, provided a bedrock of heavy elements. Any second generation stars would then already belong to Population II (Pop II). These questions, and the problem of first galaxy formation in general, have been reviewed in Bromm & Yoshida (2011), where the reader can again find pointers to the detailed literature. For a comprehensive overview of galaxy formation and evolution in general, including the situation at lower redshifts, $0 < z < 5$, see the monograph by Mo et al. (2010).

The first star and galaxy field is just entering a dynamic phase of rapid discovery. This development is primarily driven by new technology, on the theory side by ever more powerful supercomputers, reaching peta-scale machines, and on the observational side by next-generation telescopes and facilities. Among them are the *James Webb Space Telescope (JWST)*, planned for launch in ~ 2018 , and the suite of extremely large, ground-based telescopes, such as the GMT, TMT, and E-ELT. The capabilities of the *JWST* are summarized in Gardner et al. (2006), as well as in the monograph by Stiavelli (2009). Complementary to them are ongoing and future meter-wavelength radio arrays, designed to detect the redshifted 21cm radiation from the neutral hydrogen in the early Universe (see the review by Furlanetto et al. 2006). A further intriguing window into the epoch of the first stars is provided by high-redshift gamma-ray bursts (GRBs). These are extremely bright, relativistic explosions, triggered when a rapidly rotating

massive star is collapsing into a black hole (see the monograph by Bloom 2011). The first stars are promising GRB progenitors, thus possibly enabling what has been termed “GRB cosmology” (for details see Kouveliotou et al. 2012).

There is a second approach to study the ancient past, nicely complementary to the *in situ* observation of high-redshift sources. This alternative channel, often termed “Near-Field Cosmology” (Freeman & Bland-Hawthorn 2002), is provided by local fossils that have survived since early cosmic times. Among them are extremely metal-poor stars found in the halo of the Milky Way. The idea here is to scrutinize their chemical abundance patterns and derive constraints on the properties of the first SNe, and, indirectly, of the Pop III progenitor stars, such as their mass and rate of rotation (for reviews, see Beers & Christlieb 2005; Frebel 2010). Another class of relic objects is made up of the newly discovered extremely faint dwarf galaxies in the Local Group. These ultra-faint dwarf (UFD) galaxies consist of only a few hundred stars, and reside in very low-mass dark matter halos. Their chemical and structural history is therefore much simpler than what is encountered in massive, mature galaxies, and it should be much more straightforward to make the connection with the primordial building blocks (e.g., Salvadori & Ferrara 2009).

The plan for these lecture notes is to provide a theoretical ‘toolkit’, containing the basic physical principles that are the foundation to understand the end of the cosmic dark ages. We will consider the overall cosmological context, the fundamentals of star formation as applicable to the primordial Universe, the properties of the first stars, and the physical principles underlying the assembly of the first galaxies. We conclude with some useful tools of observational cosmology, allowing us to connect theory with empirical probes. For a detailed discussion of the phenomenology and the numerical simulations, we refer the reader to the review papers and monographs cited above. Again, the goal here is to focus on the basic framework, which will likely be relevant for many years to come, enabling the student to follow the rapid progress unfolding in the research literature. I invite you to join in on this grand journey of discovery!

2. The cosmological context

2.1. CDM structure formation

We now have a very successful model that describes the expansion history of the Universe, and the early growth of density fluctuations (Komatsu et al. 2011). This is the Λ cold dark matter (Λ CDM) model, as calibrated to very high precision by the *Wilkinson Microwave Anisotropy Probe (WMAP)*. Structure formation in this model proceeds hierarchically, in a bottom-up fashion, such that small objects emerge first, and subsequently grow through mergers with neighboring objects and the smooth accretion of matter. To characterize the resulting distribution of density fluctuations, we measure the “overdensity” in a spherical window of radius R and total (gas + dark matter) mass M , where $M = 4\pi/3\bar{\rho}R^3$,

$$\delta_M \equiv \frac{\rho - \bar{\rho}}{\bar{\rho}} . \quad (1)$$

Here, ρ is the mass density within a given window, and $\bar{\rho}$ that of the background Universe at the time the overdensity is measured. Next, the idea is to place

the window at random everywhere in the Universe, and to calculate the (mean-square) average $\sigma^2(M) = \langle \delta_M^2 \rangle$, where the brackets indicate a spatial average. The latter is closely related to the ensemble average, where one considers many realizations of the underlying random process that generated the density fluctuations in the very early Universe (ergodic theorem). Here and in the following, all spatial scales are physical, as opposed to comoving, unless noted otherwise.

Due to gravity, the density perturbations grow in time. This growth is described with a “growth factor”, $D(z)$, such that

$$\sigma \propto D(z) \propto a = \frac{1}{1+z} . \quad (2)$$

The second proportionality is only approximate, and would be strictly valid in a simple Einstein-de Sitter background model. The expression for the growth factor is more complicated in a Λ -dominated Universe (see Loeb 2010), but the Einstein-de Sitter scaling still gives a rough idea for what is going on at $z \gg 1$. Indeed, it is quite useful for quick back-of-the-envelope estimates. Early on, all fluctuations are very small, with $\delta_M \ll 1$; but at some point in time, a given overdensity will grow to order unity. One says that a fluctuation is in its linear stage, as long as $\delta_M < 1$, and becomes “non-linear” when $\delta_M > 1$. Formally, a critical overdensity of $\delta_c = 1.69$ is often used to characterize the transition. The behavior and evolution of the perturbations in their linear stage can be treated analytically, e.g., by decomposing a density field into Fourier modes. Once the fluctuation turns non-linear, one needs to resort to numerical simulations to further follow them to increasingly high densities.

A basic tenet of modern cosmology is that the quantum-mechanical processes that imprinted the density fluctuations in the very early Universe left behind a (near-) Gaussian random field. The probability that an overdensity has a given value, around a narrow range $d\delta_M$ is then

$$P(\delta_M)d\delta_M = \frac{1}{\sqrt{2\pi\sigma_M^2}} \exp\left[-\frac{\delta_M^2}{2\sigma_M^2}\right] d\delta_M . \quad (3)$$

One speaks of a “ ν -sigma peak” when $\delta_M = \nu\sigma_M$. Note that high-sigma peaks are increasingly unlikely, and therefore rare. One also says that such peaks are highly biased, and one can show that such peaks are strongly clustered (see, e.g., Mo et al. 2010). The sites for the formation of the first stars and galaxies are predicted to correspond to such high-sigma peaks. To predict the redshift of collapse, or “virialization” redshift (see below), we demand $\delta_M(z) = D(z)\delta_M(z=0) \simeq \delta_c$, or, using Eqn. (2)

$$\frac{\nu\sigma_M(z=0)}{1+z_{\text{vir}}} \simeq 1.69 ,$$

such that $1+z_{\text{vir}} \simeq \nu\sigma_M(z=0)/1.69$, where $\sigma_M(z=0)$ is the rms density fluctuation, extrapolated to the present. On the scale of a minihalo ($M \sim 10^6 M_\odot$), one has $\sigma_M(z=0) \sim 10$. For collapse (virialization) to occur at, say, $z_{\text{vir}} \simeq 20$, we would then need $\nu \simeq 3.5$. Thus, the first star forming sites are rare, but not yet so unlikely to render them completely irrelevant for cosmic history.

2.2. Virialization of DM halos

Once a given perturbation becomes non-linear ($\delta_M \sim 1$), the corresponding dark matter (DM) collapses in on itself through a process of violent dynamical relaxation. The rapidly changing gravitational potential, $\partial\varphi/\partial t$, acts to scatter the DM particles, and their ordered motion is converted into random motion. The result of this “virialization” is a, roughly spherical, halo, where the kinetic and gravitational potential energies approach virial equilibrium, $2E_{\text{kin}} \simeq -E_{\text{pot}}$. Note that the total energy, $E_{\text{tot}} = E_{\text{kin}} + E_{\text{pot}} = -E_{\text{kin}}$, is negative, which implies that the halo is bound.

It is now convenient to define the gravitational potential (potential energy per unit mass), as follows,

$$\varphi = \frac{E_{\text{pot}}}{M_{\text{h}}} \simeq -\frac{GM_{\text{h}}}{R_{\text{vir}}} . \quad (4)$$

Here, M_{h} is the halo mass (gas + DM), which is connected to the halo density and radius, often called “virial” density and radius, via

$$M_{\text{h}} \simeq \frac{4\pi}{3} \rho_{\text{vir}} R_{\text{vir}}^3 . \quad (5)$$

The virial density, established after the virialization process is complete, is related to the background density of the Universe at the time of collapse; at z_{vir} , $\rho_{\text{vir}} \simeq 200\bar{\rho}(z_{\text{vir}})$. In terms of the present-day background density, one has

$$\bar{\rho}(z) = (1+z)^3 \bar{\rho}(z=0) = 2.5 \times 10^{-30} \text{ g cm}^{-3} (1+z)^3 . \quad (6)$$

A very useful concept to gauge how the baryonic (gaseous) component will behave when falling into the DM halos mentioned above is the “virial temperature”. The idea is to ask what would happen to a proton, of mass $m_{\text{H}} = 1.67 \times 10^{-24}$ g, when it is thrown into such a DM potential well. Through compressional heating, either adiabatically or involving shocks, the particle would acquire a random kinetic energy of

$$k_{\text{B}} T_{\text{vir}} \simeq \epsilon_{\text{kin}} \simeq -\epsilon_{\text{pot}} \simeq \frac{GM_{\text{h}} m_{\text{H}}}{R_{\text{vir}}} , \quad (7)$$

where k_{B} is Boltzmann’s constant. Combining the equations above yields

$$T_{\text{vir}} \simeq 10^4 \text{ K} \left(\frac{M_{\text{h}}}{10^8 M_{\odot}} \right)^{2/3} \left(\frac{1+z_{\text{vir}}}{10} \right) , \quad (8)$$

where the normalizations are appropriate for a first-galaxy system, or, technically, an atomic cooling halo. For a minihalo, where $M_{\text{h}} \sim 10^6 M_{\odot}$ and $z_{\text{vir}} \sim 20$, one has $T_{\text{vir}} \sim 1,000$ K. A related quantity is the halo binding energy

$$E_{\text{b}} \simeq |E_{\text{tot}}| \simeq \frac{1}{2} \frac{GM_{\text{h}}^2}{R_{\text{vir}}} \simeq 10^{53} \text{ ergs} \left(\frac{M_{\text{h}}}{10^8 M_{\odot}} \right)^{5/3} \left(\frac{1+z_{\text{vir}}}{10} \right) , \quad (9)$$

where the normalizations are again appropriate for an atomic cooling halo. For a minihalo, the corresponding number is $E_{\text{b}} \sim 10^{50}$ erg. Comparing these values

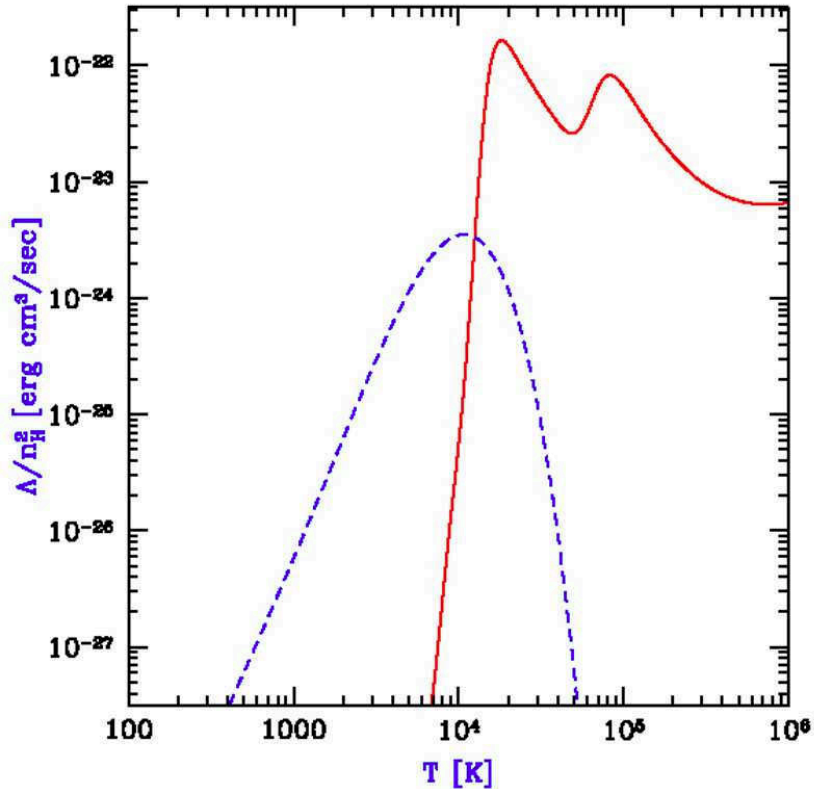


Figure 1. Cooling rate of primordial gas as a function of temperature. Shown is the contribution from atomic hydrogen and helium (*solid line*), as well as that from molecular hydrogen (*dashed line*). Atomic hydrogen line cooling is very efficient at temperatures of $T > 10^4$ K, whereas at lower temperatures, cooling has to rely on H_2 , which is a poor coolant. This is the regime of the minihalos, hosting the formation of the first stars. Adopted from Loeb (2010).

with the explosion energy of Pop III SNe, where $E_{\text{SN}} \simeq 10^{51} - 10^{52}$ erg, one gets the zero-order prediction that minihalos may already be severely affected by SN feedback, evacuating most of the gas from the DM halo (see Ciardi & Ferrara 2005). The more massive atomic cooling halos, on the other hand, are expected to survive such negative SN feedback. This expectation is roughly born out by numerical simulations (see Bromm & Yoshida 2011).

2.3. Gas dissipation

To form something interesting, such as stars, black holes, or galaxies, gas needs to be able to collapse to high densities. Initially, such collapse is triggered by the DM potential well in halos, as the DM is dynamically dominant, and the gas (the baryons) just follow along. However, different from DM, the gas is collisional, and therefore subject to compressional heating. If this heat could not be radiated

away, or dissipated, there would eventually be sufficient pressure support to stop the collapse. The key question then is: *Can the gas sufficiently cool?* A simple, but intuitively appealing and useful answer, is provided by the classical Rees-Ostriker-Silk criterion, that the cooling time has to be shorter than the free-fall time, $t_{\text{cool}} < t_{\text{ff}}$. If this criterion is fulfilled, a gas cloud will be able to condense to high densities, and possibly undergo gravitational runaway collapse. These important timescales are defined as follows, $t_{\text{ff}} \simeq 1/\sqrt{G\rho}$ and $t_{\text{cool}} \simeq nk_{\text{B}}T/\Lambda$, where Λ is the cooling function (in units of $\text{erg cm}^{-3} \text{s}^{-1}$).

In Figure 1, the cooling function for primordial, pure H/He, gas is shown. One can clearly distinguish two distinct cooling channels, one at $T > 10^4 \text{ K}$, where cooling relies on atomic hydrogen lines, and one at lower temperatures, where the much less efficient H_2 molecule is the only available coolant. In the present-day interstellar medium (ISM), metal species would dominate cooling in this low-temperature regime, but, by definition, they are absent in the primordial Universe. The first cooling channel governs the formation of the first galaxies (atomic cooling halos), since $T_{\text{vir}} \sim 10^4 \text{ K}$ for $M_{\text{h}} \sim 10^8 M_{\odot}$ and $z_{\text{vir}} \sim 10$. First star formation in minihalos, on the other hand, is governed by the low-temperature, H_2 , cooling channel. The reason is again that minihalos typically have $T_{\text{vir}} \sim 1,000 \text{ K}$.

2.4. Halo angular momentum

Another important ingredient for early star and galaxy formation is angular momentum. Current cosmological models posit that the post-recombination Universe, at $z < 1000$, was free of any circulation ($\nabla \times \vec{v} = 0$). Angular momentum is thought to have been created through tidal torques during the collapse of slightly asymmetric overdensities. The idea is that neighboring perturbations exert a net torque on a given halo, thus spinning it up. It is convenient to parameterize the resulting total angular momentum, J , of a virialized halo by a “spin parameter”

$$\lambda \equiv \frac{J|E_{\text{tot}}|^{1/2}}{GM_{\text{h}}^{5/2}} \simeq \left(\frac{E_{\text{rot}}}{|E_{\text{tot}}|} \right)^{1/2}, \quad (10)$$

where $|E_{\text{tot}}|$ is again the total halo (binding) energy, and $E_{\text{rot}} \simeq J^2/(M_{\text{h}}R_{\text{vir}}^2)$ the total rotation energy. Numerical simulations, studying the large-scale evolution of the DM component, have shown that the spin parameter is distributed in a log-normal fashion with a mean of $\bar{\lambda} \simeq 0.04$ (see Mo et al. 2010).

For the DM component, the spin parameter is conserved during collisionless evolution. During the dissipational collapse of the gas, however, the spin parameter can change. In particular, the system can be driven towards centrifugal support, where $E_{\text{rot}} \simeq |E_{\text{tot}}|$. *What is the radius of centrifugal support?* Assume that the baryons collapse further, in a fixed DM halo potential. It is then straightforward to show that the baryons have to collapse by a factor of $\sim \lambda^{-1}$ to reach centrifugal support, $R_{\text{cent}} \simeq \lambda R_{\text{vir}}$. This then is the typical dimension of any large-scale disk that forms inside a dark matter halo.

3. First star formation: basic principles

Primordial star formation shares many similarities with the present-day case, in terms of basic principles. It is therefore always a good idea to seek guidance from the rich phenomenology and understanding reached in classical star formation theory (see McKee & Ostriker 2007; Zinnecker & Yorke 2007; Bodenheimer 2011 for reviews). In the following, in the spirit of our basic toolkit approach, we will address gravitational (Jeans) instability, the physics of protostellar accretion, and the properties of a generic stellar IMF.

3.1. Gravitational instability

Consider a gaseous cloud of linear size L with a given mass density ρ and temperature T . Such a cloud will be unstable to gravitational runaway collapse, if $t_{\text{sound}} > t_{\text{ff}}$, with $t_{\text{sound}} \simeq L/c_s$ being the sound-crossing time. The sound speed is $c_s \simeq \sqrt{k_B T/m_H} \propto T^{1/2}$. The intuition here is that the free-fall time measures the strength of gravity, in the sense that a smaller t_{ff} corresponds to a stronger force of gravity. Similarly, the sound-crossing timescale provides a measure for the strength of the opposing thermal pressure, where again a smaller t_{sound} indicates stronger pressure forces. The above timescale criterion for gravitational instability can be written as

$$\frac{L}{c_s} > \frac{1}{\sqrt{G\rho}} . \quad (11)$$

This inequality defines the Jeans length

$$L > L_J \simeq \frac{c_s}{\sqrt{G\rho}} , \quad (12)$$

with the interpretation that a density perturbation has to exceed a certain critical size, such that gravitational forces take over, and cannot be balanced by thermal pressure any longer. One then defines the *Jeans mass*, as follows

$$M_J \sim \rho L_J^3 \simeq 500 M_\odot \left(\frac{T}{200 \text{ K}} \right)^{3/2} \left(\frac{n}{10^4 \text{ cm}^{-3}} \right)^{-1/2} , \quad (13)$$

where $n \simeq \rho/m_H$ is the hydrogen number density, and the normalizations reflect typical values in Pop III star forming regions. A closely related concept is the *Bonnor-Ebert mass*, where $M_J \sim 2M_{\text{BE}}$.

3.2. Protostellar accretion

Every star, regardless of whether we are dealing with Pop I or Pop III, is assembled in an inside-out fashion, such that a small hydrostatic protostellar core is formed first at the center of a Jeans-unstable cloud. This initial core subsequently grows through accretion. Feedback effects from the growing protostar will eventually terminate this process, thus setting the final mass scale of the star. The initial core mass is small, close to the so-called *opacity limit for fragmentation*, $M_F \simeq 10^{-2} M_\odot$. This lower limit to the mass of a star can be derived by considering a cloud that is roughly in free-fall collapse. Collapse can proceed as long as the gas is able to radiate away the concomitant compressional heat. At

very high densities, however, the gas becomes opaque to this cooling radiation. Soon thereafter thermal pressure forces can stop the collapse, and a hydrostatic core is born. The key question now is to address the growth via accretion, which happens in two distinct regimes, first as predominantly spherical accretion, and then as disk-dominated accretion.

Spherical accretion For a roughly spherical gas cloud with a mass close to the Jeans mass, one can estimate the average accretion rate as follows,

$$\dot{M}_{\text{acc}} \sim \frac{M_{\text{J}}}{t_{\text{ff}}} \propto \frac{T^{3/2} \rho^{-1/2}}{\rho^{-1/2}} \sim T^{3/2} . \quad (14)$$

In the first step, we have assumed that gravity cannot move any material faster than the free-fall time. Using $c_s \propto T^{1/2}$, it is sometimes convenient to rewrite this as $\dot{M} \simeq c_s^3/G$. Typically, one has for Pop I $T \sim 10 \text{ K} \Rightarrow \dot{M} \sim 10^{-5} M_{\odot} \text{ yr}^{-1}$; and for Pop III $T \sim 300 \text{ K} \Rightarrow \dot{M} \sim 10^{-3} M_{\odot} \text{ yr}^{-1}$. This two-order of magnitude difference in accretion rates is the basic physical reason why the first stars are believed to be more massive than present-day stars. Early on, protostellar accretion is mainly spherical, but with time, material with higher specific angular momentum (J/m) falls in, and results in the formation of a protostellar disk. The bulk of the accretion is then shifted to a disk mode.

Disk accretion Consider a circular shell, located at radius r , within a disk of surface mass density $\Sigma = M_{\text{disk}}/(\pi R_{\text{disk}}^2)$. For such a shell, one has

$$dM \simeq 2\pi r dr \Sigma . \quad (15)$$

Dividing by dt on both sides, yields the basic expression for the disk accretion rate, $\dot{M}_{\text{acc}} \simeq 2\pi r v_r \Sigma$, with $v_r = dr/dt$ being the radial (inflow) velocity. In a non-viscous disk, one would have $v_r = 0$. Thus the reason that there is any infall is the presence of viscous shear forces, or, put differently, of friction. Such shear forces enable the outward transport of angular momentum, and the inward transport of mass.

Intuitively, to characterize viscous transport of linear momentum, one can set

$$r v_r \sim \lambda_{\text{mfp}} \bar{v} \sim \nu , \quad (16)$$

with ν being the (kinematic) viscosity coefficient (in units of $\text{cm}^2 \text{ s}^{-1}$). The idea is that viscous transport involves the displacement of a particle (or fluid element) from a region of higher to lower momentum, e.g., a radial excursion in a Keplerian disk, where $v_{\text{rot}} \propto r^{-1/2}$. Such a displacement involves, on average, a distance equal to the mean-free path, λ_{mfp} , and proceeds with the average particle velocity, \bar{v} . The latter is often equal to the thermal velocity (or sound speed). It has long been realized that the molecular (microscopic particle) viscosity is much too small to have an effect on astrophysical systems, such as protostellar disks. Therefore, an ‘‘abnormal’’ source of viscosity is needed. Often, turbulent diffusion (transport) is implicated. Due to the inherent difficulties involved in the physics of turbulent transport, it is customary to employ the phenomenological α -prescription, introduced by Shakura & Sunyaev (1973), $\nu = \alpha H_p c_s$, where H_p is the pressure scale-height, effectively a measure of the vertical disk

height. The underlying intuition is that one is dealing with subsonic turbulence (else, for supersonic turbulence, shocks would rapidly dissipate any turbulent energy), such that $\alpha < 1$. Note, that within this picture, the turbulent eddy size is bounded by the height of the disk, and the eddy turnover velocity by the sound speed. Also note that here, mesoscopic fluid elements (small compared to the total system, but large compared to individual atoms) have taken over the role of the individual atoms (or molecules) as fundamental carriers of linear momentum transport. From numerical simulations, we have the further constraint that, typically $\alpha \simeq 10^{-2} - 1$, depending on the nature of the torques involved (gravitational, hydrodynamical, or magnetic).

We can now re-write our expression for the disk accretion rate in a form that can actually be evaluated in terms of easily accessible quantities,

$$\dot{M}_{\text{acc}} \simeq 2\pi\nu\Sigma . \quad (17)$$

The precise derivation would yield a “ 3π ” instead of our factor of 2π . Let us conclude this subsection by considering some numbers, typically encountered in Pop III disks (e.g., Clark et al. 2011), $\Sigma \sim 10^2 \text{ g cm}^{-2}$, $H_p \sim 100 \text{ AU} \sim 10^{15} - 10^{16} \text{ cm}$, and $c_s \sim 10^5 \text{ cm s}^{-1}$. Since here, angular momentum transport is dominated by gravitational torques, it is appropriate to choose $\alpha \sim 1$. We then estimate $\dot{M}_{\text{acc}} \sim 10^{-3} - 10^{-2} M_{\odot} \text{ yr}^{-1}$. Accretion onto a massive star proceeds for roughly the Kelvin-Helmholtz timescale, $t_{\text{acc}} \sim t_{\text{KH}} \sim 10^5 \text{ yr}$, which in turn is the time it takes a (massive) star to reach the hydrogen-burning main sequence. One then has as a rough upper limit for the final mass of a Pop III star, $M_* \sim \dot{M}_{\text{acc}} t_{\text{acc}} \sim 100 M_{\odot}$. In reality, final masses will typically be smaller, since accretion may be terminated earlier on due to the negative radiative feedback from the growing protostar (e.g., Hosokawa et al. 2011; Stacy et al. 2012).

3.3. Initial mass function

The stellar IMF is a complicated function of mass, but it is often convenient to simply write it as a power law, valid for a given mass range. Specifically, one considers the number of stars per unit mass,

$$\frac{dN}{dM} \propto M^{-x} , \quad (18)$$

where the present-day IMF is characterized by the famous Salpeter slope of $x = 2.35$. To understand what the *typical* outcome of the star-formation process is, one can ask: *Where does most of the available mass go?* Or, put differently: What is the average stellar mass? This can be calculated as follows,

$$\bar{M} = \frac{\int_{M_{\text{low}}}^{M_{\text{up}}} M \frac{dN}{dM} dM}{\int_{M_{\text{low}}}^{M_{\text{up}}} \frac{dN}{dM} dM} = \frac{1-x}{2-x} \frac{M_{\text{up}}^{2-x} - M_{\text{low}}^{2-x}}{M_{\text{up}}^{1-x} - M_{\text{low}}^{1-x}} \sim 3.8 M_{\text{low}} \quad (19)$$

where in the last relation, we have used the Salpeter value for x , and M_{low} and M_{up} are the lower and upper mass limits, respectively. In general, one can neglect all terms involving M_{up} above, as long as $x > 2$. This means that a Salpeter-like IMF is dominated by the lower-mass limit. For Pop I (present-day) stars, one often takes $M_{\text{low}} \simeq 0.1 M_{\odot}$ and $M_{\text{up}} \simeq 100 M_{\odot}$, such that $\bar{M} \sim 0.5 M_{\odot}$,

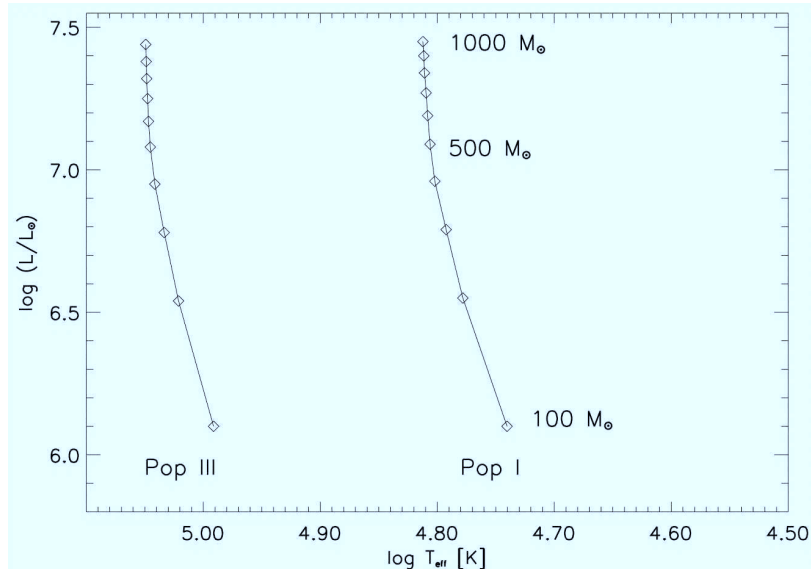


Figure 2. Zero-age main sequence (ZAMS) for very massive stars. Shown is a comparison between the Pop III (*left line*) and Pop I cases (*right line*). Stellar luminosity (in units of L_{\odot}) is plotted vs. effective temperature (in K). *Diamond-shaped symbols*: stellar masses along the sequence, from $100M_{\odot}$ (bottom) to $1000M_{\odot}$ (top). As can be seen, the Pop III ZAMS is shifted to higher values of effective temperature, asymptotically reaching $T_{\text{eff}} \simeq 10^5$ K. Note that current estimates for the Pop III mass are somewhat less extreme. Adopted from Bromm et al. (2001).

whereas for Pop III, current theory postulates a characteristic (typical) mass of $\bar{M} \sim 4M_{\text{low}} \sim \text{a few} \times 10M_{\odot}$, assuming that the Pop III IMF were to exhibit a slope similar to Salpeter. The latter assumption is not at all proven, and just serves as a zero-order guess.

4. First stars: basic properties

In the following, we will address the fundamentals of the structure and evolution of massive, Pop III stars. Many of these relations are strictly valid only for stars with $M_* > 100M_{\odot}$. The stellar physics in this high-mass regime, although involving extreme energies and temperatures, is of an appealing simplicity. Recent simulations have revised the Pop III mass-scale downwards to more modest values ($M_* \sim 10 - 50M_{\odot}$), but the simple high-mass physics nevertheless provides us with very useful order-of-magnitude estimates. The discussion here is largely based on Bromm et al. (2001), and we refer the reader to this paper, and references therein, for a more detailed (numerical) treatment.

In this spirit, we start by assuming a typical Pop III stellar mass of $M_* \sim 100M_{\odot}$. Massive stars are dominated by radiation pressure (see below), and

their structure can therefore approximately be described as a polytrope with index $n = 3$. For such a configuration, one can derive the following mass-radius relation,

$$R_* \simeq 5R_\odot \left(\frac{M_*}{100M_\odot} \right)^{1/2}, \quad (20)$$

which is valid for a star on the hydrogen-burning main sequence. It is then straightforward to estimate the average mass $\langle \rho \rangle = M_*/(4\pi/3R_*^3) \sim 1 \text{ g cm}^{-3}$, which is of the same order as for the Sun. Somewhat surprisingly, massive stars, therefore do not involve extreme densities. We next wish to estimate the temperature, both at the surface and in the deep interior. To accomplish this, one has to consider the pressure inside the star.

4.1. Radiation pressure

In massive stars ($M_* > 50M_\odot$), radiation pressure starts to be important, compared with the usual gas (thermal) pressure. For ultra-relativistic particles, in our case photons, one has the general relation between pressure and energy density (in units of erg cm^{-3}), $P_{\text{rad}} = 1/3u_{\text{rad}}$. The latter is given by the Stefan-Boltzmann law,

$$u_{\text{rad}} = \frac{8\pi^5}{15} \frac{k_{\text{B}}^4}{h^3 c^3} T^4 = a_{\text{rad}} T^4, \quad (21)$$

where h is Planck's constant. The radiation constant has the numerical value $a_{\text{rad}} = 7.57 \times 10^{-15} \text{ erg K}^{-4} \text{ cm}^{-3}$. Thus, we can write the radiation (photon) pressure, as

$$P_{\text{rad}} = \frac{1}{3} a_{\text{rad}} T^4. \quad (22)$$

4.2. Hydrostatic equilibrium

The motion of any fluid element in a star is governed by the Euler equation

$$\rho \frac{D\vec{v}}{Dt} = -\nabla P + \rho \vec{g}, \quad (23)$$

where D/Dt is the substantial (moving with the fluid) derivative, and \vec{g} the gravitational acceleration. Assuming spherical symmetry and $D/Dt = 0$, we get the equation of hydrostatic equilibrium, which is crucial for the structure of stars,

$$\frac{dP_{\text{rad}}}{dr} = -\rho \frac{Gm}{r^2}, \quad (24)$$

Here, we have assumed $P = P_{\text{gas}} + P_{\text{rad}} \sim P_{\text{rad}}$, as is appropriate for massive stars. Above, we introduce the Lagrangian mass coordinate, $m = m(r)$, which measures the total mass contained within a shell of radius r . We now re-work this equation in an order-of-magnitude fashion,

$$\frac{a_{\text{rad}} T^4}{R_*} \simeq \langle \rho \rangle \frac{GM_*}{R_*^2}, \quad (25)$$

resulting in an estimate for the typical interior temperature in a massive Pop III star,

$$T_I = \left(\frac{\langle \rho \rangle}{a_{\text{rad}}} \frac{GM_*}{R_*} \right)^{1/4} \sim 10^8 \text{ K} . \quad (26)$$

The next question is: *How is this related to the surface temperature?* In addressing it, we need to consider how energy is transported in the stellar interior via photon diffusion.

4.3. Radiative diffusion

Let us begin with a thought experiment. For the moment, (wrongly) assume that photons are free to escape from the hot interior of a star, which would imply negligible opacity (i.e., the capability of stellar gas to bottle-up radiation). The timescale for such hypothetical, direct escape would be $t_{\text{direct}} = R_*/c$. Within the same setup, we would estimate the stellar luminosity as follows,

$$L = \frac{\Delta E}{\Delta t} \sim \frac{u_{\text{rad}} R_*^3}{t_{\text{direct}}} \simeq \frac{a_{\text{rad}} c T_I^4 R_*^3}{R_*} \simeq a_{\text{rad}} c R_*^2 T_I^4 . \quad (27)$$

The radiation constant is related to the Stefan-Boltzmann constant via $a_{\text{rad}} = 4\sigma_{\text{SB}}/c$, where $\sigma_{\text{SB}} = 5.67 \times 10^{-5} \text{ erg s}^{-1} \text{ cm}^{-2} \text{ K}^{-4}$. We can thus re-phrase the equation above in a form similar to the standard blackbody expression

$$L = 4\pi R_*^2 \sigma_{\text{SB}} T_I^4 . \quad (28)$$

Now, why is this reasoning incorrect? The answer is that in reality photons are trapped inside a star. Indeed, stellar material is typically extremely opaque to radiation, such that the photons engage in a very slow diffusion process, and eventually leak out from a narrow layer close to the surface, the stellar photosphere. Effectively, we are dealing with a near-blackbody, characterized by an effective (photospheric) temperature, T_{eff} . If we further replace the (incorrect) direct escape timescale with the (correct) diffusion time, we have

$$L = \frac{\Delta E}{\Delta t} \simeq \frac{\Delta E}{t_{\text{diff}}} = 4\pi R_*^2 \sigma_{\text{SB}} T_{\text{eff}}^4 , \quad (29)$$

such that

$$T_{\text{eff}} \simeq \left(\frac{t_{\text{direct}}}{t_{\text{diff}}} \right)^{1/4} T_I . \quad (30)$$

Our remaining task is therefore to estimate the diffusion timescale.

We can do this by modeling diffusion as a (nearly-isotropic) random walk. If l_γ is the photon mean-free path, and N_{sc} the number of scatterings needed for a photon to escape from the star, basic random-walk theory yields $R_* = \sqrt{N_{\text{sc}}} l_\gamma$. Stellar material is extremely opaque, and one typically has $l_\gamma \simeq 1/(n\sigma_{\text{T}}) \simeq 1 \text{ cm}$. Here, we have assumed that the opacity is dominated by electron (Thomson) scattering, with an interaction cross-section of $\sigma_{\text{T}} = 0.67 \times 10^{-24} \text{ cm}^2$. The diffusion timescale can then be estimated via

$$t_{\text{diff}} \simeq \frac{N_{\text{sc}} l_\gamma}{c} \simeq \frac{R_*^2}{l_\gamma c} . \quad (31)$$

Combining everything, we finally get

$$T_{\text{eff}} \simeq \left(\frac{l_\gamma}{R_*} \right)^{1/4} T_I \sim 10^{-3} T_I \sim 10^5 \text{ K} . \quad (32)$$

Massive Pop III stars are thus extremely hot (compare to the solar $T_{\text{eff},\odot} \simeq 6,000 \text{ K}$), which in turn implies a number of key consequences for early cosmic history. Among them is a very high specific (per unit stellar mass) production rate of ionizing photons. It is useful to remember: $\dot{N}_{\text{ion}} \simeq 10^{48} \text{ s}^{-1} M_\odot^{-1}$. In addition, such hot stars can also produce copious amounts of He-ionizing photons, including those required for the second ionization of He (54 eV). Normally, such extremely energetic radiation is not produced by stars, and instead originates in quasar (accreting black-hole) sources.

4.4. Stellar luminosity

Combining the expressions above, we find for the Pop III stellar luminosity

$$L = 4\pi R_*^2 \sigma_{\text{SB}} T_{\text{eff}}^4 \simeq 10^6 L_\odot \left(\frac{M_*}{100 M_\odot} \right) . \quad (33)$$

To repeat, in deriving this, we have assumed that: *(i)* pressure is dominated by radiation (appropriate for all massive stars), and *(ii)* opacity is dominated by Thomson scattering (appropriate for metal-free stars). The $L \propto M_*$ scaling is characteristic for very massive stars. Indeed, the luminosity for massive Pop III stars is close to the theoretical upper limit, the so-called ‘‘Eddington luminosity’’.

The Eddington limit can be derived by demanding that the radiation pressure associated with a given luminosity does not exceed the force of gravity. Specifically, let us consider the balance of forces exerted on a combination of one proton and one electron, where the proton provides (most of) the mass, and the (free) electron the opacity (via Thomson scattering),

$$\frac{G m_{\text{H}} M_*}{r^2} \simeq \frac{\Delta p_\gamma}{\Delta t} , \quad (34)$$

where Δp_γ is the absorbed photon momentum per particle,

$$\frac{\Delta p_\gamma}{\Delta t} = \frac{\Delta E_\gamma / c}{\Delta t} = \frac{1}{c} \frac{L}{4\pi r^2} \sigma_{\text{T}} . \quad (35)$$

Thus, one has $L < L_{\text{Edd}}$, where the Eddington luminosity is

$$L_{\text{Edd}} = \frac{4\pi G c m_{\text{H}}}{\sigma_{\text{T}}} M_* = 1.3 \times 10^{38} \text{ erg s}^{-1} \left(\frac{M_*}{M_\odot} \right) . \quad (36)$$

This is very close to the estimate in equation (33), demonstrating that $L \sim L_{\text{Edd}}$ for very massive ($M_* > 100 M_\odot$) Pop III stars. Again, these relations still give reasonable ballpark numbers for less extreme masses.

In Figure 2, the Pop III zero-age main sequence (ZAMS) is shown, together with the comparison Pop I sequence, in both cases for very massive stars. As

is evident there, the effective temperatures asymptotically approach constant values, $T_{\text{eff}} \sim 10^5$ K for Pop III, and $\sim 60,000$ K for Pop I. Luminosities, however, are very similar for a star of given mass, regardless of metallicity. The reason that Pop III stars are so much hotter (bluer) is their much more compact configuration, which is in turn a reflection of the reduced opacity in the outer envelope.

Finally, let us estimate the lifetime of massive Pop III stars. Assuming that such stars radiate close to the Eddington limit, and that they are almost fully convective, one has the simple relation

$$t_* \simeq \frac{0.007 M_* c^2}{L_{\text{Edd}}} \simeq 3 \times 10^6 \text{ yr}, \quad (37)$$

where the factor of 0.007 is the efficiency of hydrogen burning. These are very short lifetimes, compared with the solar $t_{*,\odot} \sim 10^{10}$ yr. The implication is that any feedback effects exerted on the surrounding IGM by the Pop III star are almost instantaneous. For example, the pristine gas in the neighborhood of the Pop III star is rapidly converted into metal-enriched material, such that any subsequent round of star formation will already lead to Pop II stars. Also note that for very massive stars the stellar lifetime becomes independent of mass.

5. First galaxy assembly

With the emergence of the first galaxies, we witness the onset of supersonic turbulence, which is expected to have important consequences for star formation (reviewed in Mac Low & Klessen 2004; McKee & Ostriker 2007). To see this, we estimate the Reynolds and Mach numbers, as follows. The Reynolds number measures the relative importance of inertia and viscous forces,

$$Re = \frac{\text{inertial acceleration}}{\text{viscous acceleration}} \simeq \frac{V}{\nu} \simeq \frac{VL}{\nu} , \quad (38)$$

where V , L , $T = L/V$ are characteristic velocity, length, and time scales, respectively. For the first galaxies, we can estimate $V \sim v_{\text{vir}} \sim 10 \text{ km s}^{-1}$, $L \sim R_{\text{vir}} \sim 1 \text{ kpc}$, and $\nu \sim \lambda_{\text{mfp}} c_s \sim 10^{18} \text{ cm}^2 \text{ s}^{-1}$. For the last estimate, we have assumed $\lambda_{\text{mfp}} = 1/(n\sigma_{\text{coll}}) \sim 10^{13} \text{ cm}$, if the number density is typically $n \sim 10^3 \text{ cm}^{-3}$, and we consider collisions between neutral hydrogen atoms ($\sigma_{\text{coll}} \sim 10^{-16} \text{ cm}^2$). For the typical particle velocity, we assume the sound-speed of H_2 -cooled gas ($c_s \sim 1 \text{ km s}^{-1}$). The Reynolds number in the center of the first galaxies is therefore $Re \sim 10^9$, indicating a highly-turbulent situation. The Mach number is $Ma \sim V/c_s \sim v_{\text{vir}}/c_s \sim 10$, indicating supersonic flows.

Supersonic turbulence generates density fluctuations in the ISM. Statistically, these can be described with a log-normal probability density function (PDF),

$$f(x)dx = \frac{1}{\sqrt{2\pi\sigma_x^2}} \exp\left[-\frac{(x - \mu_x)^2}{2\sigma_x^2}\right] dx , \quad (39)$$

where $x \equiv \ln(\rho/\bar{\rho})$, and μ_x and σ_x^2 are the mean and dispersion of the distribution, respectively. The latter two are connected, $\mu_x = -\sigma_x^2/2$. This relation can easily

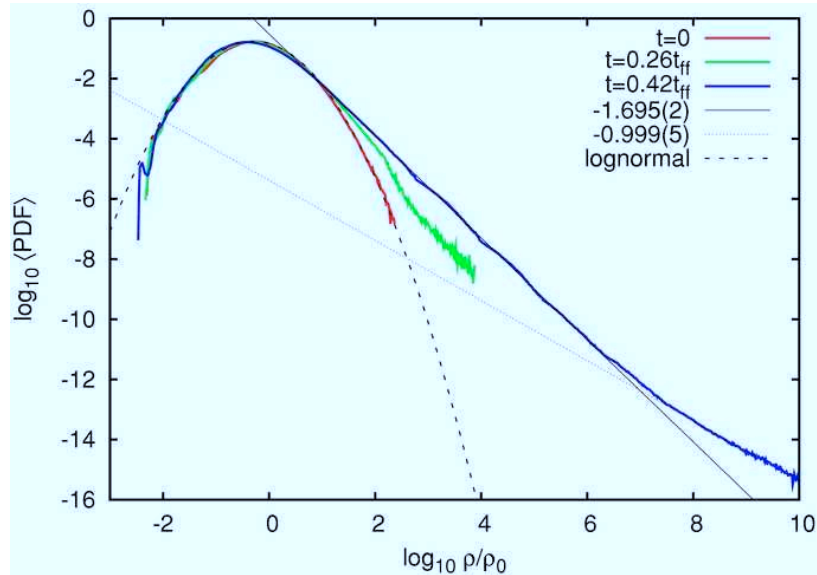


Figure 3. Density distribution in supersonically-turbulent flows. Initially ($t = 0$), the density PDF is log-normal. With time, a pronounced power-law tail develops towards high density. This is a reflection of the gas self-gravity. Adopted from Kritsuk et al. (2011).

be derived by interpreting the PDF above as a distribution (of x) by volume. One then has for the volume-averaged density $\bar{\rho} = \int \rho f(x) dx = \bar{\rho} \int e^x f(x) dx$, which yields the desired result. Numerical simulations have shown that the dispersion of the density PDF is connected to the Mach number of the flow $\sigma_x^2 \simeq \ln(1 + 0.25Ma^2)$. Inside the first galaxies, one finds values close to $\sigma_x \simeq 1$. In Figure 3, we show an illustrative example from a numerical simulation of isothermal, supersonic turbulence. There, it is also evident that the self-gravity of the gas imprints a power-law tail toward the highest densities, on top of the log-normal PDF at lower densities, which is generated by purely hydrodynamical effects.

6. Observational signature

It is useful to recall the derivations of some of the key quantities in observational cosmology, specifically luminosity and angular-diameter distance, as well as the observed flux. It is also useful to assemble estimates for their typical values as encountered in the first galaxies. Further details are given in the monographs mentioned above. In addition, a comprehensive survey of high-redshift galaxy observations, including a description of the key methods and tools, is given by Appenzeller (2009).

6.1. Cosmological distances

In analogy to the usual inverse-square law, the luminosity distance, d_L , is defined via

$$f_{\text{obs}} = \frac{\Delta E_{\text{obs}}}{\Delta t_{\text{obs}} \Delta A_{\text{obs}}} = \frac{L_{\text{em}}}{4\pi d_L^2}, \quad (40)$$

where here and in the following we refer to quantities that are measured at $z = 0$ with the subscript ‘‘obs’’, and with ‘‘em’’ to source-frame quantities (emitted at a given redshift z). Note that $\Delta E_{\text{obs}} = \Delta E_{\text{em}}/(1+z)$, and $\Delta t_{\text{obs}} = \Delta t_{\text{em}}(1+z)$ relate small differences in energy and time in the two frames. To evaluate ΔA_{obs} , carry out the following thought experiment: Imagine that you could somehow ‘step outside’ our Universe, looking down at the scene from some (higher-dimensional) bird’s-eye perspective. Such a perspective, which of course is completely inaccessible in practice, would allow you to measure distances, *as they would appear today*. Or, put differently, you somehow managed to stop the expansion of the Universe, keep everything frozen at $z = 0$, and go about measuring the distance, with some appropriate measuring rod, from the observer (the telescope) to where the source would be located today. Recall that the source was much closer when it emitted the photon that we receive today, but has hence receded due to cosmic expansion. This source-observer distance, $r(z)$, is called *comoving distance*, or *proper distance*. Although it cannot be directly measured, but instead can only be calculated by assuming a theoretical model of the Universe, this concept is nevertheless extremely useful in cosmology. Assuming a point source at a given redshift z , we can now write the (proper) size of the spherical surface over which the photons have been spread, as $\Delta A_{\text{obs}} = 4\pi r^2(z)$.

To calculate the comoving distance, consider the Robertson-Walker (RW) metric,

$$ds^2 = c^2 dt^2 - a^2 dr^2, \quad (41)$$

where we have assumed a spatially flat Universe, and where ds is the (invariant) space-time interval. Since they travel along null geodesics ($ds = 0$), one has for photons $dr = c dt/a$ (recall $a = 1/(1+z)$). The RW metric describes any homogeneous, isotropic, and expanding Universe. To fully specify the background cosmological model, we also need the Friedmann equation, governing \dot{a} . The latter can in turn be derived from the Einstein field equations of general relativity (see Mo et al. 2010), yielding

$$\left(\frac{\dot{a}}{a}\right) = H(z) = H_0 \sqrt{\Omega_m(1+z)^3 + \Omega_\Lambda}, \quad (42)$$

where H_0 , Ω_m , and Ω_Λ are the Hubble constant, the density parameter for matter, and that for dark energy, respectively, as measured to very high precision by *WMAP* (Komatsu et al. 2011). In this expression, we again assume a spatially flat Universe (zero curvature). We can now carry out the integration along the photon-geodesic,

$$r(z) = c \int_0^z (1+z') \left| \frac{dt}{dz'} \right| dz' = \frac{c}{H_0} \int_0^z \frac{dz'}{\sqrt{\Omega_m(1+z')^3 + \Omega_\Lambda}}, \quad (43)$$

where we use the Friedmann equation in the last step.

We have now all the ingredients in hand to find an expression for the luminosity distance,

$$f_{\text{obs}} = \frac{1}{4\pi(1+z)^2 r^2} \frac{\Delta E_{\text{em}}}{\Delta t_{\text{em}}} = \frac{L_{\text{em}}}{4\pi r^2 (1+z)^2} . \quad (44)$$

Comparing with the definition above, we finally have $d_L(z) = (1+z)r(z)$. It is useful to memorize the ballpark number for a source at $z \simeq 10$, appropriate for the first galaxies, $d_L(z) \sim 10^2$ Gpc.

Next, let us derive the analogous expression for *angular-diameter distance*, d_A , where we again start with a definition that follows basic, geometrical intuition. If a source at z , having a true (proper) transverse size of D , is observed to have an apparent angular size of Θ , we define $\Theta = D/d_A$. And let us again assume our bird's-eye perspective, as before. How would the source appear at the present-day ($z = 0$), if it had just been coasting along with the expanding Universe since the time that the photons, reaching us now, were originally emitted? The situation can be described with a virtual triangle, where

$$\Theta = \frac{D(1+z)}{r(z)} = \frac{D}{d_A} , \quad (45)$$

giving us our result, $d_A = r(z)/(1+z)$. Note that the two fundamental distances of observational cosmology are connected, $d_L = d_A(1+z)^2$, such that it suffices to remember only one. For a first galaxy, where $D \sim 1$ kpc, one finds $\Theta \sim D/d_A \sim 1 \text{ kpc}/1 \text{ Gpc} \sim 10^{-6} \sim 0.2''$. The near-IR camera on-board the *JWST* (NIRCam) should thus be able to marginally resolve these sources.

6.2. Observed fluxes

To estimate how bright a first galaxy is likely to be, we need to consider the observed specific flux (flux per unit frequency)

$$f_{\nu, \text{obs}} = \frac{\Delta E_{\text{obs}}}{\Delta t_{\text{obs}} \Delta A_{\text{obs}} \Delta \nu_{\text{obs}}} = \frac{\Delta E_{\text{em}}/(1+z)}{4\pi r^2 \Delta t_{\text{em}} \Delta \nu_{\text{em}}} \simeq (1+z) \frac{L_{\nu, \text{em}}}{4\pi d_L^2} . \quad (46)$$

To arrive at a zeroth-order guess, we assume that the total stellar mass involved in the starburst at the center of a first galaxy is $M_* \sim 10^5 M_\odot$. If we further assume that we are dealing with a top-heavy Pop III burst, the stellar radiation will be characterized by $T_{\text{eff}} \sim 10^5$ K, corresponding to a peak frequency of $\nu_{\text{max}} \sim 10^{16}$ Hz, and a total luminosity close to the Eddington-luminosity (see Section 4), $L \sim L_{\text{Edd}} \sim 10^{43}$ erg s $^{-1}$. The emitted specific luminosity is thus $L_{\nu, \text{em}} \sim L_{\text{Edd}}/\nu_{\text{max}} \sim 10^{27}$ erg s $^{-1}$ Hz $^{-1}$. The observed (specific) flux for a first galaxy at $z \sim 10$ is then

$$f_{\nu, \text{obs}} \sim 10^{-32} \text{ erg s}^{-1} \text{ cm}^{-2} \text{ Hz}^{-1} = 1 \text{ nJy} . \quad (47)$$

The nJy is indeed the typical brightness level that the *JWST* is designed to image with NIRCam, thus reiterating the point that with this next-generation facility, we will get the first galaxies within reach of deep-field exposures.

7. Outlook

The next decade will be very exciting as we are opening up multiple windows into the cosmic dark ages. We will finally be able to close the remaining gap in the long quest to reconstruct the entire history of the Universe, which began with the pioneers of cosmology in the 1920s. There will be many opportunities to make important discoveries, e.g., in directly detecting the first sources of light, and in working out a well-tested theoretical framework for star and galaxy formation at the dawn of time. Very likely, serendipity will play a crucial role. It is thus a good idea to equip oneself with a comprehensive set of tools, such as the basic physics covered in these lecture notes. After all, there is wisdom to the old adage that “fortune favors the prepared mind”.

Acknowledgments. I would like to thank the organizers for their warm hospitality, and for putting together a stimulating program. VB acknowledges support from NSF grant AST-1009928 and NASA ATFP grant NNX09AJ33G.

References

- Appenzeller, I. 2009, *High-Redshift Galaxies* (Berlin: Springer)
- Barkana, R., Loeb, A. 2001, *Physics Reports*, 349, 125
- Beers, T. C., Christlieb, N. 2005, *ARA&A*, 43, 531
- Bloom, J. S. 2011, *What are Gamma-ray Bursts?* (Princeton: Princeton Univ. Press)
- Bodenheimer, P. H. 2011, *Principles of Star Formation* (Berlin: Springer)
- Bromm, V., Kudritzki, R. P., Loeb, A. 2001, *ApJ*, 552, 464
- Bromm, V., Larson, R. B. 2004, *ARA&A*, 42, 79
- Bromm, V., Yoshida, N., Hernquist, L., et al. 2009, *Nature*, 459, 49
- Bromm, V., Yoshida, N. 2011, *ARA&A*, 49, 373
- Ciardi, B., Ferrara, A. 2005, *Space Science Reviews*, 116, 625
- Clark, P. C., Glover, S. C. O., Smith, R. J., et al. 2011, *Science*, 331, 1040
- Frebel, A., Johnson, J. L., Bromm, V. 2007, *MNRAS*, 380, L40
- Frebel, A. 2010, *Astronomische Nachrichten*, 331, 474
- Freeman, K., Bland-Hawthorn, J. 2002, *ARA&A*, 40, 487
- Furlanetto, S. R., Oh, S. P., Briggs, F. H. 2006, *Physics Reports*, 433, 181
- Gardner, J. P., Mather, J. C., Clampin, M., et al. 2006, *Space Science Reviews*, 123, 485
- Glover, S. C. O. 2005, *Space Science Reviews*, 117, 445
- Greif, T. H., Springel, V., White, S. D. M., et al. 2011, *ApJ*, 737, 75
- Hosokawa, T., Omukai, K., Yoshida, N., et al. 2011, *Science*, 334, 1250
- Karlsson, T., Bromm, V., Bland-Hawthorn, J. 2012, *Rev. Mod. Phys.*, submitted (arXiv:1101.4024)
- Komatsu, E., Smith, K. M., Dunkley, J., et al. 2011, *ApJS*, 192, 18
- Kouveliotou, C., Woosley, S. E., Wijers, R. A. M. J. (eds.) 2012, *Gamma-ray Bursts* (Cambridge: Cambridge Univ. Press)

- Kritsuk, A. G., Norman, M. L., Wagner, R. 2011, *ApJ*, 727, L20
- Loeb, A. 2010, *How did the First Stars and Galaxies Form?* (Princeton: Princeton Univ. Press)
- Mac Low, M. M., Klessen, R. S. 2004, *Rev. Mod. Phys.*, 76, 125
- McKee, C. F., Ostriker, E. C. 2007, *ARA&A*, 45, 565
- Mo, H., Van den Bosch, F., White, S. D. M. 2010, *Galaxy Formation and Evolution* (Cambridge: Cambridge Univ. Press)
- Oh, S. P., Haiman, Z. 2002, *ApJ*, 569, 558
- Salvadori, S., Ferrara, A. 2009, *MNRAS*, 395, L6
- Shakura, N. I., Sunyaev, R. A. 1973, *A&A*, 24, 337
- Stacy, A., Greif, T. H., Bromm, V. 2010, *MNRAS*, 403, 45
- Stacy, A., Greif, T. H., Bromm, V. 2012, *MNRAS*, in press (arXiv:1109.3147)
- Stiavelli, M. 2009, *From First Light to Reionization: The End of the Dark Ages* (Weinheim: Wiley-VCH)
- Turk, M. J., Abel, T., O'Shea, B. 2009, *Science*, 325, 601
- Whalen, D. J., Bromm, V., Yoshida, N. (eds.) 2010, *The First Stars and Galaxies: Challenges for the Next Decade* (AIP Conference Series, vol. 1294)
- Zinnecker, H., Yorke, H. W. 2007, *ARA&A*, 45, 481

Galaxy evolution throughout the cosmic epochs: an observational perspective

R. Maiolino^{1,2}

¹*Cavendish Laboratory, University of Cambridge, Cambridge, UK*

²*Kavli Institute for Cosmology, Cambridge, UK*

Abstract. During the past few years our understanding of galaxy evolution throughout the cosmic epochs has greatly improved thanks to several major observational results. In these lecture notes I shortly review some of the main findings in this field, by emphasizing the most recent results obtained through observational studies of high redshift galaxies. I will also discuss the open problems and the facilities that may enable us to tackle them.

1. Introduction

One of the main challenges of modern astrophysics is to understand the mechanisms responsible for the formation of galaxies and for their properties, as we see them today. Why some local galaxies have old stellar populations and little gas content, while others host ongoing star formation and are gas rich? What is the origin of the spheroidal components of galaxies and of their disks? What is the role of impulsive starbursts, possibly triggered by merging events, and what the role of smooth secular star formation, during the evolution of galaxies? What is the connection, if any, between the evolution of the central supermassive black holes and the evolution of their host galaxies? These and other fundamental questions on galaxy evolution have been recently tackled by extensive multi-wavelength observations of high redshift galaxies. In the limited space available for these lecture notes, it is not possible to review all of the several observational studies that have contributed to our understanding of galaxy evolution. With the exception of for a few introductory remarks, I will mostly focus on some of the recent and most significant results in the field. I will concentrate on the formation and evolution of galaxies at intermediate redshifts, while the formation of the first galaxies, close to the re-ionization epoch, is discussed in the parallel lecture notes by V. Bromm. I will eventually also mention some of the main outstanding questions that still remain open and the facilities that may enable us to address them.

2. The evolution of star formation in galaxies

In this and the next section I review some of the main observational strategies to identify galaxies across the cosmic epochs. I will also review the observational diagnostics that enable astronomers to measure the star formation rate (SFR) and stellar content in galaxies, and the main results within this context.

Most observational diagnostics of star formation are associated with the UV light emitted (and partly reprocessed by the interstellar medium, ISM) by young, massive short-lived stars. During the past twenty years, some of the most extensive surveys of star forming galaxies at high redshift have exploited the UV rest-frame emission to detect high-redshift galaxies and to measure their star formation rate. If the galaxy hosts active star formation and is not obscured by dust, then the emission from OB stars, which rises steeply in the UV, generally dominates the observed integrated stellar light at optical-UV wavelengths. However, at high redshift the Ly α Forest, due to intervening neutral intergalactic medium along the line of sight, heavily suppresses the observed flux at wavelengths shorter than Ly α . The resulting spectral cutoff, and the associated photometric “dropout” in the observed blue-UV bands, has been widely used to identify high redshift galaxies (e.g. Steidel et al. 1996, 2003, 2004). The photometric band at which the “dropout” occurs gives a first indication of the redshift of the sources.

An extension of the “dropout” technique is the “photometric redshift” method. Within this method the galaxy photometric fluxes in multiple bands are fitted with several galaxy templates by leaving the redshift of the source as a free parameter to fit (e.g. Bolzonella et al. 2000). This technique is extremely useful to constrain the redshift of faint galaxies for which spectroscopy cannot be obtained, or to simply select candidates for subsequent spectroscopic followup. The more photometric bands are available, the more accurate is the photometric redshift. This technique can be very accurate if the galaxy continuum is characterized by sharp spectral features (such as the Ly α dropout or the “4000Å break”).

Nebular emission lines (e.g. Ly α , H β , H α , [OII]3727, [OIII]5007) are obviously another important tool to identify star forming galaxies at high redshift and to measure their SFR. In star forming galaxies these lines are primarily produced in HII regions, photo-ionized by young hot stars, and emitted either by recombination or collisional excitation. Needless to say that the identification of emission lines in the spectra of high redshift galaxies provides an accurate (and, generally, unambiguous) determination of their redshift. However, spectroscopic observations are generally much more demanding than imaging, both in terms of telescope observing time and in terms of complexity of the observations and instrumentation. Most optical/near-IR telescopes are nowadays equipped with “Multi-Object Spectrographs” (MOS), which can obtain spectra of a few tens up to thousands of galaxies simultaneously.

The flux of some strong emission lines can also be used as a tool to identify high redshift galaxies in imaging surveys by exploiting narrow band filters. In particular, the flux of some lines, such as Ly α and H α , is often so strong that they can strongly boost the observed flux of a galaxy within a narrow photometric band (typically $\lambda/\Delta\lambda = 50 - 100$), provided that the galaxy is at the appropriate redshift for the line to be shifted into the filter band. Narrow band surveys have been widely exploited to identify distant galaxies (e.g. Taniguchi et al. 2005; Sobral et al. 2012), and several of the most distant objects known have been identified through this technique. However, the possibility of low redshift “interlopers” always require spectroscopic confirmation of the redshift.

Optical and UV tracers of star formation are subject to dust extinction and in many high redshift dusty galaxies the tracers discussed above are often undetected or very weak, despite the fact that these galaxies may host vigorous star formation. In these dusty systems the bulk of the radiation emitted by (young) stars is absorbed by dust and re-emitted in the thermal infrared. The Herschel Space Observatory, by observing in the $70\mu\text{m}$ to $500\mu\text{m}$ wavelength range, has recently delivered huge samples of distant galaxies by detecting their far-IR radiation (e.g. Clements et al. 2010; Nordon et al. 2010; Oliver et al. 2010). In these galaxies, the far-IR luminosity provides a good (reddening free) determination of the star formation rate.

Well before the launch of Herschel, ground based submillimeter and millimeter imaging cameras had already revealed large samples of high redshift galaxies (Hughes et al. 1998; Blain et al. 1999; Smail et al. 2002; Bertoldi et al. 2007). The interesting feature of the mm/submm bands is that they probe the Rayleigh-Jeans tail of the far-IR thermal bump of galaxies and, therefore, they are characterized by a strong *negative* k-correction. The nice implication of the latter effect is that distant galaxies (out to $z \sim 8 - 10$) are as easy to detect as low- z galaxies ($z \sim 1$), i.e. for galaxies with a given SFR the observed flux remains nearly constant in the redshift range $1 < z < 10$ (e.g. Maiolino et al. 2008). This is one of the reasons why large mm/submm groundbased facilities have been and are being developed.

In the mid-IR spectral region the dust thermal emission is much more sensitive to the dust temperature and to radiative transfer effects. However, the mid-IR wavelength range hosts the emission of strong spectral features emitted from very small carbonaceous grains, the so-called Polycyclic Aromatic Hydrocarbon (PAH) particles. These are broad features, primarily in the $6-11\mu\text{m}$ spectral range, emitted as a consequence of PAH excitation by the soft-UV photons produced in star forming regions. The Spitzer Space Observatory has exploited these features heavily to detect and identify distant star forming galaxies, as well as to estimate their star formation rate (Legache et al. 2004; Yan et al. 2005; Reddy et al. 2006; Smith et al. 2007).

All of the observable quantities discussed above are effectively proportional to the number of OB stars alive, either directly (UV continuum) or through reprocessing of their radiation by the ISM (emission lines, far-IR radiation, PAH features). Since OB stars are short lived, these observational quantities are regarded as good indicators of the current SFR in galaxies. Equations relating the luminosity of each of these tracers with the SFR have been reported in the literature (e.g. Kennicutt 1998).

The radio emission in star forming galaxies is not directly associated with the light emitted by OB stars. It is however found to correlate with other tracers of star formation (de Jong et al. 1985; Helou et al. 1985; Condon et al. 1991; Yun et al. 2001). The radio emission is primarily of synchrotron origin and it is believed to originate from the interaction of cosmic rays produced by SN explosions with the galactic magnetic field. Since the SN rate is proportional to the SFR, this would explain (if averaged on timescales longer than 10^7 yr and on scales larger than about $10 - 100$ pc) the radio-SFR correlation. The sensitivity of radio telescopes arrays, such as the VLA (and its upgrade, ELVA-JVLA) have

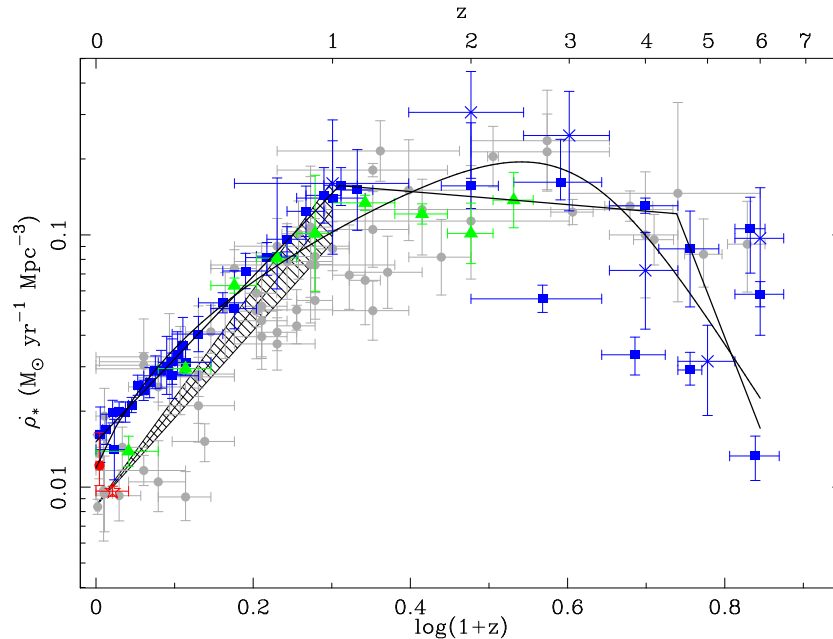


Figure 1. Redshift evolution of the cosmic star formation density as inferred from different galaxy surveys, by using SFR tracers at different wavelengths. From Hopkins & Beaumont (2006). See the original paper for a detailed description of the symbols.

allowed astronomers to detect star forming galaxies out to $z \sim 2 - 3$ (e.g. Karim et al. 2011).

Measuring these quantities in various samples of galaxies at different redshifts has been one of the major efforts of many observational campaigns, with the goal of determining the evolution of the cosmic (average) star formation rate as a function of redshift. Each of these tracers has advantages and caveats. Fig. 1 summarizes the evolution of the cosmic density of star formation rate (SFRD) as inferred by surveys exploiting different star formation tracers. Although there is a large dispersion, the various star formation tracers (once corrected for dust extinction, when needed) show a general broad agreement, at least for what concerns the shape of the SFRD evolution. The SFRD shows a steep evolution up to $z \sim 1$, by increasing, relative to the local value, by about an order of magnitude. After reaching a maximum around $z \sim 1 - 3$ the SFRD declines at higher redshift, but the trend at $z > 5$ is still highly uncertain. Understanding why the SFRD has this trend, and which mechanisms are responsible for such evolution, are some of the main goals of ongoing observing programs, as discussed in the next sections.

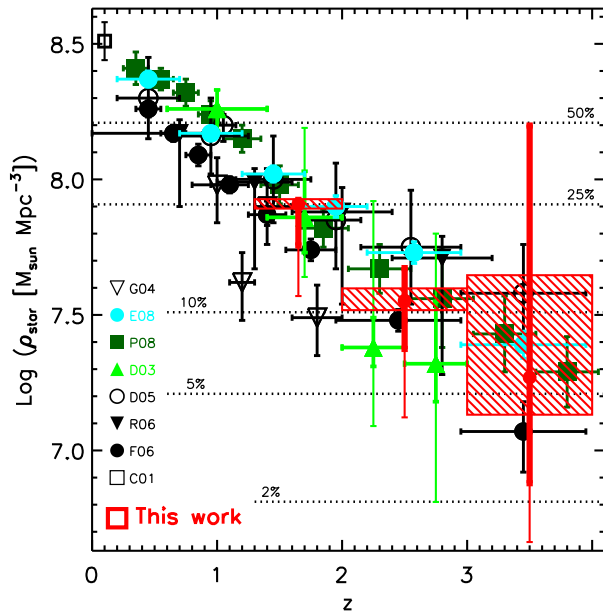


Figure 2. Redshift evolution of the cosmic density of stellar mass as inferred from different surveys. The horizontal dotted lines indicate different fractions of the cosmic density of stellar mass relative to the local universe. Note that 50% of the total stellar mass has been formed since $z \sim 1$, while the bulk of the stellar mass ($> 90\%$) has been assembled since $z \sim 3$. From Marchesini et al. (2009).

3. The evolution of stellar content in galaxies

An alternative approach to investigate the evolution of star formation in galaxies has been the investigation of the stellar content in galaxies as a function of redshift. The availability of deep near-IR observations (and in particular through Spitzer and the WFC3 camera on HST) has enabled astronomers to robustly measure the stellar mass in large samples of distant galaxies (indeed the near-IR rest frame light in galaxies is a good tracer of the stellar mass, less sensitive to the star formation history and to extinction). Fig. 2 shows the density of stellar mass formed as a function of redshift, as inferred from various surveys (Marchesini et al. 2009; see also Le Borgne et al. 2009). Although the uncertainties are large, the evolution of the stellar mass is consistent with the integrated cosmic star formation rate by that epoch. Fig. 2 illustrates that about 50% of the current stellar mass has been formed since $z \sim 1$, while the bulk of the stellar mass ($> 90\%$) has been formed since $z \sim 3$.

However, within this context, the most interesting results have emerged by looking more in detail at the evolution of the stellar content in galaxies and, more specifically, the redshift evolution of the stellar mass function. As illustrated in Fig. 3 (Perez-Gonzalez et al. 2008) the most massive galaxies were already in place by $z \sim 2 - 3$, and the stellar mass function at high masses has not changed

significantly since then. Instead, the bulk of low mass galaxies formed mostly at low redshift (see also Le Flocc’h et al. 2005). This result also reflects the observed evolution of the star formation rate in galaxies, once they are differentiated by stellar mass: massive galaxies had the bulk of their star formation at early epochs (high- z) and evolve passively afterwards, while low mass galaxies formed more slowly across a prolonged interval of time (Juneau et al. 2005). This anti-hierarchical growth, apparently inverted relative to the hierarchical growth of dark matter haloes, is known as “galaxy downsizing”. Understanding the physical origin of such galaxy downsizing has been subject of several theoretical works. Some insights on the mechanisms that may be at the origin of galaxy downsizing will also be discussed in the following sections.

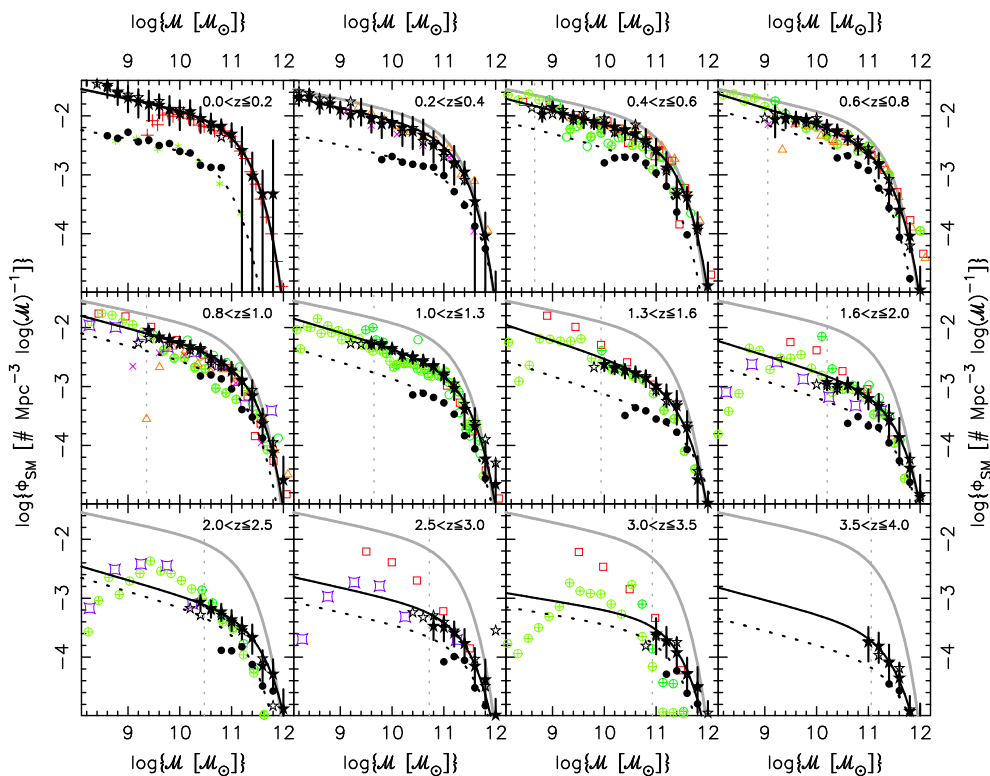


Figure 3. Redshift evolution of stellar mass function of galaxies. Note that the most massive galaxies were already in place by redshift $z \sim 2$, while the assembly of low mass galaxies has evolved more slowly to $z = 0$. From Perez-Gonzalez et al. (2008).

Massive galaxies were not only already in place by $z \sim 2$, but they appear to be already characterized, at such early epoch, by old (ages of 1 – 2 Gyr) and passively evolving stellar populations. This was confirmed through both the photometric and spectroscopic properties of such galaxies (Cimatti et al. 2004; McCarthy et al. 2004; Glazebrook et al. 2004; Saracco et al. 2005). However, they are not completely alike local massive galaxies in terms of structural

properties, indeed they appear to be much more compact than local ellipticals (e.g. Cimatti et al. 2008). Understanding how these galaxies manage to increase significantly their sizes, without undergoing significant star formation, is one of the main current challenges of our understanding of the formation of massive galaxies. Dry merging of galaxies (i.e. merging of galaxies with little or no gas content) is one of the possibilities that have been proposed.

4. The different modes of galaxy formation at high redshift

Theoretical models envisage two main modes of galaxy formation, a “starburst” mode and a “secular” mode. In the starburst mode, the bulk of star formation occurs violently on very short timescales (less than 10^8 yr). In this scenario, the star formation efficiency is enhanced by tidal forces and dynamical frictions (driving gas towards galaxy centers) during galaxy mergers (e.g. Mihos & Hernquist 1996; Cole et al. 2000, Steinmetz & Navarro 2002). The other mode of galaxy formation consists of a secular (“quiescent”) evolution, where star formation occurs smoothly on long time scales (longer than a few 10^8 yr) and it is associated with instabilities of the gaseous disk. In the latter scenario star formation simply follows the Schmidt-Kennicutt relation (where the star formation surface density is proportional to the 1.5 power of the gas surface density) and it is maintained by infall of gas from the intergalactic medium, likely through cool flows predicted to be particularly intense at high redshift (e.g. Ocvirk et al. 2008; Dekel et al. 2009). Which of the two modes dominates at high redshift and, in particular, around the peak of cosmic star formation ($z \sim 1 - 3$)?

Observations of distant galaxies, especially those exploiting HST imaging, have revealed that the fraction of merging galaxies increases rapidly at high redshift, especially among massive galaxies (Conselice et al. 2011). In these merging systems the star formation efficiency (i.e., stars formed per unit gas mass) is increased strongly. Indeed, high angular resolution observations of submillimeter detected galaxies (SMGs) at high redshifts, which are among the strongest starbursting systems at high redshift (with star formation rates around $1000 M_{\odot} \text{ yr}^{-1}$), are found to be hosted in merging or strongly interacting systems (Fig. 4, Engel et al. 2010). However, SMGs are relatively rare systems.

High- z galaxies with lower star formation rates ($10 - 100 M_{\odot} \text{ yr}^{-1}$), representative of the bulk of the star forming population at $z \sim 1 - 3$, are instead characterized by regular kinematical patterns, typical of massive rotating disks, as inferred both from near-IR integral field spectroscopy, mapping kinematics through the redshifted optical nebular lines (Fig. 5; Forster-Schreiber et al. 2006; Genzel et al. 2006; Cresci et al. 2010; Gnerucci et al. 2011) and millimeter observations (mapping galaxy dynamics through the CO rotational transitions, Tacconi et al. 2010). No signatures of ongoing merging are found in these systems. The large fraction of massive rotating disks already in place at such early epochs was unexpected and difficult to reconcile with the hierarchical galaxy formation scenarios. The main difference between such high redshift disks and their local counterparts is the large velocity dispersion and clumpiness of the former. Such properties suggest that these high- z disks are likely dynamically unstable, which is likely the reason of their enhanced star formation. The dynamical instability is probably a consequence of their the large gas content. Indeed, as

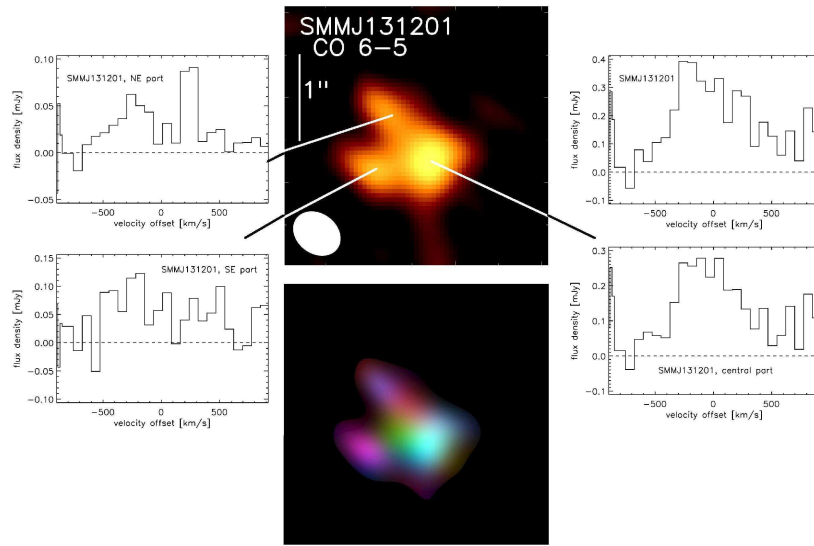


Figure 4. CO(6-5) map of the SMG galaxy SMM J131201, showing a clear irregular morphology. The RGB-image (bottom, mapping red, green and blue parts of the spectrum) does not show any indication of rotation. This and similar other results support the idea that strongly starbursting SMGs at high- z are hosted in merging/interacting systems. From Engel et al. (2010).

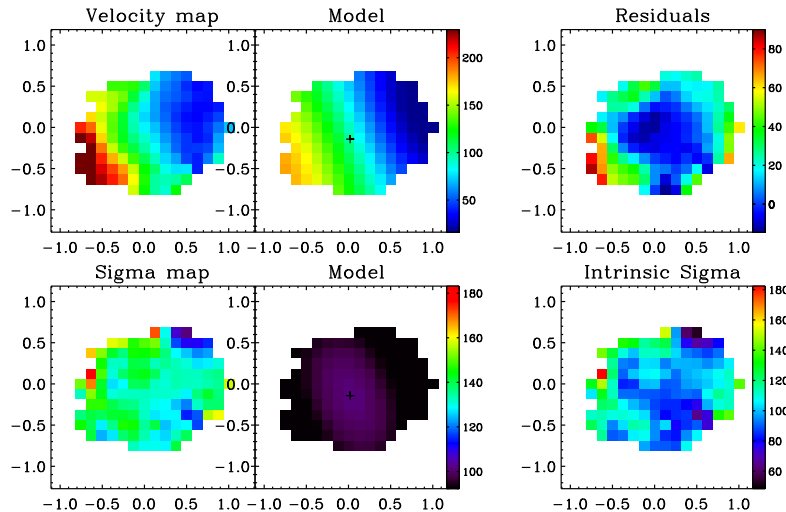


Figure 5. Velocity map (top left) and associated velocity dispersion (bottom left) of a star forming galaxy at $z \sim 3$ with a SFR of a few times $100 M_{\odot} \text{ yr}^{-1}$. The velocity field is well fitted with a regular rotating disk, although characterized by high turbulence. From Gnerucci et al. (2011).

discussed further in the next section, these high redshift systems are characterized by large masses of molecular gas. The high gas fraction is expected to make the disk gravitationally unstable (which is thought to be the mechanism behind the Schmidt-Kennicutt relation), favoring the collapse of molecular clouds and resulting into enhanced star formation. Both dynamical friction and gas loss through outflows (Genzel et al. 2011) can subsequently drive the newly formed super star clusters towards the central region to form a massive bulge.

The relative fraction of merging (starbursting) systems and secularly evolving (“quiescent”) star forming galaxies has been investigated more extensively through the distribution of high- z galaxies on the so-called “main sequence”. The latter is a tight relationship between SFR and stellar mass, which is found to characterize the bulk of (quiescent) local galaxies (e.g. Peng et al. 2010). The finding that local star forming galaxies obey this tight relation is an indication that smooth, secular processes are responsible for their star formation activity. The unexpected result has been that even high- z galaxies are also distributed along a “main sequence”, although offset with respect to the local one towards higher star formation rates (due to the larger gas content, e.g. Daddi et al. 2010a, Genzel et al. 2010). This confirms that smooth, secular evolving processes were at work also at high redshift. However, outliers from the main sequence (starbursts) are also present in the high redshift samples. Establishing the relative fraction of galaxies on the main sequence and starbursts (significantly above the main sequence) has not been simple, both because of the limited statistics and because of the observational biases affecting many of the past studies. The Herschel Space Observatory has recently delivered large samples of high redshift

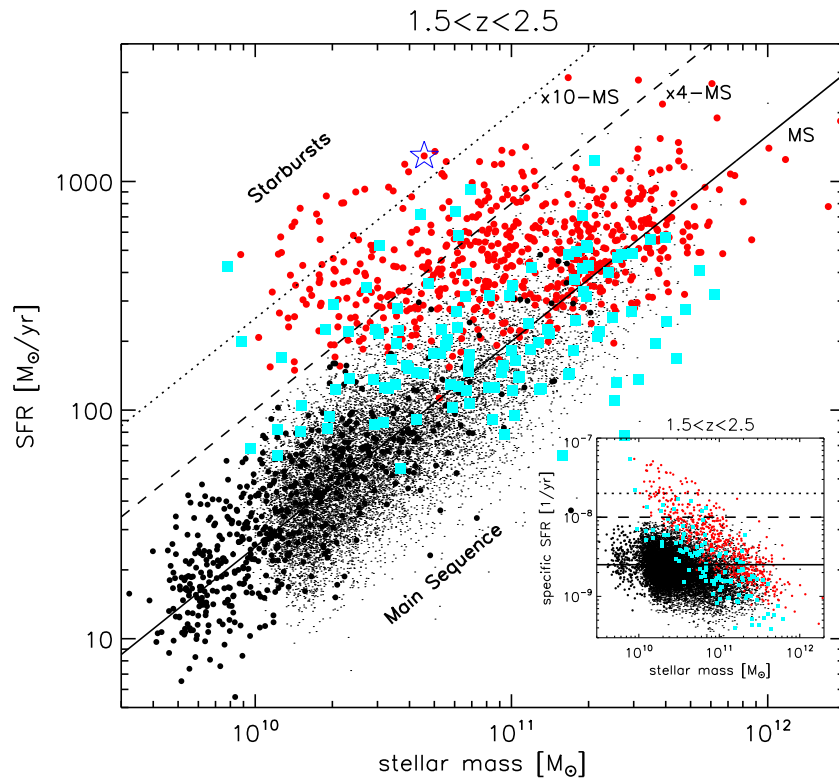


Figure 6. Stellar mass-star formation rate relation at $1.5 < z < 2.5$ as inferred from the “shallow” and “deep” Herschel far-IR data (red and cyan symbols) and from near-IR selected (BzK) sources (black symbols). The bulk of the galaxies are distributed along the “main sequence”, with only of a minority of sources (“starbursts”) distributed at significantly higher SFRs. From Rodighiero et al. (2011).

galaxies whose SFR is measured through the far-IR emission, avoiding biases and uncertainties associated with dust extinction. An analysis of the distribution of Herschel sources at $z \sim 2$ on the SFR– M_{star} diagram (Fig. 6), has revealed that the role of starbursts is minor: mergers contribute to less than 10% of the global SFR at $z \sim 2$ (Rodighiero et al. 2011). A similar conclusion has been reached through an analysis of the spectral energy distribution of high- z Herschel galaxies (Elbaz et al. 2011).

5. The molecular gas content of high redshift galaxies

The content of molecular gas in galaxies cannot be probed by directly exploiting H_2 transitions. Indeed, since H_2 does not have an electric dipole (because it is a symmetric molecule) it can only undergo quadrupole transitions (i.e. $\Delta J = \pm 2$). This, along with its small momentum of inertia, makes H_2 transitions possible

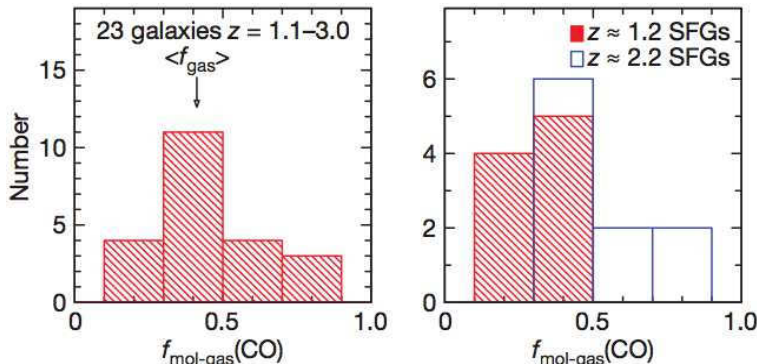


Figure 7. Distribution of molecular gas fraction of star forming galaxies at $1 < z < 3$ as inferred from CO measurements at mm wavelengths (one should note that, for comparison, the typical molecular gas fraction of local star forming galaxies is about 5%). From Tacconi et al. (2010).

only between levels with high ΔE , emitted only by warm ($T > 300$ K) molecular regions, which account only for a minor fraction of the total molecular gas.

To probe the bulk of the molecular gas, which is at lower temperatures, one has to rely on transitions from other species. Carbon monoxide, CO, is the second most abundant molecule and its lowest rotational transitions, in the millimeter bands (e.g. $\nu_{\text{CO}(1-0)} = 115$ GHz, $\nu_{\text{CO}(2-1)} = 230$ GHz and $\nu_{\text{CO}(3-2)} = 345$ GHz), are excellent tracers of the cold phase of the molecular gas. These are generally the strongest molecular transitions in galaxies.

Early measurements of CO transitions at high redshift had focussed on exceptionally luminous systems (QSOs and SMGs), with star formation rates of about $1000 M_{\odot} \text{ yr}^{-1}$ (see Solomon & Vanden Bout 2005, for a review). However, the improved sensitivity of the millimeter interferometers (and in particular the IRAM Plateau de Bure Interferometer) has recently enabled astronomers to detect CO transitions in high- z galaxies with moderate star formation rates ($\sim 100 M_{\odot} \text{ yr}^{-1}$) more typical of the star forming population at $z \sim 1 - 2$. The main result of these studies is that the mean gas fraction, $f_{\text{gas}} = M_{\text{gas}} / (M_{\text{star}} + M_{\text{gas}})$, in high- z star forming galaxies is about 50%, i.e. about an order of magnitude higher than observed in local galaxies (Daddi et al. 2010b; Tacconi et al. 2010).

The additional interesting result is that these high- z star forming galaxies obey nearly the same star formation law (i.e. relationship between SFR surface density and molecular gas surface density, the Schmidt-Kennicutt law) as local galaxies, especially if one accounts for the different dynamical times of the different systems (Fig. 8, Daddi et al. 2010a; Genzel et al. 2011; Krumholz et al. 2012). As mentioned above, the spatially resolved kinematical information inferred from the same CO maps, has revealed that the bulk of these systems are rotating disks, although fairly turbulent. So the mechanism responsible for the star formation in these galaxies is the same as local disk galaxies, and their

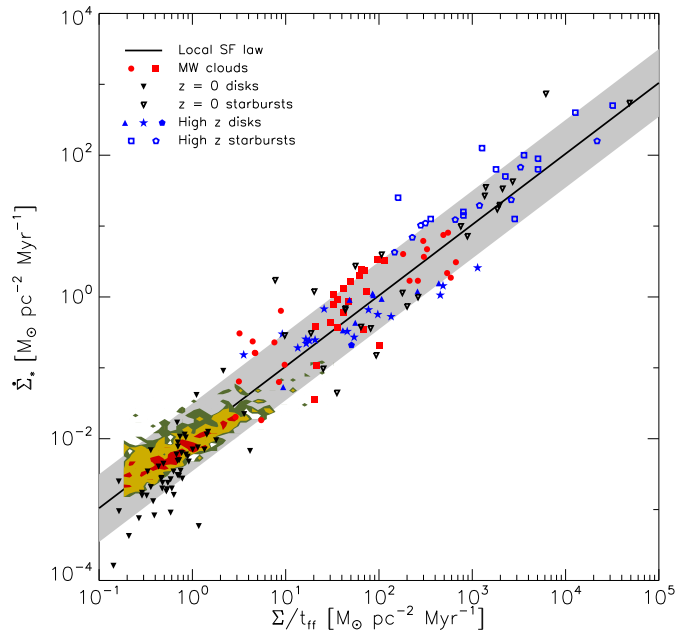


Figure 8. Schmidt-Kennicutt law for local and distant galaxies. From Krumholz et al. (2012).

enhanced star formation rate relative to local galaxies is simply a consequence of their larger molecular gas content.

The emerging picture is therefore that the evolution of galaxies is actually primarily driven by the evolution of their molecular gas content (Obreschcow & Rawlings 2009; Lagos et al. 2011), which is higher at high redshift as a consequence of the massive inflow of gas from the intergalactic medium (e.g. Ocvirk et al. 2008; Dekel et al. 2009). Within this new scenario, the evolution of the star formation rate in galaxies is only a consequence, through the Schmidt-Kennicutt relation, of the (more fundamental) evolution of the molecular gas content. Variations of the star formation efficiency, introduced by merging events, play only a secondary role in shaping the evolution of the star formation rate of galaxies at high redshift.

6. Feedback

So far we have discussed how star forms throughout the cosmic epochs. However, it is even more important to understand why stars do not form. Indeed, across the entire life of the Universe, only about 4% of baryons in the local Universe have been converted into stars (Fukugita & Peebles 2004), while the expectation from gravitational collapse and gas cooling would be that over 80% of the baryons should have formed gas. Therefore, some form of negative feedback is required by most models of galaxy evolution to keep the efficiency of star formation low.

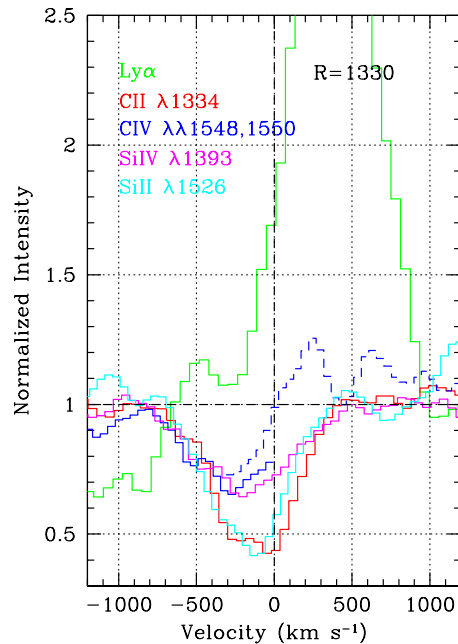


Figure 9. Velocity profile of various UV transitions obtained by stacking the spectra of several star forming galaxies at $2 < z < 3$. The blueshifted absorption features characterizing most transitions reveal prominent outflows characterizing these galaxies, with outflow velocities of several hundreds km/s. From Steidel et al. (2010).

Strong negative feedback effects are in particular required to explain the stellar mass function of local galaxies. Indeed, in absence of feedback, the stellar mass function should follow (scaled down) the dark matter halos mass function. Instead, the stellar mass function of galaxies falls short relative to theoretical prediction both at low and at high stellar masses, even by orders of magnitude.

A related issue concerns the properties of massive elliptical galaxies in the local universe, which are characterized by old stellar populations and with little gas content, while in absence of feedback models would expect them to be associated with young stellar populations and rich of gas.

The main scenario invoked to explain the low star formation efficiency in low mass galaxies assumes that negative feedback associated with supernova explosions self-regulate star formation in galaxies. Supernovae, whose rate is proportional to the star formation rate, can heat the ISM and blow large quantities of gas out of the galactic plane, hence removing gas, which is no longer available for star formation. Large outflows, driven by supernova winds have been detected in several star forming galaxies, both by mapping the kinematics of emission lines, as well as through blueshifted absorption systems (see Veilleux et al. 2005, for a review). Even stronger outflows have been detected in distant star forming galaxies, with velocities approaching several hundreds km/s and

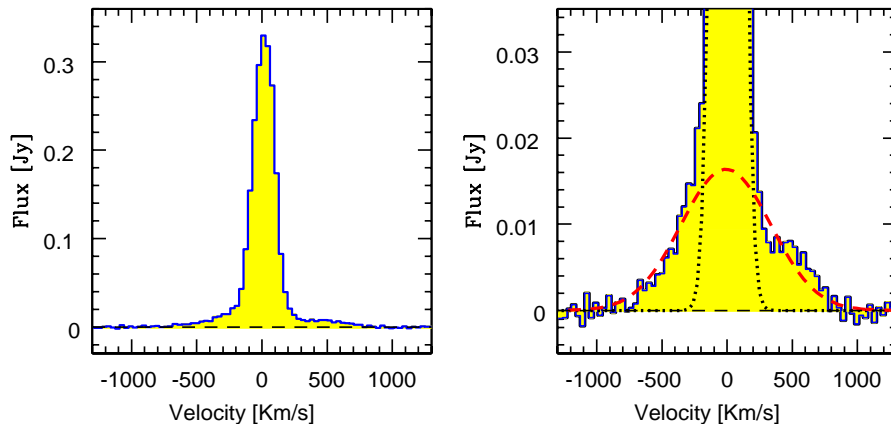


Figure 10. CO(1-0) spectrum of the closest quasar known, Mrk231, revealing broad wings extending to velocities of several hundred km/s associated with a massive molecular winds driven by the quasar radiation pressure. From Feruglio et al. (2010).

outflow rates as high as the star formation rate producing them (Fig. 9, Steidel et al. 2010; Erb et al. 2012). It should be mentioned that some studies have also highlighted the importance of radiation pressure to drive such powerful outflows (Thompson et al. 2005; Hopkins et al. 2012). Moreover, an additional source of feedback in star forming galaxies may be the heating of the ISM due to the UV radiation field generated by young hot stars (Governato et al. 2007).

However, according to models, the strength of the negative feedback associated with stellar activity is capable of reducing significantly the star formation efficiency only in low mass galaxies. In high mass galaxies an additional, stronger feedback mechanism is required to quench star formation and prevent massive galaxies to overgrow. Most theoretical models identify this additional mechanism in the negative feedback introduced by Active Galactic Nuclei associated with supermassive accreting black holes. According to various models and simulations, when the accreting black hole reaches quasar-like luminosities the released energy can blow away the bulk of the gas in the host galaxy, hence quenching star formation (e.g. Silk & Rees 1998; Fabian 1999; Granato et al. 2004; Di Matteo et al. 2005; King 2005; Lapi et al. 2005; Narayanan et al. 2008; see also Fabian 2012, for a review). The coupling between the quasar radiation pressure and the acceleration of the ISM in the host galaxy is still not fully understood and a matter of debate. After the gas has been expelled, the galaxy evolves passively, becoming a “red-and-dead” elliptical. Star formation quenching in high redshift massive galaxies, through AGN feedback, is thought to be one of the key mechanisms responsible for the “galaxy downsizing” (Croton et al. 2006; Menci et al. 2006).

Direct observational evidence of the AGN feedback at work has been first found in the closest quasar, Mrk231, through the detection of a massive molecular outflow, which is capable, at the observed rate ($\dot{M}_{\text{outflow}} \sim 700 M_{\odot} \text{ yr}^{-1}$), of cleaning the host galaxy of its gas content in only 10^7 yr (Fig. 10, Feruglio

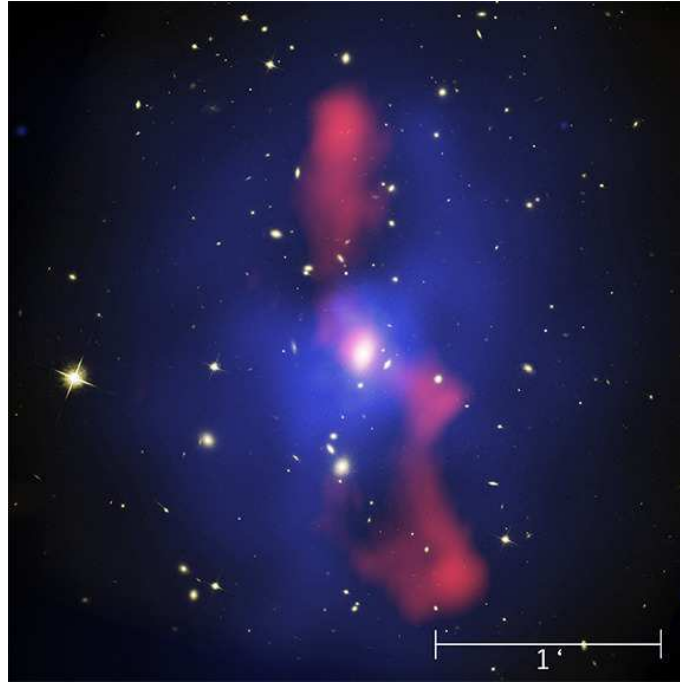


Figure 11. X-ray image (blue) of the central 700 kpc of the S0735.6+7421 cluster illustrating extended cavities in correspondence of the radio lobes (red) powered by the central radio galaxy. From McNamara et al. (2009).

et al. 2010; Fischer et al. 2010). The energetics of the outflow is in agreement with the model expectations for AGN driven outflows. In the past two years, the number of detections of AGN-driven outflows, capable of quenching star formation in massive galaxies, has increased very rapidly (Sturm et al. 2011; Rupke & Veilleux 2011; Aalto et al. 2012; Cicone et al. 2012). Most importantly, recent observations have reported the detection of such massive AGN outflows also at high redshift, where the bulk of the AGN feedback is expected to occur and which should be at the origin of the red-and-dead massive elliptical observed locally (Alexander et al. 2010; Nesvadba et al. 2010, 2011; Harrison et al. 2012a, ; Maiolino et al. 2012; Weiss et al. 2012). Very recently, there have been a few of claims for direct evidence of quasar activity quenching star formation in high- z host galaxies, either through detailed observations of individual quasars (e.g. Cano-Diaz et al. 2012) or through statistical analyses on the occurrence of star formation activity in quasar host galaxies (Farrah et al. 2012; Page et al. 2012). However, the latter claims have been recently questioned by more extensive analyses performed on larger samples (Harrison et al. 2012b).

Once the massive galaxy has been cleaned of its gaseous content (and therefore star formation has been quenched) this is not, in principle, enough to prevent further accretion from the large reservoir of hot gas in the halo, which would result in subsequent episodes of star formation. However, X-ray and radio ob-

servations have revealed that the kinetic energy injected through radio-jets into the halo prevents the hot gas to cool onto the central galaxy. This has been clearly revealed by the detection of large cavities, in the X-ray emitting halo surrounding radio galaxies, that anti-correlate with the radio-lobes fueled by the radio jets (Fig. 11; Fabian et al. 2006, 2012; McNamara et al. 2009; Blanton et al. 2011; Cavagnolo et al. 2011; Randall et al. 2011). This “maintenance” feedback mode has been dubbed “radio mode”.

This is a very hot field, developing very rapidly. Certainly, in the coming few years many more observational results will tackle the issue of feedback in galaxies more thoroughly, both through detailed observations of individual objects and through large sample of objects enabling proper statistical assessments.

7. The AGN-galaxy coevolution

The last part of the previous section smoothly introduces the last topic of these lecture notes, the connection between AGN and galaxy evolution. The local relationship between supermassive black holes and the properties of the host galaxy spheroid (primarily velocity dispersion and stellar mass, Marconi & Hunt 2003; Ferrarese & Ford 2005; Gültekin et al. 2009) suggests that the evolution of black holes and their host galaxies are intimately related. However, theoretical models have struggled in finding mechanisms capable of linking phenomena (star formation and black hole accretion) occurring on spatial scales that are different by orders of magnitude.

The AGN driven massive outflows discussed in the previous section are a clear example of how the accreting black hole can affect the star formation in its host galaxy. The AGN negative feedback, both quenches star formation and removes the gas out of which the AGN itself is being fed (effectively committing suicide!). The simultaneous suppression of star formation and black hole accretion is indeed required by models attempting to reproduce the $M_{\text{BH}} - \sigma$ relation. However, models require, in the first place, also mechanisms enabling both black hole accretion and star formation.

Until a few years ago, galaxy mergers were thought to be the main mechanism responsible for boosting both star formation and for driving gas towards the nucleus to feed a supermassive black hole. Local Ultraluminous Infrared Galaxies (ULIRGs) are a nice example of this process: these are generally violently merging systems, which often host both vigorous star formation and an accreting black hole, often with luminosities approaching the quasar regime (Veilleux et al. 1999, 2009; Armus et al. 2007; Nardini et al. 2008, 2009; Sani et al. 2008; Petric et al. 2010). Evidence for galaxy interactions and merging was also found for high- z quasars (Hutchings et al. 2002, 2009; Gallerani et al. 2012). Moreover, the finding of a correlation between SFR and AGN luminosity, both locally and at high redshift (Cid Fernandes et al. 2004; Maiolino et al. 2007; Netzer et al. 2008; Diamond-Stanic & Rieke 2012), has suggested a common, direct link between star formation and black hole accretion, which is most naturally explained in terms of galaxy interactions.

However, more recently, high resolution HST images of intermediate/high luminosity AGNs at high redshift have revealed that most of them are *not* hosted in merging/interacting systems (Fig. 12; Cisternas et al. 2010; Mainieri et al.

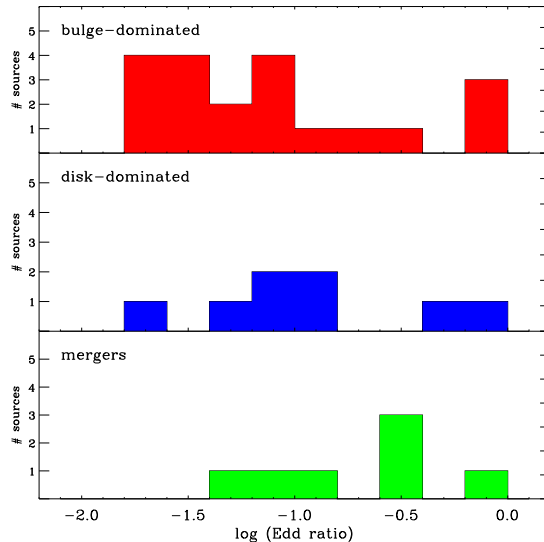


Figure 12. Morphological distribution of the host galaxies of high redshift ($1 < z < 2.5$), X-ray selected obscured AGNs. Note that the majority of these AGNs are not hosted in merging/interacting systems. From Mainieri et al. (2011).

2011; Kocevski et al. 2012). Moreover, the host galaxies of high redshift AGNs seem to follow the same “main sequence” as non-AGN star forming galaxies at the same redshift (Minieri et al. 2011; Mullaney et al. 2012; Santini et al. 2012). This finding have yielded to a revision of the standard scenario where the co-evolution of galaxies and AGNs is driven by galaxy mergers. The emerging scenario is that the bulk of the AGN-galaxy co-evolution occurs through secular processes. Models have indeed been proposed where also the Black Hole accretion is fuelled secularly through disk instabilities (Bournaud et al. 2011). The co-evolution does not even need to be necessarily co-coeval (Davies et al. 2007), indeed Shao et al. (2010) and Rosario et al. (2012) found that at intermediate-low AGN luminosities there is no correlation between star formation rate and AGN luminosity.

However, evidence is found that a correlation between SFR and AGN luminosity is actually found at very high luminosities (Lutz et al. 2007, 2008; Hatziminaoglou et al. 2010; Shao et al. 2010; Rosario et al. 2012) and that host galaxies of very luminous AGNs do deviate from the main sequence by having higher star formation rate (Fig. 13; Santini et al. 2011). These results indicate that at least for luminous AGNs, galaxy mergers and interactions do play a role. Yet, these luminous AGNs represent a minor fraction of the whole AGN population.

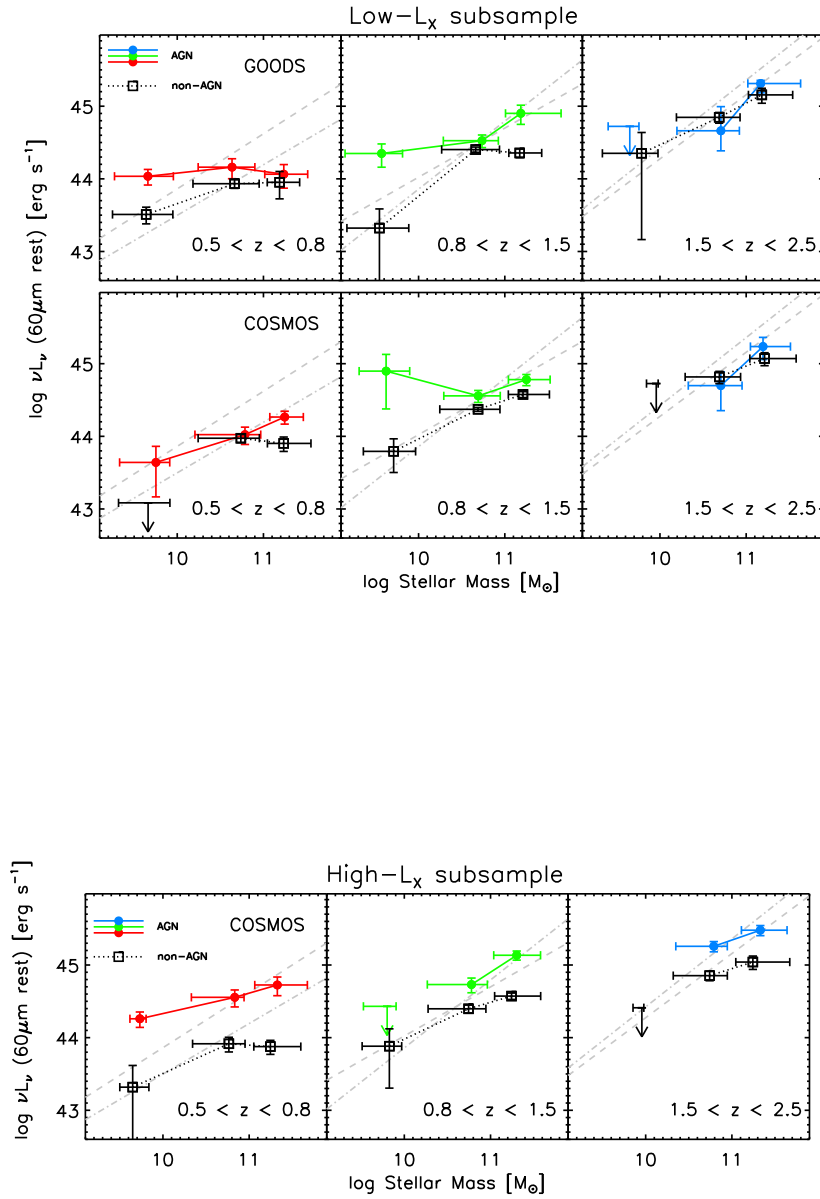


Figure 13. Far-Infrared luminosity (\sim SFR) versus stellar mass relationship for stacked high- z AGN host galaxies (colored symbols) relative to inactive galaxies (black symbols) and relative to the “main sequence” at the same redshift, for low luminosity AGNs (top) and for high luminosity AGNs (bottom). Note that high luminosity AGNs tend to systematically have an excess of star formation relative to inactive galaxies. From Santini et al. (2012).

8. Open issues and future prospects

Although our understanding of galaxy evolution has increased enormously in the past few years thanks to extensive observing programs, some of which have been summarized in these lecture notes, the new observational results have also opened new outstanding questions and new challenging fields of investigation.

The evolution of passive galaxies, from their very compact morphologies, to the extended sizes of local ellipticals, is still a puzzle. The role of minor mergers and of smooth gas inflow have still to be investigated, since these phenomena are far more difficult to investigate observationally than major mergers and galaxy disk dynamics in high- z galaxies. The emerging scenario that the star formation in galaxies, across the cosmic epochs, is mostly regulated by the molecular gas content implies that a proper understanding of the cosmic evolution of galaxies requires tracing the redshift evolution of the molecular gas (still largely unexplored), rather than the redshift evolution of the star formation rate (which has been the main focus of observing programmes until recently). The even more fundamental questions on the origin of the molecular gas and its relation with the atomic gas in galaxies and in the intergalactic medium, are even more difficult to tackle, since current radio facilities are not sensitive enough to probe HI at high- z , hence the content of HI is inferred only indirectly through Ly α absorption systems along a few lines of sight of bright quasars. The occurrence of starburst-driven and AGN-driven outflows and their role in regulating star formation in different classes of galaxies at high redshift has still to be assessed, since the objects investigated so far on this regard represent only a few extreme cases, which may not be representative of the bulk of the galaxy population at high redshift.

In the coming years a number of new facilities and instruments will enable astronomers to tackle most of these open issues. The Atacama Large Millimeter Array (ALMA, <http://www.almaobservatory.org>), which has just started its early operations, and which will be completed next year, will allow us to investigate in detail the evolution of the molecular gas for the bulk of the star forming galaxy population out to very high redshift, and with an angular resolution capable of tracing the internal kinematics of galaxies, molecular outflows, and minor merging companions. The Square Kilometer Array (SKA, <http://www.skatelescope.org>) and its precursors (MeerKAT and ASKAP, <http://www.ska.ac.za/meerkat>, <http://www.atnf.csiro.au/projects/askap>) will allow us to detect and map the HI content and HI kinematics in a huge number of galaxies out to the re-ionization epoch. The unprecedented sensitivity of the James Webb Space Telescope (JCMT, http://jwstsite.stsci.edu/webb_telescope) will enable us to detect the bulk the population of star forming and passive galaxies across the cosmic epochs out to the re-ionization epoch, properly assessing the contribution of the different classes of galaxies to the cosmic stellar assembly. The next generation of extremely large telescopes (E-ELT, <http://www.eso.org/public/teles-instr/e-elt.html>, TMT, <http://www.tmt.org>, GMT, <http://www.gmto.org>) will enable us to investigate with unprecedented detail the mechanisms responsible for star formation and the ISM and stellar properties in high redshift galaxies, thanks to their unprecedented angular resolution and by enabling high spectral resolution observations on faint targets.

Acknowledgments. I am extremely grateful to the organizers of the workshop, and in particular to Maria Emilia De Rossi, for the excellent organization of the meeting and of the associated school. I also acknowledge financial support by the Marie Curie Initial Training Network ELIXIR under the contract PITN-GA-2008-214227 from the European Commission.

References

- Aalto, S., et al. 2012, *A&A*, 537, 44
Alatalo, K., et al. 2011, *ApJ*, 735, 88
Alexander, D., et al. 2010, *MNRAS*, 402, 2211
Armus, L., et al. 2007, *ApJ*, 656, 148
Bertoldi, F. et al. 2007, *ApJS*, 172, 132
Blain, A. et al. 1999, *MNRAS*, 302, 632
Blanton, E.L., et al. 2011, *ApJ*, 737, 99
Bolzonella, M., Miralles, J.-M., Pellò, R. 2000, *A&A*, 363, 476
Bournaud, F., et al. 2011, *ApJ*, 741, L33
Cano-Diaz, M., et al. 2012, *A&A*, 537, 79
Cavagnolo, K.W., et al. 2011, *ApJ*, 732, 71
Cicone, C., et al., 2012, *A&A*, 543, 99
Cid Fernandes, R., et al. 2004, *MNRAS*, 355, 273
Cimatti, A., et al. 2004, *Nature*, 430, 184
Cimatti, A., et al. 2008, *A&A*, 482, 21
Cisternas, M., et al. 2011, *ApJ*, 726, 57
Clemens, D. et al, 2010, *A&A*, 518, L8
Cole, S. et al. 2000, *MNRAS*, 319, 168
Condon, J.J. 1992, *ARA&A*, 30, 575
Conselice, C. et al. 2011, *MNRAS*, 417, 2770
Cresci, G. et al. 2010, *Nature*, 467, 811
Cronton, D.J, et al. 2006, *MNRAS*, 365, 11
Datti, E., et al. 2010a, *ApJ*, 714, L118
Datti, E., et al. 2010b, *ApJ*, 713, 686
Davies, R., et al. 2007, *ApJ*, 671, 1388
de Jong, T., et al. 1985, *A&A*, 147, L6
Dekel, A., et al. 2009, *Nature*, 457, 451
Damond-Stnic, A.M., & Rieke, G.H., 2012, *ApJ*, 746, 168
Di Matteo, T., et al. 2005, *Nature*, 433, 604
Elbaz, D., et al. 2011, *A&A*, 533, 119
Erb, D., et al. 2012, arXiv:1209.5363
Fabian, A.C. 1999, *MNRAS*, 308, L39
Fabian, A.C. et al. 2006, *MNRAS*, 366, 417
Fabian, A.C. 2012, *ARA&A*, 50, 455

- Farrah, D., et al. 2012, *ApJ*, 745, 178
- Ferrarese, L., & Ford, H., 2005, *Space Sci.Rev.*, 116, 523
- Feruglio, C., et al. 2010, *A&A*, 518, L155
- Fischer, J., et al. 2010, *A&A*, 518, L41
- Forster-Schreiber, N.M. et al. 2006, *ApJ*, 645, 1062
- Fukugita, M., & Peebles, P.J.E., *ApJ*, 616, 643
- Gallerani, S., et al. 2012, *A&A*, 543, 114
- Genzel, R. et al. 2006, *Nature*, 442, 786
- Genzel, R. et al. 2010, *MNRAS*, 407, 2091
- Genzel, R. et al. 2011, *ApJ*, 733, 101
- Gnerucci, A. et al. 2011, *A&A*, 528, 88
- Glazebrook, K., et al. 2004, *Nature*, 430, 181
- Governato, F., et al. 2007, *MNRAS*, 374, 1479
- Granato, G., et al. 2004, *ApJ*, 600, 580
- Gultekin, K., et al. 2009, *ApJ*, 698, 198
- Harrison, C.M., et al. 2012a, arXiv:1205.1801
- Harrison, C.M., et al. 2012b, arXiv:1209.3016
- Hatziminaoglou, E., et al. 2010, *A&A*, 518, L33
- Helou, G., Soifer, B. T., & Rowan-Robinson, M. 1985, *ApJ*, 298, L7
- Hopkins, A. M., Beacom, J. F. 2006, *ApJ*, 651, 142
- Hopkins, P., et al. 2012, arXiv:1206.0011
- Hughes, D., 1998, *Nature*, 394, 241
- Hutchings, J.B., et al. 2002, *AJ*, 123, 2936
- Hutchings, J.B., et al. 2009, *AJ*, 137, 3533
- Juneau, S. et al. 1005, *ApJ*, 619, L135
- Karim, A., et al. 2011, *ApJ*, 730, 61
- Kennicutt, R. 1998, *ARA&A*, 36, 189
- King, A., 2005, *ApJ*, 635, L121
- Kocevski, D.D., et al. 2012, *ApJ*, 744, 148
- Krumholz, M.R., Dekel, A., McKee, C.F., 2012, *ApJ*, 745, 69
- Lapi, A., et al. 2005, *ApJ*, 619, 60
- Lagos, C. et al. 2011, *MNRAS*, 418, 1649
- Le Borgne, D. et al. 2009, *A&A*, 504, 727
- Le Floch, E. et al. 2005, *ApJ*, 632, 169
- Legache, G. et al. 2004, *ApJS*, 154, 112
- Lutz, D., et al. 2007, *ApJ*, 661, L25
- Lutz, D., et al. 2008, *ApJ*, 684, 853
- McCarthy, P.J. et al. 2004, *ApJ*, 614, L9
- Mainieri, V. et al. 2011, *A&A*, 535, 80
- Maiolino, R., et al. 2007, *A&A*, 468, 979
- Maiolino, R., 2008, *New Astron. Rev.*, 52, 339

- Maiolino, R., et al. 2012, MNRAS, 425, L66
Marchesini, D. et al. 2009, ApJ, 701, 1765
Marconi, A., & Hunt, L., 2003, ApJ, 589, L21
McNamara, B.R. et al. 2009, ApJ, 698, 594
Menci, N., et al. 2006, ApJ, 647, 753
Mihos, J.C., & Hernquist, L., 1996, ApJ, 464, 641
Mullaney, J.R., et al. 2012, MNRAS, 419, 95
Nardini, E., et al. 2008, MNRAS, 385, L130
Nardini, E., et al. 2009, MNRAS, 399, 1373
Nesbadba, N., et al. 2010, ApJ, 521, 65
Nesbadba, N., et al. 2011, MNRAS, 415, 2359
Netzer, H., et al. 2007, ApJ, 666, 806
Narayanan, D., et al. 2008, ApJ, 176, 331
Nordon, R. et al. 2010, A&A, 518, L24
Obreschkow, D., & Rawlings, S., 2009, ApJ, 696, L129
Ocvirk, P. et al. 2008, MNRAS, 390, 1326
Oliver, S. et al. 2010, A&A, 518, L21
Page, M. et al. 2012, Nature, 485, 213
Peng, Y. et al. 2010, ApJ, 721, 193
Perez-Gonzalez, P.G. et al. 2008, ApJ, 675, 234
Petric, A.O., et al. 2011, ApJ, 730, 28
Randall, S.W., et al. 2011, ApJ, 726, 86
Reddy, N. et al. 2006, ApJ, 644, 792
Rodighiero, G. et al. 2011, ApJ, 739, L40
Rosario, D.J., et al. 2012, A&A, 545, 45
Rupke, D., & Veileux, S., 2011, ApJ, 729, L27
Sani, E., et al. 2008, ApJ, 675, 96
Santini, P. et al. 2012, A&A, 540, 109
Saracco, P. et al. 2005, MNRAS, 357, L40
Silk, J., & Rees, M.J., 1998, A&A, 331, L1
Shao, L. et al., 2010, A&A, 518, L26
Smail, I., et al. 2002, MNRAS, 331, 495
Smith, J.D.T. et al. 2007, ApJ, 656, 770
Sobral, D. et al. 2012, MNRAS, 420, 1926
Solomon, P.M & Vanden Bout, P.A., ARA&A, 2005, 43, 677
Steidel, C. et al., 2010, ApJ, 717, 322
Steidel, C. et al., 2004, ApJ, 604, 534
Steidel, C. et al., 2003, ApJ, 592, 728
Steidel, C. et al., 1996, ApJ, 462, L17
Steinmetz, M. & Navarro, J.F., New Astronomy, 7, 155
Sturm, E., et al. 2011, ApJ, 733, L16

- Tacconi, L.J. et al. 2010, *Nature*, 463, 781
Thompson, T., et al. 2005, *ApJ*, 630, 167
Veilleux, S., et al. 1999, *ApJ*, 522, 139
Veilleux, S., Cecil, G., Bland-Hawthorn, J., 2005, *ARA&A*, 43, 769
Veilleux, S., et al. 2009, *ApJS*, 182, 628
Yan, L. et al. 2005, *ApJ*, 628, 604
Yun, M. S., Reddy, N. A., & Condon, J. J. 2001, *ApJ*, 554, 803
Weiss, A., et al. 2012, *ApJ*, 754, 102

Invited talks

State of the art of semi-analytic models

S.A. Cora^{1,2}

¹*FCAG, UNLP and IALP, CONICET, Observatorio Astronómico, La Plata, Argentina*

²*CONICET, Buenos Aires, Argentina*

Abstract. Semi-analytic models of galaxy formation and evolution are a powerful method to study how galaxies form and evolve within individual dark matter halos in a Λ -CDM cosmogony. We present the state of the art of current semi-analytic models, focusing on those properties of the galaxy population that are not properly reproduced by the model, which give hints of the astrophysical processes that still need better understanding.

1. Introduction

A theory of galaxy formation consists of the modeling of physical processes that affect the baryonic component associated to the dark matter (DM) halos of different mass. Understanding of most baryonic processes is quite incomplete, being based largely on simplified numerical simulations and on the phenomenology of observed systems. Semi-analytic models (SAMs) of galaxy formation and evolution are a powerful method to study how galaxies form and evolve within individual DM halos in a Λ CDM cosmogony. Thus, it is possible to separate the modeling of galaxy formation and evolution in two steps: *(i)* modeling the formation and evolution of the halo population using either N -body simulations or analytical methods like the extended Press-Schechter theory, and *(ii)* modeling the way in which galaxies form and evolve within DM halos using a SAM. The combination of these techniques gives rise to what is generally referred to as a hybrid model of galaxy formation and evolution.

The fundamental processes through which galaxies form are the cooling and condensation of gas in a merging hierarchy of DM halos (White & Rees 1978), and the subsequent star formation that takes place from the resulting cold gas reservoir. However, as clearly showed and discussed by Benson et al. (2003), the conversion of the DM halo mass function into the galaxy luminosity function (LF), by simply assuming a fixed mass-to-light ratio to match the knee of the latter, yields to large discrepancies at the faint and bright ends of the LF, overpredicting in both cases the number of galaxies.

In order to reproduce the observed LF, a model of galaxy formation must include feedback mechanisms to flatten the faint end of the LF, on one hand, and to suppress cooling at the centers of the massive halos of groups and clusters, on the other. It has been found that the former is achieved through the energy liberated by supernovae and stellar winds, which reheats disc gas. Although these sources of energy suppress the formation of faint galaxies, they are unable to produce a sharp cutoff at the bright end of the LF.

Most of the various SAMs proposed in the literature are attempting to model the same basic set of physical processes, which involves cooling of hot gas due to radiative losses, star formation, feedback from supernovae explosions, metal production and merging of galaxies. The first SAM was produced by White & Frenk (1991; see also Cole 1991 and Lacey & Silk 1991). After these seminal works, many research groups developed their own code (e.g., Kauffmann, White & Guiderdoni 1993; Cole et al. 1994; Heyl et al. 1995; Baugh, Cole & Frenk 1996; Kauffmann 1996; Guiderdoni, Hivon & Maffei 1998; Mo, Mao & White 1998; Devriendt et al. 1998; Kauffmann & Haehnelt 2000; Cole et al. 2000; Boisser & Prantzos 2000; Haehnelt & Kauffmann 2000; Somerville, Primack & Faber 2001, Springel et al. 2001; De Lucia, Kauffmann & White 2004). Recent works (e.g., Bower et al. 2006; Cattaneo et al. 2006; Croton et al. 2006; Menci et al. 2006; Malbon et al. 2007; Lagos, Cora & Padilla 2008; Somerville 2008) have demonstrated that feedback from active galactic nuclei, whose activity is triggered by gas accretion events onto central supermassive black holes, is crucial to reduce gas cooling in large halos, thus preventing them from forming stars at late times and allowing to obtain a good agreement with the bright end of the observed LF.

The proper treatment of the circulation of metals among the different baryonic components, e.g., hot gas, cold gas, and stars, is a key aspect since gas cooling depends on hot gas metallicity. In general, SAMs described in aforementioned works typically consider as free parameters both the fraction of metals ejected by the stars formed, and the recycled mass that has been locked in stars at their birth and re-ejected. This aspect was improved in some SAMs by including a fully consistent calculation of metal production, tracking the mass evolution of different chemical elements as provided by four kinds of sources: low- and intermediate-mass stars, and Type II and Ia supernovae (e.g., Nagashima et al. 2005; Cora 2006).

Regarding environmental effects, strangulation is a standard ingredient in nearly all SAMs. This process implies the instantaneous removal of the hot diffuse gas halo of a galaxy after its infall into a larger halo; the removed gas becomes part of the overall intragroup or intracluster medium. The affected satellite galaxy cannot accrete any more gas via cooling flows, and will consume all of its cold gas within a few Gyr, ending its star formation and becoming gradually redder as its stellar population ages (Weinmann et al. 2006; Baldry et al. 2006). The hot diffuse gas of a group or cluster of galaxies exerts ram pressure on satellites moving through it at velocities that could be close to supersonic. When ram pressure exceeds the gravitational restoring force of the galaxy, its cold gas is pushed out. This process, known as ram pressure stripping (RPS), has been implemented only in a few SAMs (Okamoto & Nagashima 2003; Lanzoni et al. 2005; Brüggén & De Lucia 2008; Tecce et al. 2010). RPS of the hot gaseous halos of satellite galaxies has been recently considered in some SAMs (e.g., Font et al. 2008; Guo et al. 2011, Kimm et al. 2011), with the aim of replacing the crude assumption of strangulation by a gradual removal of hot gas. These implementations are based on the observational evidence that large fractions of near-IR-bright, early-type galaxies in groups (Jeltema et al. 2008) and also in clusters (Sun et al. 2007) have extended X-ray emission, indicating that they retain significant hot gas halos even in these dense environments. Besides, recent hydrodynamic simulations have found that the hot gas halos of satellites are not

stripped instantly (McCarthy et al. 2008); although RPS of halo gas is much more effective than that of disc gas, satellite galaxies can keep up to 30 per cent of the initial hot halo gas for up to 10 Gyr.

The main physical processes incorporated in SAMs are described in a review by Baugh (2006). This work also compares the ways in which SAMs and direct numerical hydrodynamical simulations treat the key ingredients of galaxy formation. While hydrodynamical simulations solve hydrodynamical equations numerically treating the gas dynamics in full generality, SAMs assume spherical symmetry and solve equations analytically; these equations are simple but physically motivated analytic formulations that involve free parameters. The main advantage of a SAM is that it allows to reach a larger dynamic range than fully self-consistent hydrodynamical simulations at a far smaller computational cost. Besides, although the treatment of the physical processes is necessarily simplified, SAMs give the possibility to easily explore a wide parameter space and different sub-resolution models. The latter refers to aspects that cannot be solved by self-consistent gas simulations due to inadequate numerical resolution or because a complete physical model is simply not available.

Most of the SAMs developed by different research groups in the past decade constrain the free parameters involved in the model of the different physical processes with a set of global properties of the galaxy population at low redshift, such as the LF, the Tully-Fisher relation, the colour-magnitude relation, black hole-bulge relations, and measures of abundance and clustering as a function of the physical properties of galaxies, among others. Model results must be also consistent with the galaxy population at earlier times. However, ultra-deep surveys are just beginning to provide convincing results for the general galaxy population at high redshifts. On the other hand, galaxy group catalogues constitute a complementary tool to constraint model assumptions in detail. They have been constructed from the application of halo-based group finder to the Sloan Digital Sky Survey (SDSS) Data (Yang et al. 2005), and provide information about how galaxies of different luminosities (or stellar masses) are connected to DM halos of different masses, splitting the galaxy population in central and satellite galaxies. The different properties of these two types of galaxies clearly reveal the influence of the environment. Thus, matching such a wealth of data is a great challenge for any galaxy formation model. The degree of agreement and the discrepancies found allow to asses how realistically SAMs treat the astrophysics of galaxy formation. We present the state of the art of current SAMs, focusing on those properties of the galaxy population that are not properly reproduced, which give hints of the astrophysical processes that still need better understanding.

2. What can we learn from SAMs?

The following discussion summarizes the main conclusions of several works that compare the predictions of different SAMs with the observational data.

Kimm et al. (2009) analyze the predictions of SAMs developed by three different groups (De Lucia et al. 2006; Monaco, Fontanot & Taffoni 2007; Somerville et al. 2008) focusing on the dependence of the fraction of red and passive galaxies on halo mass and stellar mass, examining the properties of central and satellite galaxies separately. Central and satellite galaxies of a given stellar mass are

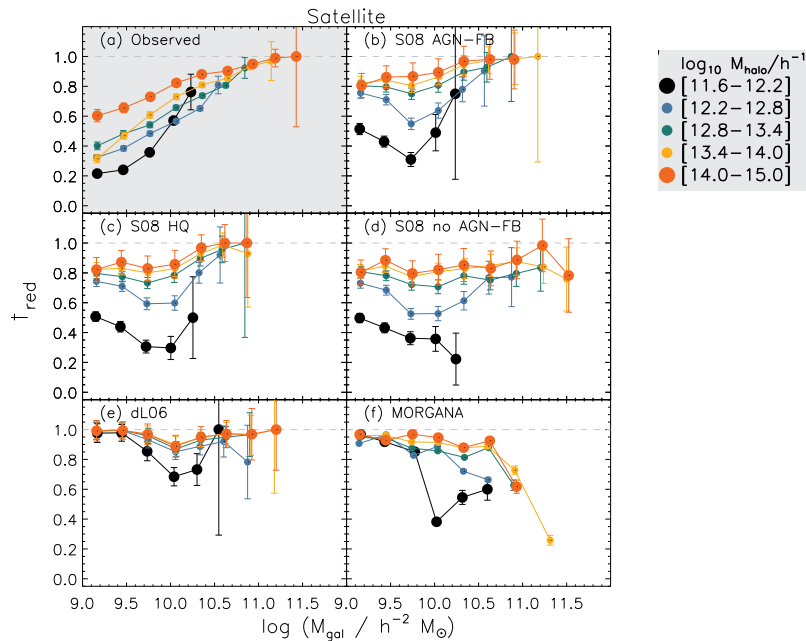


Figure 1. Red fraction f_{red} of satellite galaxies as a function of stellar mass, for different halo mass bins (see plot legend on the right), for the the observed SDSS group catalog (top left) and the five SAMs belonging to three different research groups. Taken from Fig. 5 of Kimm et al. (2009).

expected to have different properties since they are subjected to very different processes. Central galaxies are believed to reside at the centers of their DM halos and act as the recipients of new gas via cooling flows; they cannibalize satellite galaxies due to dynamical friction. Instead, satellite galaxies orbit around central galaxies, being affected by environmental effects such as tidal stripping and heating, ram-pressure stripping, galaxy harassment, and strangulation.

Model predictions are compared with empirical data provided by the halo-based Group Catalog of Yang and collaborators, which is based on the SDSS. Fig. 1 shows the red fraction f_{red} of satellite galaxies as a function of stellar mass, for different halo mass bins, obtained from both empirical and theoretical data. For observed massive satellite galaxies ($M_{\text{gal}} > 10^{10.5} h^{-1} M_{\odot}$), f_{red} does not show a significant dependence on halo mass (environment) for fixed stellar mass, similar to the corresponding dependence that is observed for central galaxies. Intermediate and low mass centrals are characterized by a very sharp drop of f_{red} over intermediate halo masses ($11.5 < \log(M_{\text{halo}} h / M_{\odot}) < 12.5$), while the red fraction of satellite galaxies in the same stellar mass range only shows some dependence on both galaxy stellar mass and halo mass, as can be seen in Figure 1. Comparing these results with those of SAMs, it is evident that f_{red} for the satellites does not have a strong enough dependence on the stellar mass

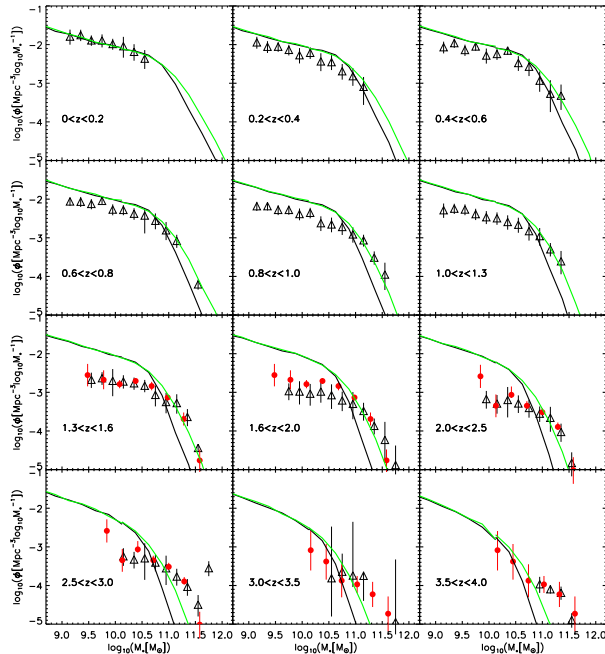


Figure 2. Stellar mass functions for different redshift intervals. Observational estimates (symbols) are based on combined very deep optical, near-IR and *Spitzer* photometry (3.6 to $8\mu\text{m}$) from Pérez-González et al. (2008) and Marchesini et al. (2009). Solid lines represent model results from the SAM of Guo et al. (2011). Those showing better agreement with observations at the high-mass end correspond to the application of the SAM to the Millenium II Simulation. Taken from Guo et al. (2011), their Fig. 23.

at fixed halo mass. All the models badly overproduce the number of low mass red satellites. This satellite overquenching problem has been detected in previous works (e.g. Weinmann et al. 2006) and is likely caused by the assumption of strangulation that is made in all the models considered, with the consequent stripping of the source of new cooling gas.

In order to evaluate if the instantaneous shock heating of the hot halo gas of satellites, which leads to its complete stripping, is the process responsible for the aforementioned mismatch between model results and observational data, Kimm et al. (2011) devise a SAM in which they implement gradual halo gas removal as a result of tidal stripping and RPS, modeling the latter according to the analytic formulation of McCarthy et al. (2008). They examine the fraction of passive satellite galaxies for different morphologies and environments (halo masses), finding that, regardless of the halo mass, the over-quenched satellite galaxies in SAMs are mostly late-type. When gradual diffuse gas stripping is considered, model late-type galaxies are more active, and the passive galaxy fraction becomes closer to the data. However, the dependence of passive fraction on galaxy mass for late-type satellites is stronger than observed. When the

dependence of this fraction on halo mass is also considered, it is found that models with gradual gas stripping preferentially lower the passive galaxy fraction of massive galaxies for all DM halo masses, reaching a better agreement with the observational data. In these cases, a larger amount of hot gas is retained because of the larger gravitational restoring force of such systems. It is also noticed that for a given galaxy mass, galaxies in less massive halos are more likely to be active since RPS is less effective. This fact can clearly be appreciated in the works of Tecce et al. (2010, 2011). Although they study the effect of RPS on cold disc gas, they show the dependence of RPS on halo virial mass and redshift using a self consistent approach instead of analytic estimations used in previous works. A model including a gradual removal of hot gas still predicts that a substantial fraction of small late-type galaxies in massive halos are passive. These results indicate that gradual removal of hot halo gas as a result of RPS is not enough to reproduce the observed level of recent star formation activity in late-type galaxies residing in massive halos, suggesting that the cold gas content of these galaxies is not yet captured by the model, and other processes like star formation and supernovae feedback should be revisited.

This conclusion is supported by the results found by Guo et al. (2011), who apply an updated and extended version of the SAM of their group to the Millennium II simulation. This model takes into account the gradual removal of hot gas as a result of RPS, in a similar fashion as Font et al. (2008), and tidal stripping. They analyse the stellar mass function (SMF) for high redshift galaxies after adjusting the free parameters to fit the observed stellar mass function at redshift $z \sim 0$, among other observational galaxy properties. Comparison between predicted and observed SMF at different redshifts is presented in Fig. 2. We can see that the good agreement with the observed SMF at $z \sim 0$ is maintained up to $z < 1$. At higher redshifts, the massive end of SMF remains consistent with observations, while the abundance of lower mass galaxies ($M_{\text{gal}} < 10^{10} M_{\odot}$) is overpredicted. This discrepancy suggests that low-mass galaxies form considerably earlier in the model than in the real Universe. This fact is consistent with the $u - i$ colour distribution also analyzed by Guo et al. (2011). At lower masses ($M_{\text{gal}} < 10^{9.5} M_{\odot}$), the predicted fraction of red galaxies is larger than observed, indicating that, even with gradual hot gas removal produced by RPS and tidal stripping, a substantial fraction of low mass galaxies in the model finish their star formation early, becoming passive.

These results are consistent with the conclusion that emerge from the analysis made by Fontanot & De Lucia (2009), who show that central galaxies are the main contributors to the overprediction of low-mass galaxies at $z < 2$. This arises from the comparison at different redshifts of the SMF given by three different SAMs (De Lucia & Blaizot 2007; Monaco et al. 2007; Somerville et al. 2008) with a set of observational data that includes those used in Guo et al. (2011). Hence, small objects are over-produced while they are central galaxies. As these systems become satellites during the assembly of galaxy groups and clusters, the low-mass satellite population shows a gradual increase at low redshift.

3. Conclusions

The excess of the red fraction of satellite galaxies predicted by SAMs focused the attention on the way in which hot halo gas of central galaxies is stripped as they become part of a larger DM halo. There is now general consensus that the shock-heating-motivated, instantaneous stripping of the hot halo gas of satellites is a crude approximation to the process, and alternative possibilities are being considered, such as tidal stripping and RPS of the hot gas, which lead to a gradual removal of this baryonic component. Gradual removal of hot gas becomes even more necessary when other environmental effects that affect the cold gas in galaxy discs are considered. As demonstrated by Tecce et al. (2010), when RPS of cold disc gas is acting, almost all galaxies in the innermost regions of clusters lose their cold gas by $z = 0$; the fraction of gas-depleted galaxies in the SAM considered, which includes strangulation, decreases at larger distances to the cluster centre, but remains significant beyond the virial radius. Hence, the combination of suppressed cooling flows due to strangulation and RPS of cold disc gas worsens the problem of excess of red fraction of satellites.

On the other hand, the abundance of low-mass galaxies, which finish their star formation early becoming red and passive, is substantially overpredicted at high redshift. This situation is not completely solved by considering gradual removal of hot gas, as expected. The scenario sketched from the results of different research works is that low-mass galaxies form considerably earlier in the model than in the real Universe, and that small objects are over-produced while they are central galaxies, supporting the idea that the mismatch between model and observations is not primarily due to inaccuracies in the modeling of satellites, and highlighting the fact that the star formation and supernovae feedback are neither yet well understood nor correctly treated in the models, particularly at high redshift.

Acknowledgments. This work was supported by Consejo Nacional de Investigaciones Científicas y Técnicas, Agencia de Promoción Científica y Tecnológica, National University of La Plata and Institute of Astrophysics of La Plata (IALP), Argentina.

References

- Benson, A. J., Bower, R. G., Frenk, C. S., et al., 2003, *ApJ*, 599, 38
- Baldry I. K., Balogh M. L., Bower R. G., et al., 2006, *MNRAS*, 373, 469
- Baugh C. M. 2006, *Reports on Progress in Physics*, 69, 3101
- Baugh C. M., Cole S., Frenk C. S., 1996, *MNRAS*, 282, L27
- Boisser S., Prantzos N. 2000, *MNRAS*, 312, 398
- Bower R. G., Benson A. J., Malbon R., et al., 2006, *MNRAS*, 370, 645
- Brüggen M., De Lucia G. 2008, *MNRAS*, 383, 1336
- Cattaneo A., Dekel A., Devriendt J., et al., 2006, *MNRAS*, 370, 1651
- Cole S. 1991, *ApJ*, 367, 45
- Cole S., Aragon-Salamanca A., Frenk C. S., et al., 1994, *MNRAS*, 271, 781
- Cole S., Lacey C. G., Baugh C. M., Frenk C. S. 2000, *MNRAS*, 319, 168

- Cora S. A. 2006, MNRAS, 368, 1540
- Croton D. J., Springel V., White S. D. M., et al., 2006, MNRAS, 365, 11
- De Lucia G., Kauffmann G., White S. D. M. 2004, MNRAS, 349, 1101
- De Lucia G., Springel V., White S. D. M., et al., 2006, MNRAS, 366, 499
- De Lucia G., Blaizot J. 2007, MNRAS, 375, 2
- Devriendt J. E. G., Sethi S. K., Guiderdoni B., et al., 1998, MNRAS, 298, 708
- Font A. S., Bower R. G., McCarthy I. G., et al., 2008, MNRAS, 389, 1619
- Fontanot F., De Lucia G., Monaco P., et al., 2009, MNRAS, 397, 1776
- Guo Q., White S. D. M., Boylan-Kolchin M., et al., 2011, MNRAS, 413, 101
- Guiderdoni B., Hivon E., Maffei F. R. B. B. 1998, MNRAS, 295, 877
- Haehnelt M., Kauffmann G. 2000, MNRAS, 318, L35
- Heyl J. S., Cole S., Frenk C. S., Navarro J. F., 1995, MNRAS, 274, 755
- Jeltema T. E., Binder B., Mulchaey J. S. 2008, ApJ, 679, 1162
- Kauffmann G. 1996, MNRAS, 281, 475
- Kauffmann G., Haehnelt M. 2000, MNRAS, 311, 576
- Kauffmann G., White S. D. M., Guiderdoni B., 1993, MNRAS, 264, 201
- Kimm T., Somerville R. S., Yi S. K., et al., 2009, MNRAS, 394, 1131
- Kimm T., Yi S. K., Khochfar S. 2011, ApJ, 729, 11
- Lacey C., Silk J. 1991, ApJ, 381, 14
- Lagos C. D. P., Cora S. A., Padilla N. D. 2008, MNRAS, 388, 587
- Lanzoni B., Guiderdoni B., Mamon G. A., et al., 2005, MNRAS, 361, 369
- Malbon R. K., Baugh C. M., Frenk C. S., Lacey C. G. 2007, MNRAS, 382, 1394
- Marchesini D., van Dokkum P. G., et al., 2009, ApJ, 701, 1765
- McCarthy I. G., Frenk C. S., Font A. S., et al., et al. 2008, MNRAS, 383, 593
- Menci N., Fontana A., Giallongo E., Grazian A., et al., 2006, ApJ, 647, 753
- Mo H. J., Mao S., White S. D. M. 1998, MNRAS, 295, 319
- Monaco P., Fontanot F., Taffoni G. 2007, MNRAS, 375, 1189
- Nagashima M., Lacey C. G., Baugh C. M., et al., 2005, MNRAS, 358, 1247
- Okamoto T., Nagashima M. 2003, ApJ, 587, 500
- Pérez-González P. G., Rieke G. H., Villar V., Barro G., et al., 2008, ApJ, 675, 234
- Somerville R. S., Primack J. R., Faber S. M. 2001, MNRAS, 320, 504
- Somerville R. S., Hopkins P. F., Cox T. J., et al., 2008, MNRAS, 391, 481
- Springel V., White S. D. M., Tormen G., Kauffmann G. 2001, MNRAS, 328, 726
- Sun M., Jones C., Forman W., Vikhlinin A., et al., 2007, ApJ, 657, 197
- Tecce T. E., Cora S. A., Tissera P. B., et al., 2010, MNRAS, 408, 2008
- Tecce T. E., Cora S. A., Tissera P. B. 2011, MNRAS, 416, 317
- Weinmann S. M., van den Bosch F. C., Yang X., et al., 2006, MNRAS, 372, 1161
- White S. D. M. and Frenk C. S. 1991, ApJ, 379, 52
- White S. D. M. and Rees M. J. 1978, MNRAS, 183, 341
- Yang X. Mo H. J., van den Bosch F. C., Jing Y. P. 2005, MNRAS, 356, 1293

Gas and metal distributions within simulated disk galaxies

B.K. Gibson^{1,2,3}, S. Courty⁴, D. Cunnama⁵ and M. Mollá⁶

¹*Dept of Phys & Astro, Saint Mary's Univ, Halifax, Canada*

²*MoCA, Clayton, Australia*

³*Jeremiah Horrocks Institute, UCLan, Preston, UK*

⁴*Université Lyon 1, France*

⁵*Physics Dept, Univ of the Western Cape, Cape Town, South Africa*

⁶*Depto de Investigación Básica, CIEMAT, Madrid, Spain*

Abstract. We highlight three research strands related to our ongoing chemodynamical Galactic Archaeology efforts: (i) the spatio-temporal infall rate of gas onto the disk, drawing analogies with the infall behaviour imposed by classical galactic chemical evolution models of inside-out disk growth; (ii) the radial age gradient predicted by spectrophotometric models of disk galaxies; (iii) the radial distribution of low column density neutral hydrogen in the halos of field and group disk galaxies. At low-redshift, we find that half of the infall onto the disk is gas associated with the corona, while half can be associated with cooler gas streams; we also find that gas enters the disk preferentially orthogonal to the system, rather than in-plane. We recover age gradient troughs/inflections consistent with those observed in nature, without recourse to radial migrations. Finally, we find radial HI profiles consistent with those observed in nature, suggesting the magnitude of our energy feedback is not significantly over- or under-estimated; environmental differences in the inferred radial HI scale-lengths are found, consistent with the impact of increased ram pressure stripping, tidal interactions, etc., in group (versus field) environments.

1. Introduction

The infall of gas onto galaxies is a fundamental constituent of any cosmologically-motivated models of galaxy evolution, whether they be classic galactic chemical evolution models (e.g. Lineweaver et al. 2004; Renda et al. 2004) or hydrodynamical simulations (e.g. Kawata & Gibson 2003; Brook et al. 2004). The shape of the metallicity distribution function of a given ensemble of stars can be a powerful tool to constrain the (otherwise, little known) interplay between infalling and outflowing material (e.g. Fenner & Gibson 2003; Pilkington et al. 2012b). In the local Universe, we often associate (rightly or wrongly) this infalling fuel for future star formation with the high-velocity clouds which permeate our halo (e.g. Gibson et al. 2001; Pisano et al. 2004).

Classic chemical evolution models, constrained by both the metallicity distribution function and gradients (abundance and surface density) in the disk, suggest “inside-out” growth of the disk is required (e.g. Chiappini et al. 2001; Fenner & Gibson 2003; Mollá & Díaz 2005; Pilkington et al. 2012a,b). By “inside-out”, we mean a scenario in which the timescale for gas infall onto the

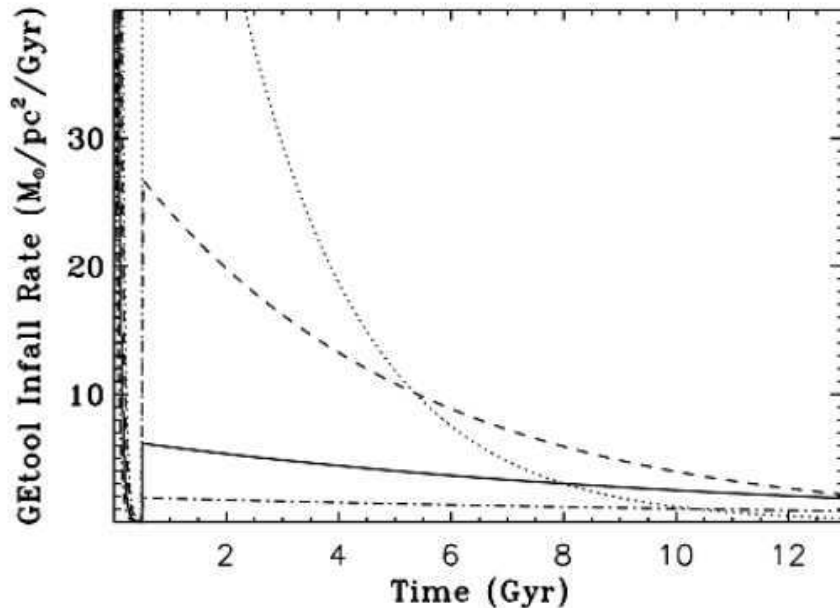


Figure 1. Gas infall rate onto the disk as a function of time (x -axis) and radius (ranging from inner to outer disk, going from the upper to the lower curves). The infall timescale here (from the models of Renda et al. 2004) grows linearly with galactocentric radius.

disk increases as a function of galactocentric radius; whether this timescale is linear (e.g. Chiappini et al. 2001) or a higher-order parametrisation (e.g. Mollá & Díaz 2005) is less important than the fact that (a) the overall infall rate is (roughly) exponential, and (b) the timescale increases with radius. Fig. 1 shows one such parametrisation from the chemical evolution model of Renda et al. (2004).

As alluded to above, energetic outflows (driven by a combination of thermal/kinetic energy from supernovae and massive star winds/radiation) also play a critical role in regulating star formation, infall of both fresh and re-cycled disk material, and setting the chemistry of the resulting system. The heating and chemical profiles of the halo are an ideal place to examine the veracity of one's feedback scheme through a comparison of the radial profiles of various neutral and ionised species (e.g. HI, OVI, MgII) with those observed in nature.

Each of the above points – specifically, (i) the spatio-temporal infall pattern of gas onto the disk, (ii) age gradients within spectrophotometric disk models, and (iii) radial HI profiles in the halo of simulated disk galaxies – are touched upon the following sub-sections. These are each, very much, works in progress, rather than finished products, so we ask the reader to bear that in mind!

2. How does gas get into galaxies?

Making use of RAMSES-CH (Few et al. 2012), a new self-consistent implementation of chemical evolution within the RAMSES cosmological adaptive mesh refinement code (Teyssier 2002), we re-simulate the disk described by Sánchez-Blázquez et al. (2009) and analyse the temporal and spatial infall rates of hot/coronal and cooler/stream gas onto the disk. Our task is a (seemingly) straightforward one: confirm/refute the aforementioned fundamental tenet of chemical evolution, that the gas infall onto simulated disks (in a cosmological context) proceeds in an inside-out fashion.

In the upper-left panel of Fig. 2, we show in black (magenta) the inflowing (outflowing) gas flux through parallel (0.5 kpc thick) slabs situated ± 5 kpc from the mid-plane (extending to a galactocentric radius of 25 kpc),¹ over the range of time for which the disk could be ‘readily’ identified (see Sánchez-Blázquez et al. 2009 for details pertaining to the ‘disk identification’). In the upper-right panel of Fig. 2, we decompose the infalling gas (black curve from the left panel, repeated again here, also in black) into polytropic/hot gas (what we label as ‘corona’) in red, and non-polytropic/cooler gas (what we label as ‘streams’) in blue. Within this simulation, *(i) the infall from the corona is roughly constant in time, and (ii) at low-redshift, each component accounts for half of the current gas infall.* In the lower-left panel of Fig. 2, we show the infalling (outflowing) gas flux, again in black (magenta), through a cylinder of radius 25 kpc and height ± 5 kpc; i.e., the sum of the fluxes shown here, plus those shown in the upper-left panel of Fig. 2, correspond to the real/total accretion rate. For this simulation, *the rate of gas infall/inflow entering the disk through the cylinder (i.e., ‘in-plane’ infall/inflow) is fairly negligible.* Finally, in the lower-right panel of Fig. 2, we show the gas inflow rate through three small ‘holes’ situated ± 5 kpc from the mid-plane, at different radii. While noisy, due to the small sampling employed here, we can see the emergence of the fundamental tenet of inside-out disk growth: specifically, the lack of gas accretion at small galacto-centric radii at low-redshift (i.e., a trend for flatter infall profiles at larger radii).

3. Age gradients

The existence of U-shaped radial age profiles (inferred via radial colour profiles, in consort with stellar population modeling) in disk galaxies (particularly those with so-called Type II surface brightness profiles - i.e., those showing a ‘break’ in the surface brightness) is now well-established (e.g. Bakos et al. 2008; Sánchez-Blázquez et al. 2011; Roediger et al. 2012). Such troughs in age, near the break radius, were found in the exquisite models of Roskar et al. (2008), where the ‘up-bend’ in the age profile in the outer disk was produced by stars that had migrated from the inner parts of the disk; in our cosmological simulation (Sánchez-Blázquez et al. 2009), a similar trough/inflection in the age profile was found at the break radius, where the presence of a warp in the gas disk resulted

¹The choice of ± 5 kpc heights is a compromise between being as close to the disk as possible, without being ‘swamped’ by the galactic fountain/re-circulation signal (Gibson et al. 2009; §7).

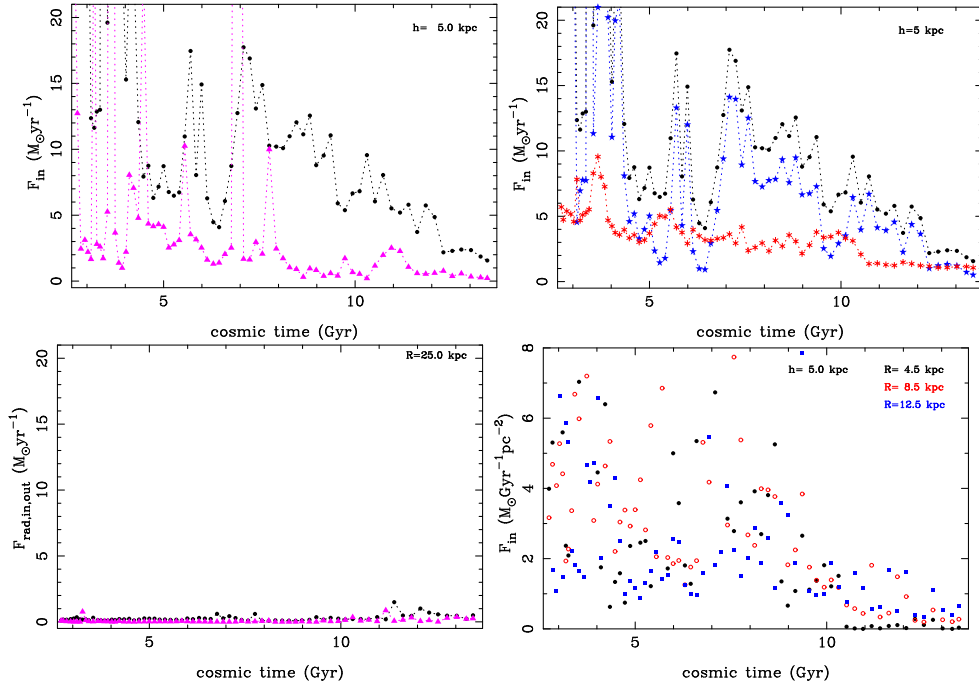


Figure 2. Upper-left: inflowing (outflowing) gas through slabs ± 5 kpc from the mid-plane in black (magenta); Upper-right: inflowing hot/coronal (cooler/stream) gas through the same ± 5 kpc slabs in red (blue); Lower-left: inflowing (outflowing) gas through a ± 5 kpc high cylinder of radius 25 kpc in black (magenta); Lower-right: inflowing gas through small 'holes' ± 5 kpc from the mid-plane, at three different radii. See text for details.

in a decrease in the volume density and, hence, a ‘break’ in the star formation density. The trough persists, regardless of the presence (or lack thereof) of radial migration (although migration *clearly* takes place and *is* critical!).

Whether U-shaped age profiles are a natural byproduct within classical galactic chemical evolution models is less certain; to that end, we examined the spectrophotometric predictions associated with the same fiducial Milky Way models (Mollá & Díaz 2005; $N=28$) that were employed in our recent work on the temporal evolution of metallicity gradients in L^* galaxies (Pilkington et al. 2012a). In Fig. 3, we show predicted present-day mass-weighted age gradients for a Milky Way analog, employing a range of star formation efficiencies (from high efficiency to low efficiency, in going from the top to the bottom curves at small galactocentric radii). We find that within these classical models, which by construct neglect radial migration, U-shaped age profiles are a natural outcome of the infall/star formation prescriptions. It is interesting to note that the position and depth of the trough is sensitive to the adopted star formation efficiency; high efficiencies drive the trough to be (i) positioned at larger galactocentric radii, and (ii) shallower (and vice versa for low star formation efficiencies). In the outer parts of the disk, beyond the minima of the age profiles, the high efficiency models show inverted age profiles, while the low efficiency models show declining age profiles. A more thorough investigation is clearly warranted.

4. Radial HI profiles of halo gas

Many of the empirical constraints to classical chemical evolution models and fully cosmological chemodynamical simulations are provided by observations of the disk and the bulge, as they (not surprisingly) dominate the light output of most galaxies. That said, the gas phase (both hot and cold) also holds a wealth of information, ranging from surface density distributions, velocity dispersions, metal content, clumpiness, etc. (e.g. Pilkington et al. 2011, and references therein). One particular component of chemodynamical galaxy modeling that has been under-represented is that of the hot halo/corona; we have discussed in Sect. 2., one aspect of coronal gas physics that lends itself to study – here we discuss another – specifically, the radial profile of neutral hydrogen in the halo of simulated field and group disk galaxies and its comparison with the radial profiles derived in the local Universe by Prochaska et al. (2011). Such profiles are very sensitive to the degree of (highly uncertain) energy feedback adopted within simulations (which is ultimately the mechanism for pushing metals and energy from the disk into the halo).

Because of the need for statistics, we re-simulated the $\sigma=0$ region of the GIMIC suite (Crain et al. 2009) down to redshift $z=0$ with a fixed physical softening length of 500 pc and a baryonic particle mass of $\sim 10^6 M_\odot$. We identified ~ 350 disk galaxies with stellar masses in excess of $10^9 M_\odot$, $\sim 60\%$ ($\sim 40\%$) of which reside in field (group) environments.

In Fig 4, we show the stacked radial HI column density profiles for galaxies in the stellar mass range $10^{10} - 10^{11} M_\odot$. Of the 184 galaxies in this mass range, 109 (75) are categorised as being in field (group) environments; individual stacked profiles are shown for these ‘group’ (upper, red curve) and ‘non-group’ (lower, blue curve) galaxies. We also overlay the empirical HI column density

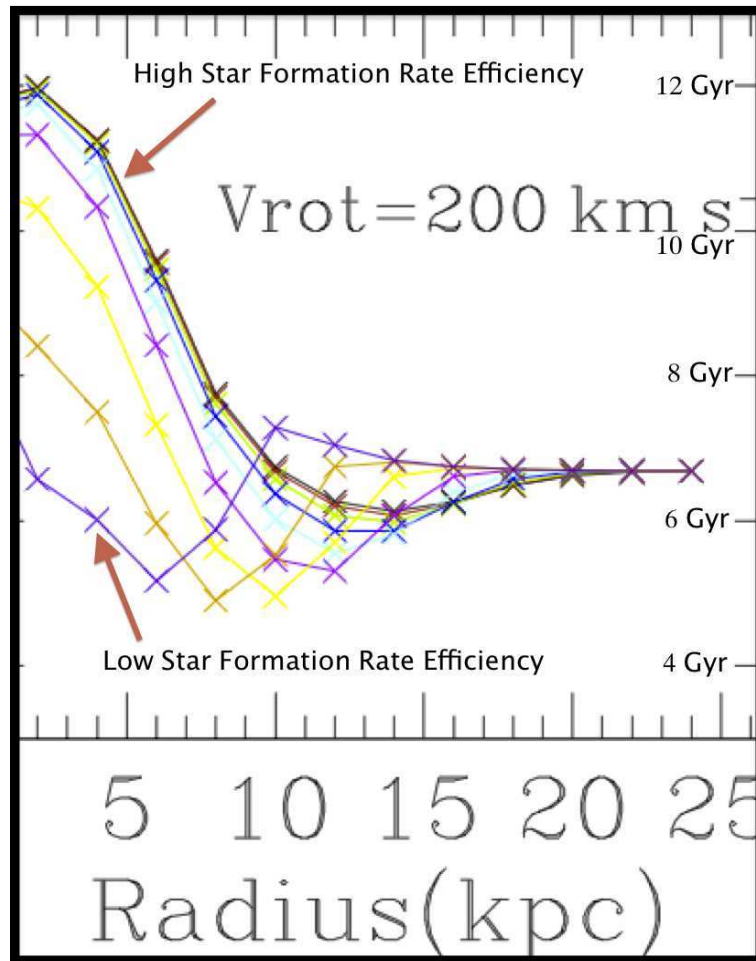


Figure 3. Radial, mass-weighted, age profiles for the fiducial Milky Way models of Mollá & Díaz (2005), for a range of star formation efficiencies. All models possess U-shaped age profiles, with the position and depth of the trough being depending upon the adopted star formation efficiency. See text for details.

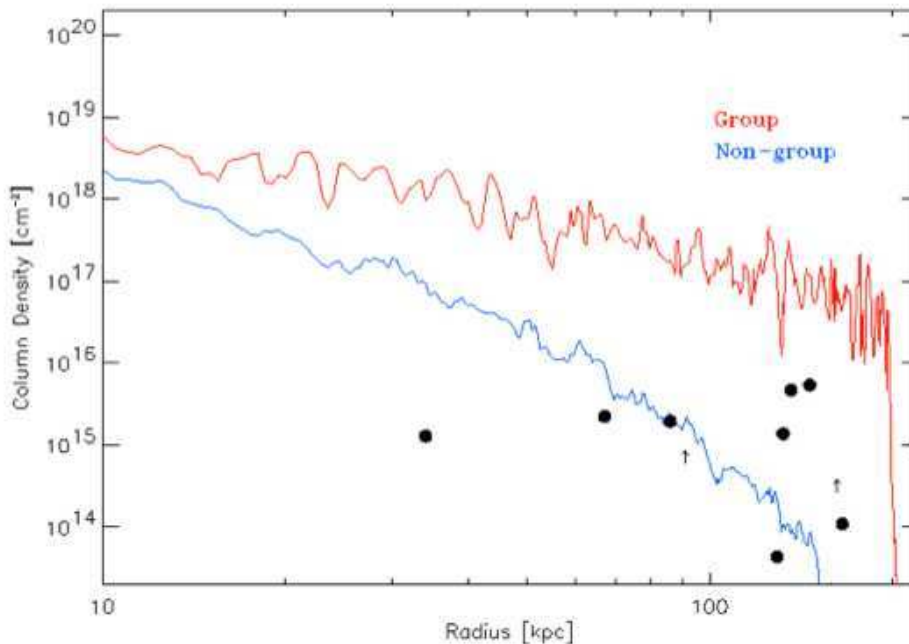


Figure 4. Stacked radial HI halo gas profiles of the 109 (74) field (group) galaxies in the $10^{10} - 10^{11} M_{\odot}$ stellar mass range (upper red and lower blue curves, respectively). Black dots and arrows (limits) are observed column densities from the nearby QSO absorption line work of Prochaska et al. (2011).

observations from Prochaska et al. (2011). Without any ‘fine-tuning’ of the feedback scheme, it would seem that the strong kinetic feedback employed here results in predicted radial HI profiles which are not dissimilar to those observed in nature. A beautiful illustration of how that agreement can go very wrong, when a less satisfactory feedback scheme is adopted, can be found in Stinson et al. (2012), to which all interested readers should refer. An ancillary result of our analysis is the apparent environmental effect in the radial HI profiles - specifically, our group galaxies have more extended HI halo profiles than their field counterparts. In our case, this is an intrinsic physical characteristic (driven by the increased effects of ram pressure stripping, etc., in the group environment) rather than a superposition effect; the importance of such differences between intrinsic and apparent superpositions, is discussed eloquently by Bordoloi et al. (2011).

Acknowledgments. Without the help of our collaborators, this work would not have been possible; we thank them all for their ongoing advice and guidance. BKG thanks both Monash and Saint Mary’s Universities for their generous visitor support, and the organisers of what was an incredibly exciting, rewarding, and collegial School and Workshop. BKG, SC, MM and DC acknowledge the

support of the UK's Science & Technology Facilities Council (ST/F002432/1 & ST/H00260X/1). SC acknowledges support from the the BINGO Project (ANR-08-BLAN-0316-01).

References

- Bakos, J., Trujillo, I., Pohlen, M. 2008, *ApJ*, 683, L103
- Bordoloi, R., Lilly, S.J., Knobel, C., et al. 2011, *ApJ*, 743, 10
- Brook, C.B., Kawata, D., Gibson, B.K., et al. 2004, 349, 52
- Chiappini, C., Matteucci, F., Romano, D. 2001, *ApJ*, 554, 1044
- Crain, R.A., Theuns, T., Dalla Vecchia, C., et al. 2009, *MNRAS*, 399, 1773
- Cunnam, D., Gibson, B.K., Faltenbacher, A., et al. 2012, *MNRAS*, submitted
- Fenner, Y., Gibson, B.K. 2003, *PASA*, 20, 189
- Few, C.G., Courty, S., Gibson, B.K., et al. 2012, *MNRAS*, 424, L11
- Gibson, B.K., Giroux, M.L., Penton, S.V., et al. 2001, *AJ*, 122, 3280
- Gibson, B.K., Courty, S., Sánchez-Blázquez, P., et al. 2009, in *The Galaxy Disk in Cosmological Context*, J. Andersen et al. (ed.)
- Kawata, D., Gibson, B.K. 2003, *MNRAS*, 346, 135
- Lineweaver, C.H., Fenner, Y., Gibson, B.K. 2004, *Science*, 303, 59
- Mollá, M., Díaz, A.I. 2005, *MNRAS*, 358, 521
- Pilkington, K., Gibson, B.K., Calura, F., et al. 2011, *MNRAS*, 417, 2891
- Pilkington, K., Few, C.G., Gibson, B.K., et al. 2012a, *A&A*, 540, A56
- Pilkington, K., Gibson, B.K., Calura, F., et al. 2012b, *MNRAS*, 425, 969
- Pisano, D.J., Barnes, D.G., Gibson, B.K., et al. 2004, *ApJ*, 610, L17
- Prochaska, J.X. Weiner, B., Chen, H.-W., et al. 2011, *ApJ*, 740, 91
- Renda, A., Fenner, Y., Gibson, B.K., et al. 2004, *MNRAS*, 354, 575
- Roediger, J.C., Courteau, S., Sánchez-Blázquez, P. 2012, *ApJ*, 758, 41
- Roskar, R., Debattista, V.P., Quinn, T.R., et al. 2008, *ApJ*, 684, L79
- Sánchez-Blázquez, P., Courty, S., Gibson, B.K., et al. 2009, *MNRAS*, 398, 591
- Sánchez-Blázquez, P., Ocvirk, P., Gibson, B.K., et al. 2011, *MNRAS*, 415, 709
- Stinson, G., Brook, C., Prochaska, J.X., et al. 2012, *MNRAS*, 425, 1270
- Teyssier, R. 2002, *A&A*, 385, 337

Structure and galaxy evolution from clustering or environment measurements

N. Padilla^{1,2}

¹*Depto de Astronomía y Astrofísica, PUC, Santiago, Chile*

²*Centro de Astro-Ingeniería, PUC, Santiago, Chile*

Abstract. We present a study of the evolution of early-type galaxies that combines luminosity function and clustering measurements. The latter allows to infer the typical dark-matter halo mass of the hosts of $z = 1$ early-type galaxies. Using Λ CDM predictions, it is then possible to follow haloes of this mass to $z = 0$ and search for a local observational sample of early-type galaxies with clustering consistent with that of these descendant haloes. Our assumption is that the $z = 0$ early-type galaxies constitute a statistical sample of descendants of those at $z = 1$. This technique shows that early-type galaxies at a given redshift evolve into brighter galaxies in the rest-frame, passively evolved optical band at lower redshifts. Notice that this indicates that a stellar-mass selection at different redshifts does not necessarily provide samples of galaxies in a progenitor-descendant relationship. The comparison between high-redshift early-type galaxies and their likely descendants at $z = 0$ points to a higher number density for the progenitors by a factor 3–11, implying the need for mergers to decrease their number density by today. Because the progenitor-to-descendant ratios of luminosity density are consistent with the unit value, our results show no need for strong star-formation episodes in early-type galaxies since $z = 1$, which indicates that the needed mergers are dry, i.e., gas free.

1. Introduction

The study of the population of early type galaxies (ETGs) at different redshifts has been used extensively to test our knowledge of the galaxy formation process, in particular, the assembly of the stellar content of massive galaxies. Analyses of the evolution of the stellar mass and luminosity functions (LF) have found that high stellar mass ($M > 10^{11} h^{-1} M_{\odot}$), passive galaxies do not show evolution in their comoving space density since $z \sim 1$ (Cimatti et al. 2002, 2004; McCarthy et al. 2004; Glazebrook et al. 2004; Daddi et al. 2005; Saracco et al. 2005; Bundy et al. 2006; Pérez-González et al. 2008; Marchesini et al. 2009). This result has been interpreted as evidence that the stellar content of such galaxies is already in place at high redshifts, ruling out the involvement of mergers (even dry i.e., gas-free) since $z \sim 1$.

Recent statistical measurements of $z \sim 1-3$ galaxies, such as the stellar mass function (Perez-Gonzalez et al. 2008; Marchesini et al. 2009; but see Benson & Devereux 2010), the galaxy luminosity function (Marchesini & van Dokkum 2007), and SCUBA (Holland et al. 1999) number counts of $z \simeq 3$ galaxies

detected in sub-millimetre bands, show little evolution in this galaxy population since these even higher redshifts. However, these results may still be subject to observational biases. For instance, Marchesini et al. (2010) showed that allowing for the existence of a previously unrecognized population of massive, old, and very dusty galaxies at $z \sim 2.6$ produces results consistent with an evolution of the number density of ETGs since $z = 3$, and also provides good agreement between the observed abundance of massive galaxies at $z = 3.5$ and that predicted by semi-analytic models (e.g., Lagos, Cora & Padilla 2008; Baugh et al. 2005).

The way in which the selection of a given population and its descendants is done, is usually via a fixed stellar mass selection (e.g., Robaina et al. 2010). Only in the case of ETGs, this can also be done using passively evolved luminosities, since these should scale linearly (and independently of the redshift) with the stellar mass in systems of old stars with no recent star formation activity (eg. Cimatti et al. 2006). However, events such as mergers would produce a change in the stellar masses or passively evolved luminosities of the galaxies, which opens the possibility that this selection may not be appropriate for the purpose.

The approach we present here is intended to improve the selection of statistical descendants of a sample of high redshift ETGs. In order to do this we will use clustering information of the progenitor galaxies (the sample at high redshift, from Padilla et al. 2010, P10), that will give us the mass of the host dark matter halo, which in a numerical simulation can be followed down to any given redshift. Then we will compare the number densities of the samples of progenitor and descendant galaxies (the lower redshift galaxies selected to have the clustering of the host haloes at this later cosmic time) obtained from luminosity function measurements (from Christlein et al. 2009, C09). We will interpret differences in these number densities in terms of mergers and their characteristics.

This article presents the measured correlation and luminosity functions used in our method in Sect. 2, and shows the results and presents our conclusions in Sect. 3.

2. Luminosity functions and clustering information

We will analyse the evolution of the Multi-wavelength Survey by Yale-Chile (MUSYC) ETGs using the LFs measured by C09. MUSYC comprises over 1.2 square degrees of sky imaged to 5σ AB depths of $U, B, V, R = 26$, $I = 25$, $z = 24$ and $J, K(AB) = 22.5$, with extensive follow-up spectroscopy. The source detection is done on the combined BVR image down to a magnitude of 27 (see Gawiser et al., 2006, for further details).

C09 proposed and applied a new technique, the photometric maximum likelihood (PML) method, to a subset of MUSYC comprising the Extended Chandra Deep Field South (ECDF-S), covering approximately 0.25 sq. degrees on the sky. The PML algorithm was used to measure the underlying luminosity function of galaxy populations characterised by different spectral types. The latter are parameterised with a set of SED templates from Coleman, Wu & Weedman (1980, CWW) or fixed superpositions of two CWW templates, extended into the UV regime using Bruzual & Charlot (1993) models. For the present analysis, we will only use the LF corresponding to the two earliest-type templates in this set, which correspond to an elliptical galaxy and to a E+20%Sbc mix. P10 demon-

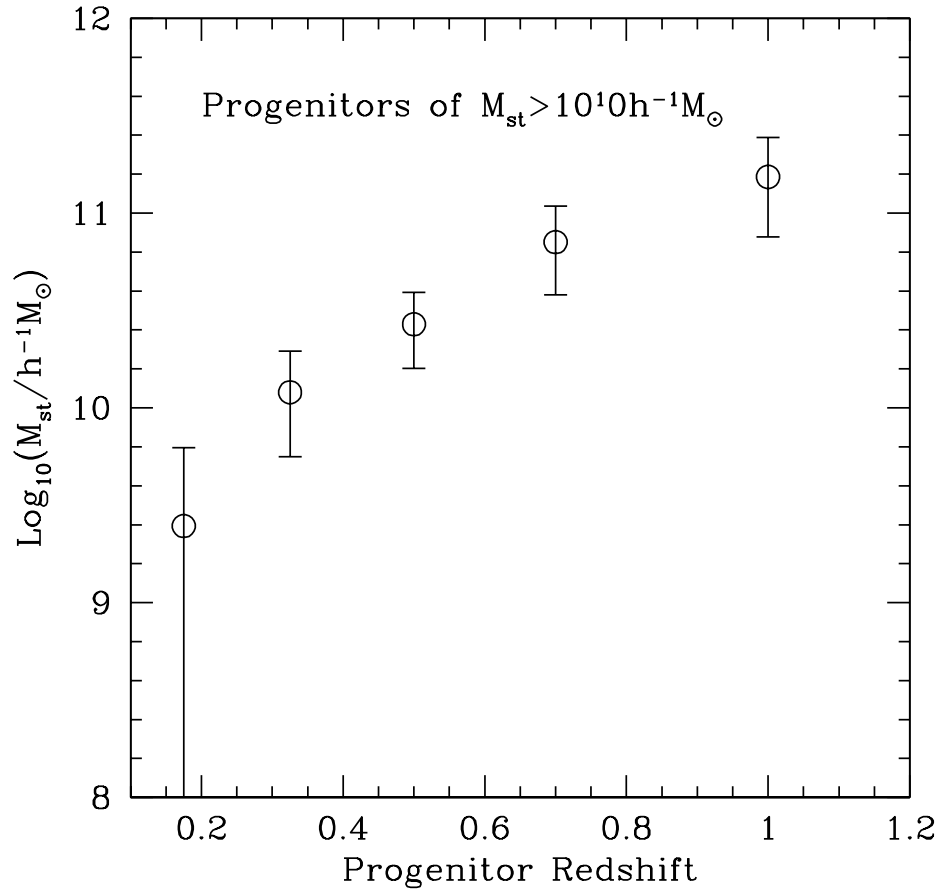


Figure 1. Stellar masses of $z = 0$ descendants as a function of progenitor redshift. In all cases the progenitor selection is done using a lower limit on passively evolved luminosities equivalent to a stellar mass of $> 10^{10} h^{-1} M_{\odot}$. The progenitors are selected so as to have the clustering of the evolved population of progenitor dark matter halo hosts (following numerical simulations). As can be seen, the stellar mass of descendants is generally higher than that of the progenitors. Error bars are determined from the scatter in descendant masses as obtained from the clustering uncertainties in P10.

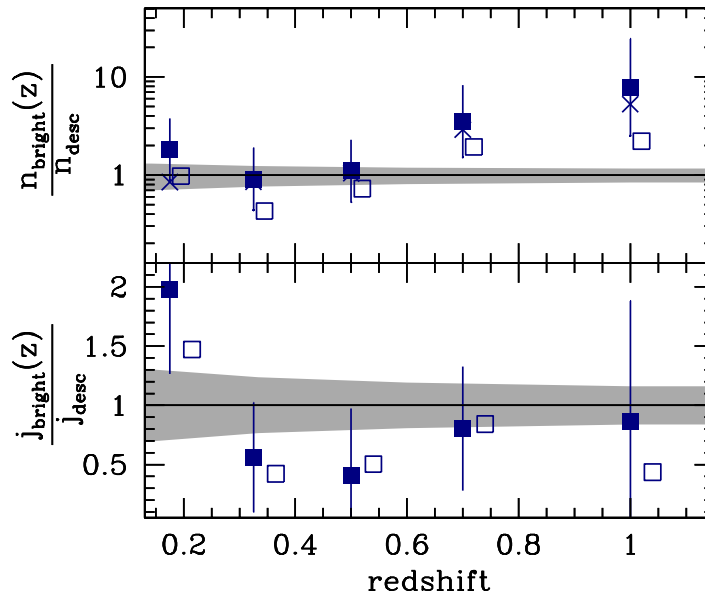


Figure 2. *Top panel:* Ratio between the number density of ETGs at a given redshift and their expected $z = 0$ descendants, as inferred from the clustering analysis of P10. The filled squares show the results from the PML r -band LF estimates; open squares show the results for the B -band. Error bars are only shown for the r -band result to improve clarity. The crosses correspond to the results from the photometric- z -based maximum likelihood method to calculate the LF in the r -band. The solid line shows the unit ratio and the grey shaded area the estimated cosmic variance in a 0.25 square degree light-cone survey divided in slices of $\Delta z = 0.1$. *Bottom panel:* Ratio between the luminosity density of progenitor ETGs and that of their $z = 0$ ETG descendants in the r - and B -bands (filled and open squares, respectively).

strate that the sample of ETGs selected in this way is comparable to a selection of the red-sequence at each redshift (as adopted in e.g., Bell et al. 2004, B04 from now on; CDR; Brown et al. 2008). They also indicate that these ETGs are compatible with a sample resulting from a $K < 22.5$ selection. For the present article we will also use the PML estimate of the ETG LF obtained from the Extended Hubble Deep Field South (EHDF-S), increasing the area of this analysis to an area on the sky of approximately 0.5 square degrees.

We use the rest-frame r - and B -band PML LF estimates from MUSYC ETGs in ECDF-S and EHDF-S. For comparison we will also use the LFs measured using the classic maximum likelihood estimate that uses photometric- z measurements; these estimates are also provided by C09. All the ETG LFs are passively evolved down to $z = 0$ by applying an empirical passive evolution recipe whereby the evolved luminosity can be obtained via

$$M_B(z = 0) = M_B(z) + 1.15z, \quad (1)$$

as proposed by CDR, following results from van Dokkum & Stanford (2003), Treu et al. (2005), and diSerego Alighieri et al. (2005). P10 showed that this passive evolution recipe is well followed by a $[\text{Fe}/\text{H}] = 0.3$ single stellar population (SSP) which is 3.5 Gyr old at $z = 1$, and used this SSP to work out the equivalent recipe for the r -band, which is well fit by

$$M_r(z = 0) = M_r(z) + 0.98z. \quad (2)$$

We apply these evolution corrections to B - and r -band LF measurements from relatively high redshift samples, and compare them to results at $z \simeq 0.165$ from the Sloan Digital Sky Survey (SDSS; York et al. 2000) for ETGs by B04 in the B -band (selected using the red-sequence), and in the r -band by Benson et al. (2007, Be07), who selected ETGs as sources with a dominant bulge component (an alternative ETG LF measurement from SDSS is provided by Ball et al. 2006).

These luminosity function measurements will allow us to measure the space density of galaxies selected using limits in luminosity at different redshifts. The limiting luminosities will be selected using clustering information.

We use the clustering results from P10, in particular those for the MUSYC sample of galaxies corresponding to the brightest absolute magnitude cut, $M_R(0) < -19.7$ corrected by passive evolution, for samples of ETGs in ECDF-S and EHDF-S. As was shown by these authors, ETGs show a higher clustering than the samples that include all galaxy types. When comparing to the clustering of $z = 0$ ETG SDSS galaxies of different luminosities, and using the evolution of clustering of dark-matter haloes of different masses, P10 show that ETG samples of equal passively evolved luminosity (i.e. stellar mass selected) at different redshifts do not seem to be connected in a progenitor-to-descendant relationship. Luminous galaxies at $z \simeq 1.15$ with stellar masses $\simeq 10^{10} h^{-1} M_\odot$, evolve into objects with higher clustering than galaxies of similar rest-frame passively evolved luminosity at $z \simeq 0.35$. The present-day descendants of the bright volume-limited ECDF-S and EHDF-S $z = 1.15$ subsamples are roughly within $0.1 < L/L^* < 2.5$, with masses up to 10 times higher, $\simeq 10^{11} h^{-1} M_\odot$. Fig. 1 shows the $z = 0$ descendant stellar masses as obtained from the P10 results for progenitors at different redshifts.

3. Results and conclusions

We calculate the number density of $z = 0$ descendants using the B04 and Be07 SDSS ETG LFs, for galaxies with median luminosities corresponding to the descendants of a given sample of MUSYC ETGs at redshift z . The number density of progenitors is calculated at redshift z , using a lower limit in $M_r(z = 0) = -19.7$, or equivalently, $M_B(z = 0) = -18.55$, consistent with the lower limits used in P10. The results are shown as squares in the upper panel of Fig. 2 (open symbols for the B -band, filled symbols for the r -band). The error bars in this panel correspond to the uncertainties in the descendant luminosity, extracted from P10. As can be seen, the ratio is significantly higher than unity at $z > 0.6$ in both bands, indicating the need for mergers between ETGs in order to diminish their number density towards $z = 0$. Lower redshift samples show number densities similar to their expected descendants. As can be seen, the photometric- z -based maximum likelihood method (crosses, shown only for the r -band for clarity) provides results in agreement with those from the PML-based LFs.

Taking advantage of the measured LFs for the high-redshift ETG samples, we calculate the ratios between the luminosity densities of the high- z ETGs and that of their $z = 0$ likely descendants, using the PML and B04/Be07 LF measurements for the MUSYC and SDSS ETGs, respectively. This is shown in the lower panel of Fig. 2 as squares (solid symbols correspond to results in the r -band, open symbols to the B -band). As can be seen, regardless of the photometric band, the data show that as the redshift decreases, the ratio of luminosity densities of progenitor and descendant ETGs becomes consistent with the unit value (bear in mind that our different high redshift ETG samples are *not* in the same evolutionary line).

The results from this analysis show that ETGs at $z = 1$ are likely to descend into $z = 0$ ETGs undergoing a decrease in space density of a factor between 3 and 11 (the ranges cover the results from the B and r bands). But, due to the constant luminosity density, mergers would provide the required increase in luminosity without the need for important episodes of star formation. Notice that the amount of mergers derived here (of two or more mergers since $z = 1$ for each $z = 0$ galaxy) is higher than that estimated from close pairs of stellar mass selected samples at different redshifts; Robaina et al. (2010) find that galaxies undergo ~ 0.7 mergers between $z = 1.2$ and 0. We suggest that a more consistent measurement of merger rates using close pairs would require the use of samples in a more likely progenitor-descendant relationship than that provided by a stellar mass selection.

Upcoming surveys such as those planned for the Large Synoptic Survey Telescope (Abell et al., The LSST Science Book, 2009), will allow much better statistics by increasing the solid angle with respect to the currently available deep photometric surveys such as MUSYC and COMBO17. With a higher signal it will be possible to apply this method and measure with high accuracy the importance of mergers in the evolution of the ETG population. Furthermore, with a careful treatment of sources and sinks in the samples of progenitors and descendants, it could also be possible to produce measurements of the expected merger rates and star formation history of combined samples of early and late-type galaxies, and via comparisons with models of galaxy formation, help improve

our understanding of the evolution of galaxies from high redshifts to the present day.

Acknowledgments. This work was supported in part by Fondecyt Regular no. 1110328, by the "Centro de Astrofísica FONDAP" 15010003 and by project Basal PFB0609. The computations carried out in this work were performed using the Geryon cluster at the Centro de Astro-Ingeniería UC.

References

- Ball N., Loveday J., Brunner R., et al. 2006, MNRAS, 373, 845
Baugh C. M., Lacey C. G., Frenk C. S., et al. 2005, MNRAS, 356, 1191
Bell E., et al. 2004, ApJ, 608, 752
Benson A., Dzanovic D., Frenk C.S., et al. 2007, MNRAS, 379, 841
Benson A., Devereux N. 2010, MNRAS, 402, 2321
Brown M., Zheng Z., White M., et al. 2008, ApJ, 682, 937
Bruzual A., Charlot S., 1993, ApJ, 405, 538
Bundy K., et al. 2006, ApJ, 651, 120
Christlein D., Gawiser E., Marchesini D., et al. 2009, MNRAS, 400, 429
Cimatti A., et al. 2002, A&A, 381, L68
Cimatti A., et al. 2004, Nature, 430, 184
Cimatti A., Daddi E., Renzini A. 2006, A&A, 453, L29
Coleman G., Wu C., Weedman D. 1980, ApJS, 43, 393
Daddi E., et al. 2005, ApJ, 626, 680
Gawiser E., et al. (The MUSYC Collaboration) 2006, ApJS, 162, 1
Glazebrook K., et al. 2004, Nature, 430, 181
Holland W., et al., 1999, Nature, 392, 788
Lagos C., Cora S., Padilla N. 2008, MNRAS, 388, 587
Marchesini D., van Dokkum P. 2007, ApJ, 663, 89
Marchesini D., van Dokkum P., Forster Schreiber N.M., et al. 2009, ApJ, 701, 1765
Marchesini D. et al. 2010, ApJ, submitted, arXiv:1009.0269
McCarthy P.-J., et al. 2004, ApJ, 614, L9
Padilla N.D., Christlein D., Gawiser E., et al. 2010, MNRAS, 409, 184
Pérez-González P., et al. 2008, ApJ, 675, 234
Robaina A., Bell E., van der Wel A., et al. 2010, ApJ, 719, 844
Saracco P., et al. 2005, MNRAS, 372, L40
Treu T., et al. 2005, ApJ, 633, 174
van Dokkum P., Stanford S. 2003, ApJ, 585, 78
York D., et al. (The SDSS Team) 2000, AJ, 120, 1579

Contributed talks

Synthetic high-mass X-ray binary populations in a cosmological frame

M. C. Artale^{1,2}, L. J. Pellizza^{1,2}, P. B. Tissera^{1,2} and I. F. Mirabel^{1,3}

¹ *IAFE (CONICET/UBA), Buenos Aires, Argentina*

² *CONICET, Argentina*

³ *CEA-Saclay, IRFU/DSM/Service d'Astrophysique, France*

Abstract. High-mass X-ray binaries are systems constituted by a massive star and a compact object. The study of these systems is important to understand the origin and evolution of compact objects. Considering recent results from other authors, which propose a dependence of the number of these binary systems on their chemical abundances, we present a model for the populations of high-mass X-ray binaries in nearby galaxies grafted onto hydrodynamical cosmological simulations. The simulations include star formation and chemical evolution, which allow us to obtain a self-consistent description of the high-mass X-ray binary populations in galaxies. We investigate the properties of high-mass X-ray binary populations in our models, and compare them with those observed in nearby galaxies.

1. Introduction

High-mass X-ray binaries (HMXBs) are systems composed by a compact object (neutron star, NS or black hole, BH) and a massive companion star. In these systems the X-ray emission is due to the accretion of mass from the companion star onto the compact object via Roche lobe overflow or stellar wind capture. The matter reaches temperatures of several million Kelvin in the accretion process. For HMXBs, the companion star has a mass above $2.5M_{\odot}$ producing systems with lifetimes of about 10^6 – 10^7 yr (Fabbiano 2006), hence the X-ray emission occurs shortly after their formation (Shtykovskiy & Gilfanov 2007). This renders HMXBs potential star formation tracers in their host galaxies. Indeed, recent studies (Grimm et al. 2003, Mineo et al. 2012) found that the X-ray luminosity of star-forming galaxies correlates with their star formation rates (SFR).

Several studies have investigated the properties of HMXB populations using Monte Carlo schemes and considering stellar evolution (Belczynski et al. 2004; Dray et al. 2005; Linden et al. 2010). These authors have analyzed the chemical dependence of HMXBs populations, finding that the number of sources increases as the metallicity decreases. These results can be useful to study galaxy properties at high redshift and to comprehend their role in the early times of the Universe (Mirabel et al. 2011).

In this work, we investigate the properties of HMXBs in galaxies. Considering the metallicity as an important ingredient to regulate their production, we produce synthetic HMXB populations coupling the results of stellar population synthesis model to numerical hydrodynamical cosmological simulations of

galaxy formation, which include star formation and chemical evolution in a self-consistent way. In Sect. 2 and 3, we describe the simulations used to create a galaxy catalog, and our method to compute the HMXB populations respectively. Finally, in Sect. 4 we present our preliminary results.

2. Cosmological simulation

The galaxy catalog was developed using hydrodynamical cosmological simulations performed with a version of GADGET-3 which includes star formation, metal-dependent cooling, chemical enrichment, multiphase gas, and energy feedback by Type II and Type Ia Supernovae (Scannapieco et al. 2005, Scannapieco et al. 2006). The simulation represents a periodic volume of $10 \text{ Mpc} h^{-1}$ side and assumes a Λ -CDM cosmogony with cosmological parameters $\Omega_\Lambda = 0.7$, $\Omega_m = 0.3$, $\Omega_b = 0.04$, $\sigma_8 = 0.9$ and $H_0 = 100h \text{ km s}^{-1} \text{ Mpc}^{-1}$, with $h = 0.7$.

A Salpeter (1955) Initial Mass Function is considered with lower and upper masses cut-offs of $0.1M_\odot$ and $40M_\odot$, respectively. For progenitors of Type II supernovae, the code selects stars with masses greater than $8M_\odot$ and uses metal-dependent lifetimes, while for Type Ia Supernovae the code uses the W7 model of Thielemann et al. (1993) and a random uniform distribution for their lifetimes in the range $[0.1 - 1] \text{ Gyr}$. For details of the SN feedback algorithm see Scannapieco et al. (2006). Chemical enrichment is included in the code, which follows 12 isotopes: ^1H , ^2He , ^{12}C , ^{16}O , ^{24}Mg , ^{28}Si , ^{56}Fe , ^{14}N , ^{20}Ne , ^{32}S , ^{40}Ca and ^{62}Zn (Mosconi et al. 2001) and adopts metal-dependent yields of Woosley & Weaver (1995).

A FoF technique was applied to select virialized structures, and the substructures were identified with the SUBFIND algorithm (Springel 2001) to produce the galaxy catalog. The mass-metallicity relation of the simulated galaxies was studied by De Rossi et al. (2010), finding discrepancies at low redshifts with the results of Tremonti et al. (2004). For this reason, we renormalized the abundances of the simulated galaxies using the results of Maiolino et al. (2008), and obtaining a good agreement with the observed mass-metallicity relation at different redshifts.

3. Synthetic population

We generate a synthetic population of HMXBs assuming that only young stellar populations can produce these kind of sources, since the companion star is a massive star (with lifetimes $\sim 10^{6-7} \text{ yr}$).

Using a Salpeter (1955) Initial Mass Function and the stellar evolution model discussed in Georgy et al. (2009), we estimate the number of BH and NS in the selected stellar populations according to their metallicity. Nevertheless only a fraction of these compact objects will be in binary systems with a massive star companion. Belckynski et al. (2004) studied the chemical dependence of this fraction using synthetic models through a Monte Carlo technique, noticing an increase of the BH binary number as metallicity decreases. We use their fractions to compute the number of compact objects in HMXBs. In this way, our model includes the metallicity dependence of the number of compact objects and binary fraction produced by each stellar population in the simulated galaxy

catalog. The detectability is included by assuming an X-ray luminosity function (Fabbiano 2006), and lower luminosity cut-offs depending on the galaxy SFR to reproduce the correlation of the sample of Mineo et al. (2012).

The total number of HMXBs is then normalized by requiring our model to reproduce available observations (Mineo et al. 2012). The normalization factor represents astrophysical phenomena that we can not model such as the exact lifetime and duty cycle of the X-ray emission.

4. Preliminary results

In this work, we investigate the HMXB populations in star forming galaxies, using the results of stellar population synthesis models from Belczynski et al. (2004) and Georgy et al. (2009), coupled to numerical hydrodynamical cosmological simulations of galaxy formation. We take into account the chemical dependence of the HMXB progenitors in galaxies, considering the dependence of the number of HMXB on the metallicity of stellar populations. We also take into account the detectability of these sources in order to compute the observable number of sources and X-ray luminosity of each galaxy.

For nearby galaxies we reproduce the observed trend of increasing number of sources with increasing SFR, which allows us to normalize the HMXB populations to take into account the effects of the duty cycle of the binaries. The normalized model shows a good agreement with observations of the X-ray luminosity of nearby galaxies as a function of star formation rate.

Our preliminary results suggest that the HMXB populations of the galaxies in the local Universe are well described by our scenario. A more stringent tests are underway which will allow us to predict their evolution with redshift (Artale et al., in preparation).

References

- Belczynski, K., Sadowski, A., Rasio, F. 2004, *ApJ*, 611, 1068
De Rossi, M. E., Tissera, P. B. 2010, *Proc. IAU Symp.* 262, p.325
Dray, L. M. 2006, *MNRAS*, 370, 2079
Georgy, C., Meynet, G., Walder, R., et al. 2009, *A&A*, 502, 611
Grimm, H. J., Gilfanov, M., Sunyaev, R. 2003, *MNRAS*, 339, 793
Fabbiano, G. 2006, *ARA&A*, 44, 323
Linden, T., Kalogera, V., Sepinsky, J. F., et al. 2010, *ApJ*, 725, 1984
Maiolino, R., Nagao, T., Grazian, A., et al. 2008, *A&A*, 488, 463
Mineo, S., Gilfanov, M., Sunyaev, R. 2012, *MNRAS*, 419, 2095
Mirabel, I. F., Dijkstra, M., Laurent, P., et al. 2011, *A&A*, 528, 149
Mosconi M. B., Tissera P. B., Lambas D. G., et al. 2001, *MNRAS*, 325, 34
Salpeter, E. E. 1955, *ApJ*, 121, 161
Scannapieco, C., Tissera, P. B., White, S. D. M., et al. 2006, *MNRAS*, 371, 1125
Scannapieco C., Tissera P. B., White S. D. M., et al. 2005, *MNRAS*, 364, 552
Shtykovskiy, P. E., Gilfanov, M. R., 2007, *AstL*, 33, 437

- Springel, V., White, S. D. M., Tormen, G., et al. 2001, MNRAS, 328, 726
- Tremonti, C. A., Heckman, T. M., Kauffmann, G., et al. 2004, ApJ, 613, 898
- Thielemann, F. K., Nomoto, K., Hashimoto, M. 1993, in Prantzos, N., Vangoni-Flam, E., Cassé, N. (eds.) "Origin and evolution of elements". Cambridge Univ. Press, p.299
- Woosley, S. E., Weaver, T. A. 1995, ApJS, 101, 181

Towards a panchromatic picture of galaxy evolution during the reionization epoch

Jaime E. Forero-Romero¹, Gustavo Yepes², Stefan Gottlöber³
and Francisco Prada^{4,5,6}

¹*Department of Astronomy, UCB, Berkeley, USA*

²*Grupo de Astrofísica, UAM, Madrid, Spain*

³*AIP, Potsdam, Germany*

⁴*Campus of International Excellence UAM+CSIC, Madrid, Spain*

⁵*Instituto de Física Teórica, (UAM/CSIC), Madrid, Spain*

⁶*IAA (CSIC), Glorieta de la Astronomía, Granada, Spain*

Abstract. There are thousands of confirmed detections of star forming galaxies at high redshift ($z > 4$). These observations rely primarily on the detection of the spectral Lyman Break and the Lyman- α emission line. Theoretical modelling of these sources help to interpret the observations in the framework of the standard cosmological paradigm. We present results from the *High- z MareNostrum Project*, aimed at constructing a panchromatic picture of the high redshift galaxy evolution that will improve our understanding of young star forming galaxies. Our simulation successfully reproduces the observational constraints from Lyman Break Galaxies and Lyman- α emitters at $5 < z < 7$. Based on this model we make predictions on the expected far infrared emission that should be observed for Lyman- α Emitters. These predictions will help to settle down the question on the dust content of massive high- z galaxies, an issue that will be feasible to probe observationally with the Atacama Large Millimetre Array.

1. Introduction

Observationally, there are two main ways to detect high redshift star forming galaxies. The first technique uses broad band measurements in order to detect the drop in flux due to the Lyman Break in the spectral energy distribution (SED) of the galaxy. Galaxies detected through this technique receive the name of Lyman Break Galaxies (LBGs). The second technique aims at detecting the Lyman- α emission line either by narrow band filtering techniques or by direct spectral measurements. Galaxies detected through this selection technique receive the name of Lyman- α Emitters (LAEs). Some of the high- z LBGs have also been detected in their rest-frame near-IR, which allows to provide an estimation of their stellar masses.

In this work we describe our efforts to build a panchromatic picture of high- z galaxies at $5 < z < 7$. Our work is based on the results from a large hydrodynamical simulation that follows the gravitational collapse of dark matter and gas, and includes radiative processes and the ensuing star formation, together with associated chemical and mechanical feedback from exploding stars. Based

on the analysis of the simulated galaxies, we have proposed a model to account for the dust extinction and the radiative transfer of the Lyman- α line. We have shown how this model is in fair agreement with the observed properties of LBGs and LAEs (Forero-Romero et al. 2010, 2011). Special attention was paid to the reproduction of the observed fraction of LBGs with a strong Lyman- α emission (Forero-Romero et al. 2012). In what follows, we will describe the main features of our model and will conclude by pointing out the expected trends for the FIR emission that will be probed by the Atacama Large Millimetre Array (ALMA) in the near future.

2. Simulation and galaxy finding

The High-Z MareNostrum Simulation follows the nonlinear evolution of a cubic region of $50 h^{-1}$ Mpc (comoving) on a side. The dark matter and gas distributions are sampled with 1024^3 particles for each component. The gas physics includes radiative cooling and photoionisation from an homogeneous UV background switched on at $z = 6$. Star formation and feedback (chemical and dynamical) are included following the Springel and Hernquist (2003) model. We identified all gravitationally bound objects using the Amiga Halo Finder (Knollman & Knebe 2009). All objects with at least 1000 particles are kept for further analysis. More details can be found in Forero-Romero et al. (2010).

3. Modelling the UV continuum and the Lyman- α line

The stellar SED is constructed from the stellar particles contained in the galaxies detected as described in Sect. 2. The main assumption under this calculation is that each stellar particle in the simulation can be treated as a burst of star formation with a given mass, age and metallicity. We assume a constant Salpeter initial mass function (IMF).

We implement a phenomenological model to quantify the extinction produced by dust in the stellar SED. The physical model assumes that extinction can be divided into two contributions that affect different stellar populations of different ages. Old stellar populations have an effective extinction from an homogeneous interstellar medium (ISM), while young stellar populations suffer additional extinction due to the molecular clouds in which they are embedded at birth.

The calculation of the escape fraction of Lyman- α radiation assumes the same geometry as the UV continuum extinction. We have developed the Monte Carlo radiative transfer code CLARA to follow the path of Lyman- α photons through the ISM in simplified geometrical configurations. Details of the implementation of this model can be found elsewhere (Forero-Romero et al. 2011).

4. Results

- **LBGs, LAEs and stellar masses:** Our numerical results for the luminosity function (LF) for LBGs are in good agreement with the observational results. Only a minor disagreement is noticeable at the faint end

of the luminosity function, where there seems to be an overabundance of simulated dwarfs with respect to the observations. UV colours as parameterised by the β slope as a function of restframe UV magnitudes are also in agreement with the results derived from observations. This shows that the dust correction we have applied to the simulated galaxies is reasonable (Forero-Romero et al. 2010). The simulated LF of LAEs shows a good agreement with observations at the bright end, while showing an overabundance at the faint end, which is somewhat more noticeable than in the restframe UV (Forero-Romero et al. 2011). Recently, we have shown that the stellar masses as a function of intrinsic UV luminosities are also in good agreement with the observational estimates, at least for the most massive systems (Forero-Romero et al. 2012b).

- **LBGs as LAEs:** As part of an international observational effort to probe the reionisation epoch using LAEs and LBGs, a new kind of observations were conducted. Galaxies detected primarily as LBGs were then followed up spectroscopically. From these measurements one can determine whether a LBG is also a LAE by requiring the Lyman- α equivalent width to be larger than a fixed threshold value. Using these results we can consider now a new kind of statistic, the fraction of LBGs showing strong Lyman- α emission, $X_{\text{Ly}\alpha}$. The results from our simulations, without any further change, fully agree with the observational measurements of this fraction. We have also shown that the Lyman- α escape fraction decreases with galaxy mass (Forero-Romero et al. 2012).
- **FIR Emission** For each galaxy in the simulation we calculate the expected flux in the ALMA band at 353 GHz as a function of the observed Lyman- α luminosity. We find that the brightest LAEs do not have a high FIR luminosity, passing completely undetected by ALMA (Fig. 1). This prediction of our model can be quantitatively understood as follows. Bright galaxies in the FIR have a high star formation rate and dust mass contents. These high dust values and neutral hydrogen associated with the most massive FIR bright galaxies naturally correspond to very low escape fractions.

5. Conclusions and outlook

We have constructed a model for high redshift galaxies (LBGs and LAEs) based on the results of the *High- z MareNostrum Simulation*. From the numerical results we are able to estimate the observed restframe UV and Lyman- α emission in these galaxies.

We find that our results are broadly consistent with the current observational constraints. The largest discrepancy is an overabundance in the faint end LF, both for LBGs and LAEs. The agreement between our model and observations for objects brighter than $M_{\text{UV}} < -20$ is remarkable.

We also predict the expected flux at 353 GHz as a function of the observed Lyman- α emission. In our model, the brightest LAE galaxies are too faint FIR emitters. Correspondingly, bright IR sources will be detected by ALMA, but they will not be detected as bright LAEs.

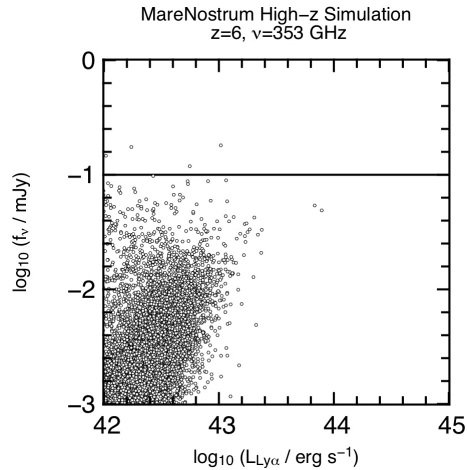


Figure 1. Flux in the ALMA band at 353 GHz as a function of the observed Lyman- α emission. The horizontal line represents the threshold for detection. In our model the brightest Lyman- α galaxies won't be detected by ALMA.

Acknowledgments. J.E. F-R is supported by the Peter and Patricia Gruber Foundation, through their fellowship administered by the International Astronomical Union. We thank the Barcelona Supercomputing Center for giving us access to the MareNostrum Supercomputer. We also thank MICINN (Spain) for financial support under projects AYA2009-13875-C03-02 and FPA2009-08958.

References

- Forero-Romero J. E., Yepes G., Gottlöber S., et al. 2010, *MNRAS*, 403, L31
 Forero-Romero J. E., Yepes G., Gottlöber S., et al. 2011, *MNRAS*, 415, 3666
 Forero-Romero J. E., Yepes G., Gottlöber S., et al. 2012, *MNRAS*, 419, 952
 Forero-Romero J. E., Yepes G., Gottlöber S., et al. 2012b, *MNRAS* sub.
 Knollmann S. R., Knebe A., 2009, *ApJS*, 182, 608
 Springel V., Hernquist L., 2003, *MNRAS*, 339, 289,

On the mass assembly of sub-Milky-Way galaxies

A. González-Samaniego¹ and V. Avila-Reese¹

¹*Instituto de Astronomía, UNAM, México, D.F., México*
(ags@astro.unam.mx)

Abstract. The emerging empirical picture of galaxy mass assembly seems to be in conflict with current models/simulations based on the Λ CDM scenario, specially for sub-Milky-Way galaxies. In order to get insight into this potential issue, we developed a parametric Λ CDM-based model for calculating average star formation rates, and halo and stellar mass (M_h and M_s) assembly histories of galaxies as a function of mass. The parameters of the model are constrained with the observed star formation rate- M_s and M_s - M_h relations out to $z \sim 3$.

1. Introduction

Recent observational works helped us to understand how the stellar mass build-up proceeds in galaxies: the lower the stellar mass (M_s), the higher is the specific star formation rate (sSFR = SFR/ M_s) on average at least up to $z \sim 1$ (*downsizing in sSFR*; e.g., Salim et al. 2007; Karim et al. 2011). This implies that the assembly of M_s occurs later as the smaller is the mass. On the other hand, the halo mass assembly in the Λ CDM scenario is by *hierarchical clustering*, with the smallest halos forming on average earlier than the larger ones (an *upsizing trend*). Then, the smaller the halo mass M_h , the more delayed is the M_s growth of the galaxy (e.g., Firmani & Avila-Reese 2010), a trend that is difficult to reproduce in current numerical simulations of galaxy evolution (e.g., Avila-Reese et al. 2011). In this work, we present a “toy model” aimed to quantify the deviations of the average galaxy stellar mass growth from that of the halo as a function of mass and redshift. Since these inferences are based on observations, they help to constrain the physical processes involved in galaxy evolution and serve as a guide to evaluate the results from numerical simulations.

2. The model and results

We start by assuming that the baryonic infall rate is driven by the dark matter halo aggregation rate, $\dot{M}_{\text{bar}}(z) = f_{\text{b,u}} \times \dot{M}_h(z)$, where $f_{\text{b,u}} \approx 0.17$ is the universal baryonic fraction, and $\dot{M}_h(z)$ is the average halo mass aggregation rate taken here from the fits to the Millennium simulation as a function of mass and z by Fakhouri et al. (2010; their Eqn. 2). Our second step is to define the galaxy SFR as a function of M_h and z as:

$$\text{SFR}(M_h, z) \equiv \dot{M}_{\text{bar}} \times T(M_h, z) \times \epsilon, \quad (1)$$

where $T(M_h, z)$ represents the “stellar deviation function” and ϵ is the normalization (efficiency). The deviation function encodes all the highly complex astrophysical mechanism that affect the M_s assembly in galaxies. We assume that it affects galaxies of different masses in a different way: for low-mass galaxies, mainly the UV background and the stellar-driven feedback reduce systematically the amounts of SF, and for high masses, the longer gas cooling times as well as the AGN-driven feedback, diminish the possibility of SF, too. Accordingly, for simplicity we assume that $T(M_h, z)$ is a double power law,

$$T(M_h, z) = \frac{2T_0}{\left[\left(\frac{M}{M_1} \right)^{-\alpha} + \left(\frac{M}{M_1} \right)^{\beta} \right]}, \quad (2)$$

normalized in such a way that $T(M_{\max}, z) = 1$, where M_{\max} is the mass at which the function has its maximum; it is related to the other parameters by $M_{\max} = (\alpha/\beta)^{1/(\alpha+\beta)} M_1$. In addition, we allow the parameters to change with time as linear functions of $\log(1+z)$ and $(1+z)$ for α and β , respectively, and $\propto c_1 + c_2(1+z)^\gamma$ for M_{\max} . In the following, we assume that M_s actually grows by in-situ and ex-situ modes; the latter represents the accretion of stars formed outside the galaxy and assembled to it by mergers,

$$\Delta M_s = \text{SFR} \times \Delta t \times (1 - R) + \Delta M_{\text{ex}}(M_h, z), \quad (3)$$

where $R = 0.5$ is the recycling factor due to stellar mass loss. We assume that the SFR is constant over a period of $\Delta t = 0.1$ Gyr. The ex-situ mode is parameterized by a function that increases with mass and time since $z \sim 2$.

By generating a grid of evolutionary tracks, the parameters of the toy model are constrained to fit the empirical sSFR- M_s and M_s - M_h relations (isochrones) out to $z \sim 3$ (Fig. 1). In spite of the several free parameters, this task is not easy: (1) There is a tension at low masses between the steep sSFR- M_s relation and the relatively slow evolution of the M_s/M_h - M_h relation; however, recent new inferences of the latter relation by Yang et al. (2011) show a faster evolution. (2) It is difficult to fit the M_s/M_h - M_h high-mass slopes (Fig. 1, bottom panel); the shift with z of the peak of this relation and the drop in the sSFR for high masses require such slopes. (3) An increasing with mass of the ex-situ M_s growth contribution is required (Fig. 2, left panel) in order to reproduce the peak decrease in the M_s/M_h - M_h relation with z (up to $z \sim 2$). This left panel resumes the results of our approach, showing the average M_s growth of galaxies as a function of mass: while massive galaxies finished their growth by SF in the remote past (they grow yet a little but by dry mergers), the lowest mass galaxies are actively growing by SF at late epochs. Results from cosmological numerical simulations by de Rossi et al. (2012, in prep.) show this trend, but not as pronounced as our inference.

The best fit to observations of the Λ CDM-based parametric model (Fig. 1) was attained with the stellar deviation functions and efficiencies shown in Fig. 2, right panel. They are strongly dependent on mass and z . The M_h where the galaxy formation efficiency is maximal, M_{\max} , decreases with time, and this peak efficiency is roughly the same at all epochs. At $z = 0$, $M_{\max} \approx 2.5 \times 10^{11} M_\odot$ ($M_s \approx 6 \times 10^9 M_\odot$). For individual evolutionary tracks, the more massive the present-day galaxy, the higher the z at which it has its maximum

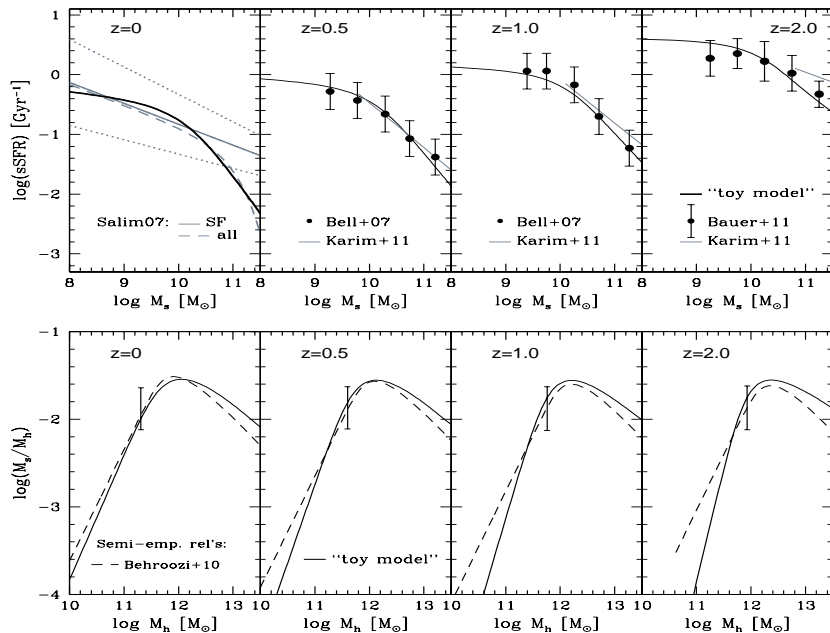


Figure 1. *Top*: sSFR vs M_s at $z = 0.0, 0.5, 1.0$ and 2.0 (solid black lines) as given by the best “constrained toy model”. The grey solid line at $z = 0$ is the linear fit carried out by Salim et al. (2007) to the sub-sample of star-forming galaxies from $\sim 50,000$ SDSS galaxies (the intrinsic scatter is shown with dotted lines), while the long-dashed line is the fit to the entire sample. The points and fit lines in the high-redshift panels correspond to different observational estimates reported in the works indicated inside the panels. *Bottom*: Stellar mass fractions vs M_h (solid black line). The long-dashed curves in each panel are semi-empirical inferences as reported in Firmani & Avila-Reese (2010) based on Behroozi et al. (2010). The error bars represent the typical 1σ uncertainty of these inferences.

galaxy formation efficiency. Galaxies less massive than $M_s \approx 3 \times 10^9 M_\odot$ did not yet attain this maximum, i.e. their efficiencies are yet increasing.

3. Conclusions

By means of a Λ CDM-based evolutionary “toy model” we showed that:

- the observed “downsizing trends” can be reproduced if strong mass and z dependent deviations from CDM halo mass aggregations rates are introduced. These deviations are physically motivated (see Sect. 2, after Eqn. 1) but at lower masses are probably too extreme (new astrophysical mechanisms might be required).
- it is difficult to reconcile the observed high sSFRs of low-mass galaxies since $z \sim 1$ with the inferred evolution of their M_s/M_h ratios.

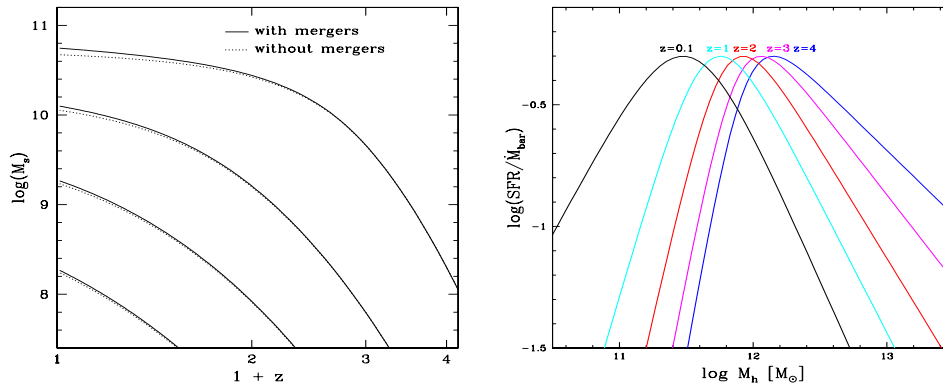


Figure 2. *Left:* Mass aggregation histories for the constrained toy model considering both modes of increment in M_s (solid lines), and only with the in-situ mode (dotted lines). *Right:* Star formation efficiency ($\text{SFR}/\dot{M}_{\text{bar}}$) as function of M_h for different z .

What is behind the delay of stellar mass assembly in low-mass galaxies (*downsizing in sSFR*)? It is possible that molecular gas formation is systematically delayed in low-mass low-metallicity galaxies (e.g., Krumholz & Dekel 2011), or that the local SFR is less efficient in these small systems at higher redshifts. It should be also taken into account that the SFR, at lower masses could proceed in more bursting episodes; hence, the measured SFRs represent only the "on" population giving this rise to the steep sSFR– M_s relations. A more radical possibility is that the underlying Λ CDM scenario needs a modification related to the mass assembly of low-mass halos.

Acknowledgments. We thank the LOC for partial support to us for attending the Workshop. A.G-S acknowledges to DGEP-UNAM, for partial support and to DGAPA-UNAM for a PhD fellowship.

References

- Avila-Reese, V., Colín, P., González-Samaniego, A., et al. 2011, ApJ, 736, 134
 Bauer, A. E., et al. 2011, MNRAS, 417, 289
 Behroozi, P. S., Conroy, C., & Wechsler, R. H. 2010, ApJ, 717, 379
 Bell E. F. et al. 2007, ApJ, 663, 834
 Fakhouri, O., Ma, C.-P., & Boylan-Kolchin, M. 2010, MNRAS, 406, 2267
 Firmani, C., & Avila-Reese, V. 2010, ApJ, 723, 755
 Fontanot, F., De Lucia, G., Monaco, P., et al. 2009, MNRAS, 397, 1776
 Karim, A. et al. 2011, ApJ, 730, 61
 Krumholz, M. R., & Dekel, A. 2011, arXiv:1106.0301
 Salim, S., Rich, R. M., Charlot, S., et al. 2007, ApJS, 173, 267
 Yang, X., Mo, H. J., van den Bosch, F. C., et al. 2011, arXiv:1110.1420

On the size evolution of early type galaxies

Gian Luigi Granato¹, Cinthia Ragone-Figueroa² and Mario G. Abadi²

¹*Istituto Nazionale di Astrofisica INAF, OATS, Trieste, Italy*

²*IATE, CONICET-Observatorio Astronómico, Córdoba, Argentina*

Abstract. We present numerical simulations of the effect of baryonic mass loss on the structure of a spheroidal stellar system, embedded in a dark matter halo. This process, invoked as a possible explanation of the observed size increase of early-type galaxies since $z \sim 2$, could be caused either by quasi-stellar objects/starburst driven galactic winds, promptly ejecting from early-type galaxies the residual gas and halting star formation (galactic winds), or by stellar mass returned to the interstellar medium (ISM) in the final stages of stellar evolution. Indeed, we find that a conceivable loss of $\sim 50\%$ of the baryonic mass can produce a significant size increase. However, the puffing up due to galactic winds occurs when the stellar populations are much younger than the estimated ages > 0.5 Gyr of compact high- z early-type galaxies. Therefore, while it may have had a role in deciding the final structure of early-type galaxies, it cannot explain the evolution observed so far of their size-mass relation. Conversely, the mass loss due to stellar evolution could cause a modest expansion of passively evolving stellar systems, contributing to, without dominating, the observed evolution of their mass-size relationship.

1. Introduction

During the last years, it has been established that most massive early-type galaxies (ETGs) observed at redshift $z \gtrsim 1$ exhibit sizes smaller by a factor of a few than local ETGs of analogous stellar mass. Nowadays most authors agree that the observational results are dominated by a real size evolution, rather than by some subtle systematic effect. Proposed interpretations are related either to the effects of mergers or to the loss of a substantial fraction of mass from the galaxy.

The only promising *merging* mechanism to explain the size increase seems to be a series of minor dry merging events. Indeed, in *wet* mergers, the presence of a dissipative gas component limits the gain in size, while major dry mergers move galaxies too slowly toward the local size-mass relationship (the size increases linearly with the mass) to explain the evolution in a reasonable number of events. By converse, minor dry mergers would add stars in the outer parts of passive high- z galaxies, in such a way to produce a size increase that can scale, optimistically, as steep as M^2 . However, recent detailed analysis concluded, from different points of view, that even minor mergers fall short to explain the observed size evolution, particularly at redshift greater than 1.5 (Newman et al. 2012; Nipoti et al. 2012; but see e.g., Lopez et al. 2012).

In this context, we tested, by means of controlled numerical experiments, the possible contribution of the *puffing-up* process. This envisages that the expansion in size is driven by the expulsion of a substantial fraction of the gas out of the galaxy either by active galactic nuclei (AGN) and/or supernova (SN) driven galactic winds (Fan et al. 2008), or by the expulsion of gas associated to stellar evolution (Damjanov et al. 2009). In the former case the expulsion timescale would be short, likely not much longer than the dynamical timescale, at least when driven by the AGN, whilst in the latter an important mass loss could last even $\sim 0.5 - 1$ Gyr. Virtually all modern models of galaxy formation give a prominent role to AGN and/or SNe driven galactic winds, ejecting from the galactic region a substantial fraction of gas. Thus, it is very likely that this puffing up played a role in deciding the final sizes of ETGs, at some point over their history. However, it is still an open question whether this role has been major, and, in particular, whether it can explain the available observations. Additionally, during the passive evolution of ETGs, it is conceivable that they have lost another significant fraction of its baryonic mass, due to stellar evolution (supernova explosions and stellar winds). The aim of the present work is to provide a step to clarify these issues.

2. Numerical method and setup

We refer the reader to Ragone & Granato (2011) and to Ragone, Granato & Abadi (2012) for all the technical details of our simulations, providing here just a quick overview. The purpose is to investigate the evolution of collision-less particles (stars and dark matter – DM) under a change of gravitational potential due to a loss of baryonic mass of the system. The escaping mass can be either the gas which has not been converted into stars during the star forming phase of the spheroid, or the mass lost by stars in the form of stellar winds and SNe explosions. In any case, we assume as given, and due to causes external to the simulations (such as SNe and AGN feedback, or stellar evolution), the temporal dependence of this mass loss, and we simulate the ensuing evolution of collision-less mass distributions. Therefore we don't have to treat the gas dynamics.

We used the N -body code *GADGET-2* (Springel 2005) to perform simulations with 10^6 particles. The density distribution of DM particles follows the NFW shape, while for the baryonic particles (stars and gas), we adopted a Hernquist profile. Given the density runs, we obtain the 1D velocity dispersion by integrating the Jeans equation. Starting from this initial setup, we introduce a mass loss, intended to emulate the various possible effects described above, by removing exponentially over an ejection time Δt a fraction $1 - \epsilon$ of the baryonic mass. The mass loss is attained by decreasing in time the mass of the baryonic particles. After the end of the mass loss period Δt , we let the system to evolve till it reaches a new equilibrium configuration.

The initial conditions have been thought to get a configuration, after the loss of a substantial fraction of baryons, consistent with our basic knowledge of the properties of local large ETGs. Thus, we adopted a reference value for the initial ratio of virial mass to baryonic mass is $M_{\text{vir}}/M_{\text{B}}(t = 0) = 25$. We set $M_{\text{vir}} = 10^{13} M_{\odot}$ in all simulations. We adopt a concentration parameter $c = 4$, a typical value at galactic halo formation, and $R_{\text{vir}} \simeq 170$ kpc, as expected for

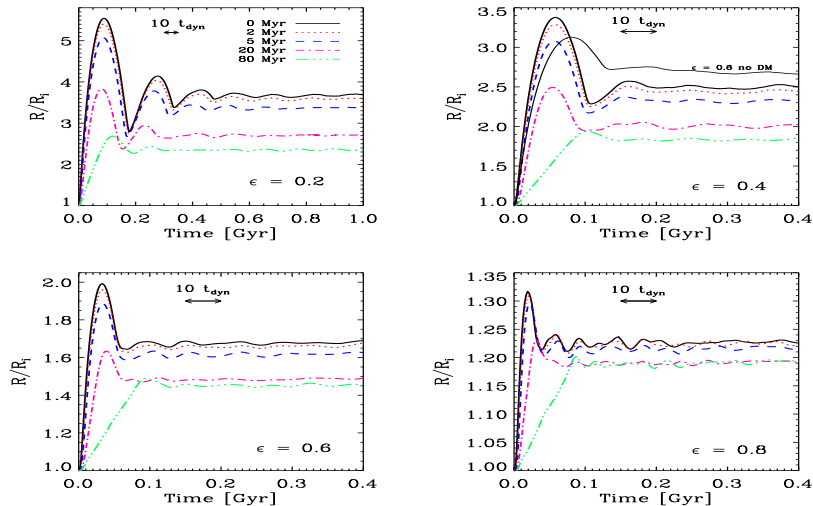


Figure 1. Ratio R/R_i of the current to the initial half-mass radius as a function of time, for different values of the diet parameter ϵ and of the ejection times Δt (from Ragone & Granato 2011).

a $M_{\text{vir}} = 10^{13} M_{\odot}$ halo virialized at $z = 3$. The baryon scale-length has been set to $a = 1.5$ kpc ($R_e \simeq 2.7$ kpc). Assuming that about half of the initial baryonic mass is in the form of stars, the system would lie initially a factor $\simeq 2.5$ below the local mass-size relationship for ETGs. The parameters affecting the results of our simulations are the ratios $M_{\text{vir}}/M_{\text{B}}(t = 0)$ and R_{vir}/a ; the fraction of baryonic mass lost ($1 - \epsilon$), and the time Δt over which the loss occurs. We performed simulations covering broad ranges of the latter two quantities, while in most runs we kept the former two at the values reported above. None of our conclusions is affected by reasonable variations of them.

3. Results: why puffing up cannot explain observed size evolution

Fig. 1 reveals the main problem to explain the *observed* size evolution of ETGs with the puffing-up scenario. On the one hand, our simulations confirm that, even in presence of a DM component, a factor ~ 2 increase in size can be expected in any galaxy formation model in which the spheroid quickly loses $\sim 50\%$ of its baryonic mass. However, if this mass is constituted by the star-forming gas, in scenarios in which a galactic wind suddenly sterilizes the galaxy, the puffing-up occurs far too close to the last episode of star formation. The galaxy is predicted to be smaller than the final size only for a very short time after expulsion, less than $\sim 20 - 30$ Myr, i.e. a factor 20 less than the minimum estimated ages of the stellar populations in high- z compact galaxies ($> 0.5 - 1$ Gyr). Even in the case of expansion driven by stellar mass loss the problem of the excessive shortness of the expansion timescale is important, though less clear cut (see Ragone & Granato 2011 for details).

To better illustrate this, Fig. 2 shows the result of a sample simulation, applied to a specific semi-analytic galaxy formation model including both processes

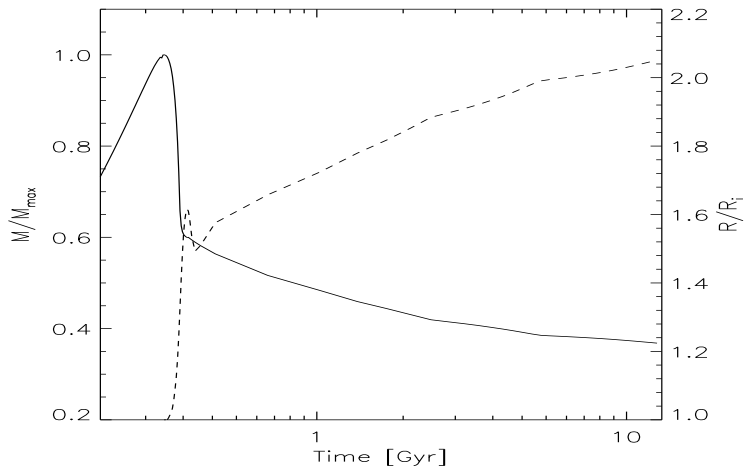


Figure 2. Evolution of the total baryonic mass (star forming gas+stars) in an ETG, according to the Granato et al. (2004) model for co-evolution of SMBH and spheroids (solid line, left axis), and the corresponding size increase (dashed line, right axis) predicted by our simulation (from Ragone & Granato 2011).

(Granato et al. 2004). The abrupt decrease of the mass after ~ 0.3 Gyr marks the ejection of gas by the AGN-driven wind. The later slow decrease of mass and moderate increase in size, is due to stellar mass returned to the ISM, assuming that the galaxy potential cannot retain it. The size expansion achieved after the epoch in which stellar populations are older than $\sim 0.5 - 1$ Gyr is about 20%,

In conclusion, the puffing up related to large scale galactic winds, quickly ejecting a substantial fraction of colored the baryonic mass, can be an important phenomenon, but is still not observed. By converse, the secular adiabatic expansion, related to the mass returned to the ISM by dying stars, could contribute, but not dominate, the observed size evolution of ETGs. Nevertheless, it is relevant to investigate this contribution, since it seems that none of the processes considered so far can explain alone the expansion (e.g., Newman et al. 2012; Nipoti et al. 2012).

References

- Damjanov, I., et al. 2009, ApJ, 695, 101
 Fan, L., Lapi, A., De Zotti, G., et al. 2008, ApJ, 689, L101
 Granato, G.L., et al. 2004, ApJ, 600, 580
 Newman A. B., Ellis R. S., Bundy K., et al. 2012, ApJ, 746, 162
 Nipoti C., et al. 2012, arXiv, arXiv:1202.0971
 Ragone-Figueroa C., Granato G. L., 2011, MNRAS, 414, 3690
 Ragone-Figueroa C., Granato G. L., Abadi M. G., 2012, MNRAS, 423, 3243
 Springel V., 2005, MNRAS, 364, 1105

PEGAS: Hydrodynamical code for numerical simulation of the gas components of interacting galaxies

Igor Kulikov

*Institute of Computational Mathematics and Mathematical Geophysics
SB RAS, Novosibirsk, Russia*

Abstract. A new hydrodynamical code for numerical simulation of the gravitational gas dynamics is described in the paper. The code is based on the Fluid-in-Cell method with a Godunov-type scheme at the Eulerian stage. The numerical method was adapted for GPU-based supercomputers. The performance of the code is shown by the simulation of the collision of the gas components of two similar disc galaxies in the course of the central collision of the galaxies in the polar direction.

1. Introduction

The movement of galaxies in dense clusters turns the collisions of galaxies into an important evolutionary factor, because during the Hubble time an ordinary galaxy may suffer up to 10 collisions with the galaxies of its cluster. The gas component plays a major role in the scenario of the collision of galaxies (Tutukov et al. 2011).

During the last 15 years, for the solution of astrophysical flow problems, two main approaches were employed from the wide range of the hydrodynamical methods: The Lagrangian smoothed particle hydrodynamics (SPH) method, and the Eulerian methods with adaptive mesh refinement (AMR). Based on the SPH method, the following simulation packages were developed: Hydra (Pearcea & Couchman 1997), Gasoline (Wadsley et al. 2004), GrapeSPH (Matthias 1996), GADGET-2 (Springel 2005). Using the Eulerian methods (in some cases with adaptive mesh refinement), the following packages were implemented: AMR-CART (Walder & Folini 1996), NIRVANA (Ziegler 2005), FLASH (Mignone et al. 2005), ENZO (Bryan & Norman et al. 2005), RAMSES (Teyssier 2002), ART (Kravtsov et al. 2002), Athena (Stone et al. 2008), Pencil Code (Brandenburg & Dobler 2002), ZEUS-MP (Norman et al. 2006), GAMER (Schive et al. 2010). The packages BETHE-Hydro (Murphy & Burrows 2008) and AREPO (Springel 2010) are implemented by means of a combination of Eulerian and Lagrangian methods. The main properties of the widely used software packages are given in Table 1.

2. The system of equations for gravitational gas dynamics

Let us consider the 3D model for self-gravitating gas dynamics in a Cartesian coordinate system. The model involves the overdetermined system of gas dynamics equations in the divergence form. The system is closed with the ideal gas equation of state. The system of gas dynamics equations is supplemented

by the Poisson equation for the gravitational potential, by the cooling function, and also by the contribution to the potential from the central body (Vshivkov et al. 2011a).

The stellar component and the dark matter of the galaxies is simulated by a single central body that has the shape of an ellipsoid with the given mass M . The central body also contributes to the general value of the potential. This contribution is set by an analytical expression (Tutukov et al. 2011).

The galactic gas, that was heated during the collision up to the temperature $\sim 10^4 - 10^8 K$, cools with the course of time. The plasma cooling rate estimated with the temperature over $\sim 10^4$ is $\epsilon_c \simeq 10^{-22} n^2 \text{ erg cm}^{-3}$, where n is the plasma density given as the number of hydrogen atoms in a cubic centimeter (Sutherland & Dopita 1993).

3. Numerical method description

Let us introduce a uniform grid in the 3D computational domain. The method for the solution of gas dynamics equation is based on the Fluid-in-Cell method. The initial system of equations of gas dynamics is solved by the two, Eulerian and Lagrangian stages.

3.1. The Eulerian stage

At the first, Eulerian stage, the system of equations describes the changing of gas values in the arbitrary flow domain due the the pressure forces and also due to the difference of potential and to the cooling. The modification of the Eulerian stage is done by the employment of the Godunov type scheme. It means that at all the boundaries of the computational cells, the linearized equation system of the Euler stage is considered along a coordinate direction n :

$$\frac{\partial v}{\partial t} = -\frac{1}{\rho} \frac{\partial p}{\partial n}, \quad \frac{\partial p}{\partial t} = -(\gamma - 1)p \frac{\partial v}{\partial n}.$$

Let us consider this quasilinear hyperbolic system without the impact of potential and cooling at the boundary of two adjacent cells. The 'left' cell with the quantities ρ_L, p_L, v_L , and the 'right' cell with the quantities ρ_R, p_R, v_R . Let us linearize the system as an arithmetic mean. The obtained system is a linear hyperbolic system and it has an analytic solution at the boundary of two cells.

$$V = \frac{v_L + v_R}{2} + \frac{p_L - p_R}{2} \sqrt{\frac{\rho_L + \rho_R}{\rho_L \rho_R (\gamma - 1) (p_L + p_R)}},$$

$$P = \frac{p_L + p_R}{2} + \frac{v_L - v_R}{2} \sqrt{\frac{\rho_L \rho_R (\gamma - 1) (p_L + p_R)}{\rho_L + \rho_R}}.$$

The values P and V are used at the scheme for the Eulerian stage.

3.2. The Lagrangian stage

At the second, Lagrangian stage, the system of equations contains divergence items,

$$\frac{\partial u}{\partial t} + \text{div}(u\vec{v}) = 0.$$

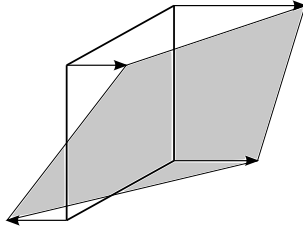


Figure 1. Flow in the Lagrangian stage.

The Lagrangian stage itself describes the convective transport of the gas quantities with the scheme velocity through the border of the cell (Fig. 1). This flow is adapted for GPU implementation (Vshivkov et al. 2007),

$$\frac{u_{ikl}^{n+1} - u_{ikl}^n}{\tau} + \frac{F_{i+1/2,kl} - F_{i-1/2,kl}}{h} = 0,$$

$$F_{i+1/2,kl} = \frac{\Sigma v_{i+1/2,k\pm 1,l\pm 1} \times \begin{cases} u_{ikl}, v_{i+1/2,k\pm 1,l\pm 1} \geq 0 \\ u_{i+1,kl}, v_{i+1/2,k\pm 1,l\pm 1} < 0 \end{cases}}{4}.$$

3.3. Poisson equation solution method

After the gas values are computed, the Poisson equation is solved to obtain the gravitational potential. Poisson equation is solved by the Fourier transform method. A 27 point stencil is used for the approximation of Poisson equation. All details of the numerical method and parallel implementation can be found in Vshivkov et al. (2011a,b) and Vshivkov et al. (2009).

4. Test of the implementation

The numerical method was verified on the following problems: 3 problems of shock tube (3 tests of Godunov); the problem of the equilibrium configuration of a rotating gas cloud; the comparison of the author's numerical method with other methods (2 implementation of SPH method, Lagrangian code, and TVD method) by the solution of the problem of collapse; Wengen cloud collision test; author's cloud collision test; Aksenov's test with continuous solution; Sedov's test.

5. Numerical simulation of a collision of the gas components of galaxies

The experiments allowed to perform a pioneering study of the model problem of the central collision of the gas components of two galaxies. It was shown that the scenario of collision of two galaxies might be their coalescence, free expansion, expansion with the formation of a new galaxy with no stellar component, dissipation of the gas components of the galaxies. For the first time, the range of parameters that is necessary for the development of each scenario was obtained.

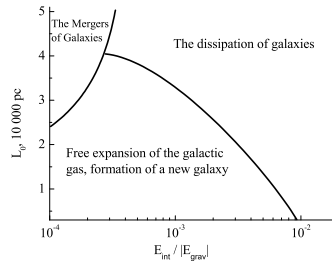


Figure 2. Collision results depending on the initial distance L_0 and the ratio of the internal energy to the gravitational energy $\alpha = E_{int}/|E_{grav}|$.

This is very important since collisions of galaxies play a great role in the dense clusters of galaxies.

It is shown that the collision leads not only to the occurrence of tidal tails and of spirals of various shapes, but also to the destruction of galaxies. Another possible collision result is the formation of a new galaxy in some cases. A new galaxy is formed from the gas components of the colliding galaxies. The results of numerical simulation of the collision scenarios with $\log(\frac{M_G}{M_\odot}) = 11$ confirmed the observation-based hypothesis about the dependence of the galaxy collision outcome on their velocity at the moment of collision.

6. Conclusions

A new numerical method is described for a class of non-stationary problems of gravitational gas dynamics considering cooling and the central body influence. The algorithm enables to perform computational experiments for the study of the self-gravitating gas dynamics in a 3D case with a wide range of parameters. A software package PEGAS for supercomputer computation was developed on the basis of the proposed algorithm. The capabilities of the package include: rotation-invariant solutions, gas-vacuum boundary simulation, estimate of the solution precision, cooling function setting, central body contribution setting, energy imbalance minimization.

Acknowledgments. The research work was supported by the Federal Program "Scientific and scientific-pedagogical cadres innovation Russia for 2009-2013" and Federal Programme for the Development of Priority Areas of Russian Scientific & Technological Complex 2007–2013, Russian Ministry of Education and Science, RFBR grants 11-01-12106-ofi-m-2011, 10-01-00040 and 12-01-31352 for junior researchers, and by the Grant of the President of the Russian Federation for the support of young scientists number MK–4183.2013.9.

References

Brandenburg, A., Dobler, W. 2002, *Comp. Phys. Comm.*, 147, 471

- Bryan, G., Norman, M.L. et al. 2005, *Lec. Not. Comp. Sci. Engng.*, 41, 341
 Hayes, J., Norman, M., Fiedler, R. et al. 2006, *ApJS*, 165, 188
 Kravtsov, A., Klypin, A., Hoffman, Y. 2002, *ApJ*, 571, 563
 Matthias, S. 1996, *MNRAS*, 278, 1005
 Mignone, A., Plewa, T., Bodo, G. 2005, *ApJ*, 160, 99
 Murphy, J., Burrows, A. 2008, *ApJS*, 179, 209
 Pearce, F.R., Couchman, H.M.P. 1997, *New Astronomy*, 2, 411
 Schive, H., Tsai, Y., Chiueh, T. 2010, *ApJS*, 186, 457
 Springel, V. 2010, *MNRAS*, 401, 791
 Springel, V. 2005, *MNRAS*, 364, 1105
 Stone, J. et al. 2008, *ApJS*, 178, 137
 Sutherland, R.S., Dopita, M.A. 1993, *ApJS*, 88, 253
 Teyssier, R. 2002, *A&A*, 385, 337
 Tutukov, A., Lazareva, G., Kulikov, I. 2011, *Astron. rep.*, 55, 9, 770
 Vshivkov, V., Lazareva, G., Snytnikov, A., et al. 2011, *ApJS*, 194, 47
 Vshivkov, V., Lazareva, G., Kulikov, I. 2007, *Opt. Instr. Data Proc.*, 43, 530
 Vshivkov, V., Lazareva, G., Snytnikov, A., et al. 2011, *J. Inv. Ill-pos. Prob.*, 19, 1, 151
 Vshivkov, V., Lazareva, G., Snytnikov, A., et al. 2009, *Lect. Not. Comp. Sci.*, 5698, 414
 Wadsley, J.W., Stadel, J., Quinn, T. 2004, *New Astronomy*, 9, 137
 Walder, R., Folini, D. 1996, *A&A*, 315, 265
 Ziegler, U. 2005, *A&A*, 435, 385

Name of code	Numerical method	Correctness checking	Collision of galaxies
GADGET-2	SPH	—	•
Hydra	SPH	•	—
Gasoline	SPH	—	—
GrapeSPH	SPH	—	—
AMRCART	Lax-Friedrichs	—	—
NIRVANA	PPM	—	—
FLASH	PPM	•	—
ENZO	PPM	—	—
RAMSES	PPM	•	—
ART	PPM	—	—
Athena	Roe's solver	—	—
Pencil Code	Finite difference	•	—
ZEUS-MP	Finite difference	—	—
GAMER	PPM	—	—
BETHE-Hydro	ALE	—	—
AREPO	Godunov	—	•
PEGAS	FIIC & Godunov	•	•

Table 1. The main properties of the widely used software packages

Dark matter halo properties at low and high redshift

Juan C. Muñoz-Cuartas, Volker Müller and Stefan Gottlöber

Leibniz-Institut Für Astrophysik Potsdam, Potsdam, Germany.

Abstract. We use high resolution cosmological N-body simulations to study the concentration of dark matter haloes up to redshift ~ 8 . We focus our attention on the observed upturn of the concentration of haloes at $z > 3$ and investigate its connection to the growth of these objects. In agreement with previous works, we confirm the presence of an upturn in the median $c_{\text{vir}}-M_{\text{vir}}$ relation, and observe it to happen also at low halo masses. We show that such an upturn in the $c_{\text{vir}}-M_{\text{vir}}$ relation implies a mild upturn in the evolution of the concentration of individual haloes at high redshift. Such an upturn would have implications in the properties of high redshift galaxies such as size, structure and star formation. Our results suggest that the upturn in the concentration is associated with a phase in which the inner region of the halo was growing at a higher rate than the outer region.

1. Introduction

In the currently most accepted cosmological scenario, the properties of galaxies are expected to be related to the properties of the distribution of mass in dark matter haloes (White & Rees 1978). This makes imperative to understand the simpler evolution of the dark matter structures first, to allow us to approximately model and understand the process of formation and evolution of galaxies.

The concentration parameter (c_{vir}) is one of the most important halo parameters since it characterises the properties of the halo mass density distribution. This, defined as the ratio between the virial radius, R_{vir} , and the scale length radius of the spherically averaged dark matter halo density profile, r_s , encapsulates all the information on the shape of the dark matter halo density profile. Understanding the mass dependence and time evolution of the concentration parameter leads to the understanding of the evolution of the dark matter halo density profile. In a previous work, Navarro et al. (1997) have stated that the concentration of dark matter haloes is related to the mean density of the Universe at the time of formation of the halo. Bullock et al. (2001) have studied the mass and redshift dependence of the concentration parameter. Since then, it is clear that there is an anti-correlation between halo mass and concentration and that the concentration parameter decreases at increasing redshifts. Wechsler et al. (2002), Zhao et al. (2009) and Muñoz-Cuartas et al. (2011; hereafter MC11) have studied the correlation between the mass assembly history of haloes and the concentration parameter. Specifically, Wechsler et al. (2002) and Zhao et al. (2009) confirm a relationship between the time of formation of the halo and its concentration parameter. Recently Klypin et al. (2011, K11) and Prada et al. (2011, P11) have

revisited the problem of the evolution and mass dependence of the concentration parameter. They report a novel feature of the concentration parameter. They show the $c_{\text{vir}}-M_{\text{vir}}$ relation to exhibit a flattening at high masses and an upturn at high redshifts. These features are not expected in the current models for the evolution of c_{vir} . This behaviour of the concentration parameter should have important implications for the evolution of the stellar content in young galaxies in the early universe.

In this work we aim to confirm the upturn shown in the $c_{\text{vir}}-M_{\text{vir}}$ relation at low halo masses. We also want to study if such an upturn in the $c_{\text{vir}}-M_{\text{vir}}$ relation implies an upturn on the evolution of the concentration of individual haloes.

2. Procedure

In this work we use three high resolution simulations from the CLUES project (Gottlöber et al. 2010), with a box size of $64 h^{-1}\text{Mpc}$, and run with the code GADGET2 using 1024^3 sampling particles. The particle mass is $1.89 \times 10^7 h^{-1}M_{\odot}$, and the starting redshift is 50. The high resolution of these simulations allow us to follow haloes with more than 200 particles down to $z \sim 8$. The cosmological parameters are consistent with those of the WMAP5 cosmology, using $\Omega_{\text{m}} = 0.279$, $\Omega_{\Lambda} = 0.721$, $h = 0.7$, $\sigma_8 = 0.817$ and $n = 0.96$.

In each simulation snapshot, haloes are identified with a friends-of-friends (FoF) method using a linking length of 0.17 times the mean interparticle distance. Then, for each FoF group, we compute the center of the halo as the position of the particle with the lowest potential energy. Around this position we search for a spherical overdensity enclosing a mean mass density of $\Delta_{\text{vir}}(z)$ times the critical density of the Universe $\rho_{\text{c}}(z)$ (Bryan & Norman 1998).

To estimate the concentration of each halo we compute the density distribution from the halo's particle distribution and fit the density profile with a NFW profile. During the fitting procedure we keep both the characteristic length r_{s} and the characteristic density δ_{c} as free parameters. Finally, we define the concentration of the halo as $c_{\text{vir}} \equiv R_{\text{vir}}/r_{\text{s}}$. See MC11 for a detailed description on the procedures.

3. Results

Fig. 1 (left panel) shows the redshift evolution of the $c_{\text{vir}}-M_{\text{vir}}$ relation for fixed halo mass for five different mass bins. The three low-mass bins are drawn from the simulations with a box of $64 h^{-1}\text{Mpc}$, while the two more massive ones are from a simulation with a box of 1 Gpc. No halo with less than 500 particles has been used to compute the median values shown in Fig. 1. As it can be seen in this figure, and in agreement with the reports from K11 and P11, the median $c_{\text{vir}}-M_{\text{vir}}$ relation increases at high redshift after reaching a minimum value. As it is shown in the figure, the position of the upturn depends on the mass of the halo, being the most massive haloes the ones reaching the upturn at later cosmic times.

In Fig. 2 we show the evolution of the median concentration parameter for the most massive progenitor halo. Merger histories have been binned by final mass ($M_{\text{vir}}(z = 0)$) and by length (or equivalently, halo formation time). As it

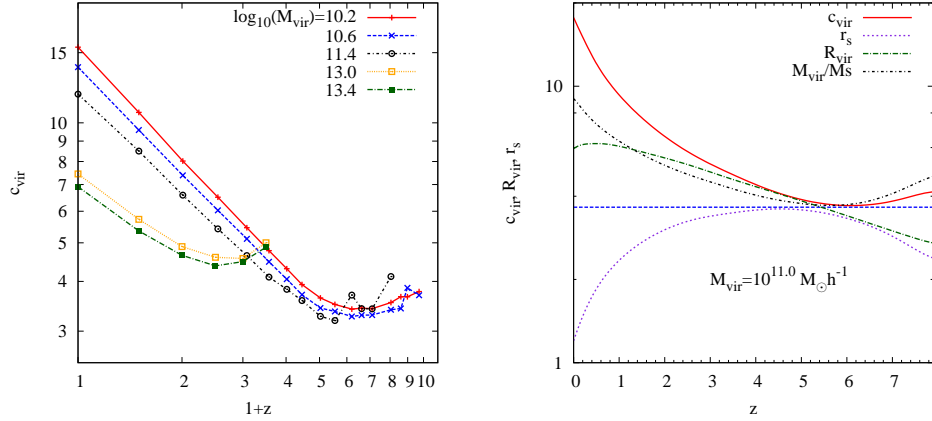


Figure 1. *Left:* Median concentration parameter as a function of redshift for different haloes at fixed halo mass. The three low mass bins ($10^{10.2}$, $10^{10.6}$ and $10^{11.4} h^{-1} M_{\odot}$) are taken from the simulations with a box of $64 h^{-1} \text{Mpc}$, while the last two ones ($10^{13.0}$ and $10^{13.4} h^{-1} M_{\odot}$) are from that with a box of 1Gpc . *Right panel:* Concentration c_{vir} , halo scale length r_s and virial radius R_{vir} (both in comoving units) arbitrarily scaled to reach comparable values. The horizontal line shows the minimum value of c_{vir} . The quantities are evaluated for the most massive progenitor of the halo.

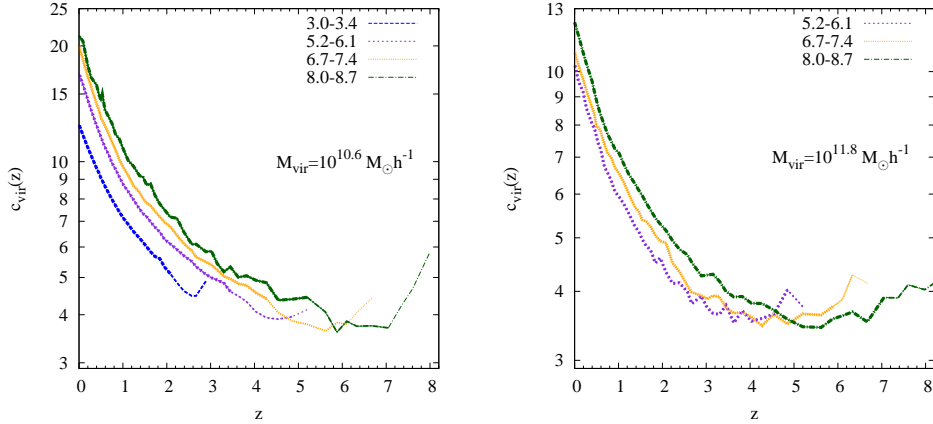


Figure 2. Evolution of the median concentration parameter as a function of redshift for the most massive progenitor of the tree. Each panel shows the evolution of c_{vir} along the merger tree for haloes with the same final mass. Note that haloes of the same mass show different evolution depending on the length of their merger histories. The set of numbers in the labels shows the range of limit redshifts used for the selection of the merger trees.

can be seen in this figure, the evolution of the concentration parameter depends on the length of the merger history. There, one can see that in general all curves show a weak upturn at early times, during the formation of the halo. The position of the minimum depends on the length of the merger history. We have used different tests, and verified that the mild upturn is not due to numerical, statistical or resolution effects.

Based on the same arguments used in MC11, to propose a physical scenario to explain the evolution of the $c_{\text{vir}}-M_{\text{vir}}$ relation, we investigate the evolution of the concentration parameter through the explicit evolution of R_{vir} and r_s . Fig. 1 (right panel) shows the redshift dependence of R_{vir} , r_s and c_{vir} . R_{vir} and r_s have been scaled arbitrarily to values comparable to those of c_{vir} . We stress that this arbitrary normalisation is intended to help to visualise the relationship between c_{vir} , R_{vir} and r_s . Note that the minimum in c_{vir} occurs approximately at the same redshift at which R_{vir} and r_s have the same slope. For redshifts larger than this, the rate of growth of r_s becomes slightly larger than that for R_{vir} , inducing the upturn in the concentration parameter.

4. Conclusions

We confirm the upturn shown in the $c_{\text{vir}}-M_{\text{vir}}$ relation presented in K11 and P11. We observe it at low halo masses, and determine it to be mass dependent, being the most massive haloes the ones reaching the upturn at lower redshifts.

We show, following the evolution of the most massive progenitor halo in the merger tree, that such an upturn in the $c_{\text{vir}}-M_{\text{vir}}$ relation implies a mild upturn in the evolution of the concentration of individual haloes at high redshift.

We have found that the upturn in the concentration is due to a different rate of growth between R_{vir} and r_s , where we see that before the minimum in $c_{\text{vir}}(z)$, $R_{\text{vir}}(z)$ has a slope that is slightly smaller than that after the upturn, and smaller than the slope in $r_s(z)$ at the same redshift. It leads us to conclude that the upturn in the concentration is induced by the growth of the halo at early times, which at the beginning favours the fast collapse of the inner region of the halo, compared to the outer region.

References

- Bullock, J. S., Kolatt, T. S., Sigad, Y., et al. 2001, MNRAS, 321, 559
 Klypin, A. A., Trujillo-Gomez, S., & Primack, J. 2011, ApJ, 740, 102
 Muñoz-Cuartas, J. C., Macciò, A. V., Gottlöber, S., et al. 2011, MNRAS, 411, 584
 Navarro, J. F., Frenk, C. S., & White, S. D. M. 1997, ApJ, 490, 493
 Prada, F., Klypin, A. A., Cuesta, A. J., et al. 2011, arXiv:1104.5130
 Wechsler, R. H., Bullock, J. S., Primack, J. R., et al. 2002, ApJ, 568, 52
 White, S. D. M., & Rees, M. J. 1978, MNRAS, 183, 341
 Zhao, D. H., Jing, Y. P., Mo, H. J., et al. 2009, ApJ, 707, 354

Modelling Ly α emitters in a hierarchical Universe: a hybrid approach

Alvaro Orsi^{1,2}, Cedric G. Lacey³ and Carlton M. Baugh³

1. Depto de Astronomía y Astrofísica, PUC, Santiago, Chile.

2. Centro de Astro-Ingeniería, PUC, Santiago, Chile.

3. ICC, Department of Physics, DU, Durham, UK.

Abstract. We present the results of combining the GALFORM semi-analytical model of galaxy formation with a Monte Carlo Ly α radiative transfer code to study the properties of Ly α emitters between $0 < z < 7$. In this hybrid approach, Ly α photons escape from galaxies in galactic outflows. The model results are consistent with a set of key observations, such as the inferred Ly α escape fraction and, remarkably, with the shape of the Ly α line from composite spectra. The predicted fractions of Ly α emitters in Lyman-break galaxy samples at high redshift are in partial agreement with observations, and suggest that the intergalactic medium may not play a dominant role in attenuating the Ly α line at $z \sim 6 - 7$.

1. Introduction

Understanding the physical mechanisms which drive the escape of Ly α radiation from a galaxy remains a challenge. Ly α photons undergo resonant scattering when interacting with hydrogen atoms, resulting in an increase of the path length that photons need to travel before escaping the medium. Therefore, the probability of photons being absorbed by dust grains is greatly enhanced, making the escape of Ly α photons very sensitive to even small amounts of dust.

Recent observational studies have revealed that the escape fraction in Ly α emitters can be anything between 10^{-3} and 1 (e.g. Hayes et al. 2011). The analysis of metal lines in local starbursts and high-redshift galaxies reveals the presence of outflows in Ly α emitting galaxies (Mas-Hesse et al. 2003; Shapley et al. 2003; Hu et al. 2010), suggesting that galactic outflows play an important role in driving the escape of Ly α photons.

Motivated by this idea, we developed in Orsi, Lacey & Baugh (2012) a model that incorporates a physical treatment of the propagation of Ly α photons, including radiative transfer through an HI region. Our approach makes use of a Monte Carlo algorithm, in which the paths of a set of photons are followed one at a time through many scattering events, until the photon either escapes or is absorbed by a dust grain.

We explore the properties of Ly α emitters in our hybrid model for two outflow geometries: a shell of neutral gas and a wind ejecting material, both expanding at constant velocity. In the following, we briefly highlight some of the main predictions of our model, exploring the nature of Ly α emitters within this framework.

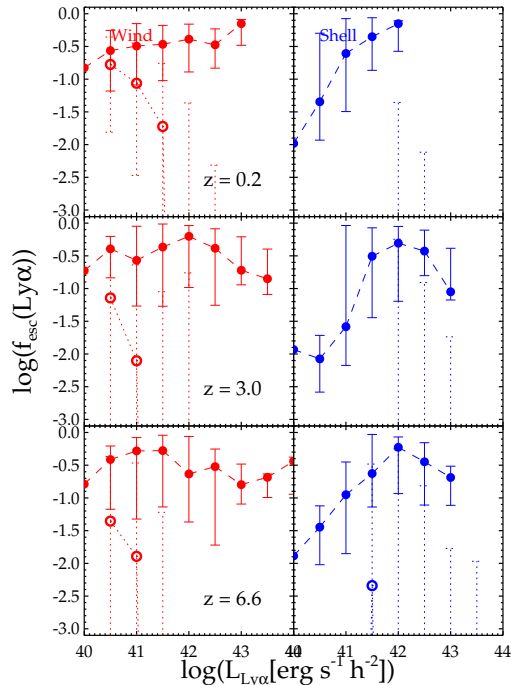


Figure 1. The escape fraction as a function of Ly α luminosity at $z = 0.2$ (top), $z = 3.0$ (middle) and $z = 6.6$ (bottom). The wind geometry predictions are shown in red (left), and the shell geometry in blue (right). Solid circles show the median of the escape fraction as a function of attenuated Ly α luminosity. Open circles show the same relation as a function of intrinsic Ly α luminosity instead. Error bars represent the 10-90 percentiles around the median of the escape fraction at a given Ly α luminosity.

2. Model predictions

In our model, the properties of each galaxy predicted by the semi-analytical model GALFORM are used to define the properties of a galactic outflow, which is then used by the Monte Carlo radiative transfer model to compute an escape fraction, $f_{\text{esc}}(\text{Ly}\alpha)$, for each galaxy. A set of free parameters relate the size, expansion velocity and mass (or mass ejection rate) of the outflows to the half-mass radius, circular velocity and cold gas mass of the galaxies. The parameter values are fixed by matching the observed abundance of Ly α emitters over the redshift range $0 < z < 7$.

The resulting Ly α escape fraction of galaxies predicted by our models is shown in Fig. 1. Overall, we find that typical Ly α emitters (with luminosities of $L_{\text{Ly}\alpha} \sim 10^{42} h^{-2} \text{erg s}^{-1}$) have $f_{\text{esc}} > 0.1$, regardless of redshift. In detail, however, the two outflow models predict different escape fractions for galaxies with the same Ly α luminosity. Hence, Fig. 1 illustrates the impact of the model of galactic outflows on the predicted properties of Ly α emitters.

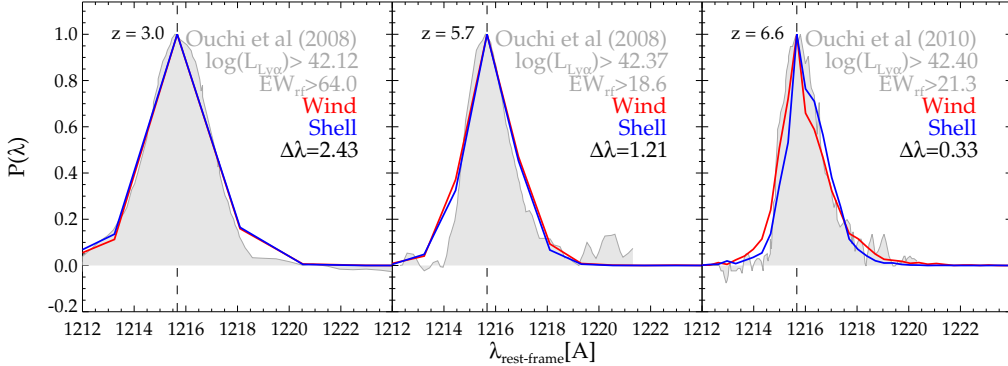


Figure 2. Composite Ly α line profiles of the samples at different redshifts, as indicated in each panel. The gray shaded regions show the Ly α line profiles from composite observational samples taken from Ouchi et al. (2008, 2010), whereas the solid curves show the model predictions using the wind geometry (red), and the shell geometry (blue).

We also predict composite Ly α profiles at different redshifts. The average Ly α profiles shown in Fig. 2, constructed using the methodology of Ouchi et al. (2008, 2010), show reasonable agreement with the data, thus supporting the idea that Ly α photons escape mainly in galactic outflows. Notice that our outflow geometries are not tuned to reproduce the observed line shapes, and therefore these represent genuine predictions of the model.

Finally, we study the fraction of galaxies exhibiting Ly α in emission predicted by our models. Fig. 3 compares our model predictions with the observed fraction of Ly α emitters found in Lyman-break galaxies (LBGs) at high redshifts. Ly α emitters are defined here as galaxies with a Ly α equivalent width, $EW \geq 25 \text{ \AA}$ (in the rest-frame). Observational data were split into two rest-frame UV magnitude ranges, which we reproduce in the models by computing UV magnitudes at 1500 \AA rest frame.

Both outflow geometries predict an increase in the fraction of Ly α emitters with redshift, which is qualitatively consistent with the observations up to $z \sim 6$. However, the model predicts lower fractions of Ly α emitters at the faint magnitude bin, as shown in Fig. 3. At higher redshifts, the observations of Schenker et al. (2011) and Pentericci et al. (2011) suggest a decline in the fraction of Ly α emitters at $z \sim 7$. They interpret this decline as being due to the neutral intergalactic medium (IGM) attenuating the Ly α luminosity from galaxies. However, our model reproduces this decline in the fraction of Ly α emitters at high redshift despite not including any attenuation of the Ly α line due to the IGM. Therefore, our predictions imply that the decline in the Ly α fraction in LBG samples found at high redshifts is not necessarily caused by the presence of neutral HI in the IGM.

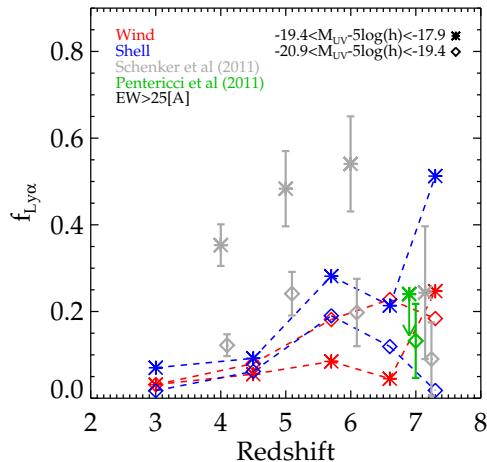


Figure 3. The fraction of Ly α emitters as a function of redshift. Predictions of the wind and shell geometries are shown in red and blue, respectively. The observational measurements of Schenker et al. (2011) and Pentericci et al. (2011) are shown in gray and green, respectively.

3. Conclusions

The models presented here (see also Orsi, Lacey & Baugh, 2012) for the emission of Ly α represent an important step towards a detailed understanding of the physical properties of these galaxies. With the advent of large observational campaigns in the forthcoming years focusing on detecting Ly α emitters at high redshifts, new data will help us refine and improve our physical understanding of these galaxies, and thus enable us to improve our knowledge of galaxy formation and evolution, particularly in the high redshift Universe.

References

- Atek H., Kunth D., Hayes M., et al. 2008, A&A, 488, 491
 Hayes M., Östlin G., Schaerer D., et al. 2010, Nature, 464, 562
 Hayes M., Schaerer D., Östlin G., et al. 2011, ApJ, 730, 8
 Hu E. M., Cowie L. L., Barger A. J., et al. 2010, ApJ, 725, 394
 Mas-Hesse J. M., Kunth D., Tenorio-Tagle G., et al. 2003, ApJ, 598, 858
 Orsi A., Lacey C. G., Baugh C. M., 2012, MNRAS, 425, 87
 Ouchi M., Shimasaku K., Akiyama M., et al. 2008, ApJS, 176, 301
 Ouchi M., Shimasaku K., Furusawa H., et al. 2010, ApJ, 723, 869
 Pentericci L., Fontana A., Vanzella E., et al. 2011, ArXiv e-prints, 11071376
 McLure R. J., Kneib J. ., Richard J., 2011, ArXiv e-prints 11071261
 Shapley A. E., Steidel C. C., Pettini M., et al. 2003, ApJ, 588, 65

Cosmic voids as a tool to constrain cosmology

Santiago G. Patiri

¹*IANIGLA-CONICET, Apartado Postal 330, Mendoza, Argentina*

Abstract. In this presentation we introduce the statistics of voids in the large-scale distribution of galaxies, i.e. the number of voids found in the final data release (DR7) of the Sloan Digital Sky Survey as a function of their radius. We also discuss how this statistics can be used to estimate the σ_8 and $\Omega_m h$ cosmological parameters with an accuracy of $\sim 5\%$ at the 68% CL.

1. Introduction

In recent years, thanks to new data obtained with the WMAP experiment (Hinshaw et al. 2009) on the Cosmic Microwave Background (CMB) radiation, it has been possible to measure with high precision the value of the fundamental cosmological parameters. However, CMB constraints are greatly improved when combined with results from other methods, such as the number counts of galaxy clusters, gravitational lensing and galaxy clustering extracted from large redshift surveys (e.g., Vikhlinin et al. 2009; Sánchez et al. 2009; Komatsu et al. 2011).

Since independent measurements based on different aspects of the clustering and large scale structure of galaxies (LSS) are essential to improve the parameter estimation, one possibility is to extract information from the large regions with very low density of galaxies, commonly called *voids*. The attention toward these regions has rapidly increased, thanks to the advent of large galaxy redshift surveys and improvements in theoretical modeling. However, robust methods to extract information about cosmological parameters have been difficult to implement (see e.g., Plionis & Basilakos 2002; Lavaux & Wandelt 2011).

In this work, we present the void statistics obtained from the largest galaxy redshift survey available for the local Universe, the SDSS DR7. We also discuss a specific method to constrain σ_8 and $\Omega_m h$ using the statistics of voids. Recently, in Betancort-Rijo et al. (2009, BPPR09 hereafter) we have shown theoretically that the void statistics can be used to constrain cosmological parameters. In particular, we have noted that it might be specially interesting to measure the normalization of the amplitude of density fluctuations (in scales of $8h^{-1}\text{Mpc}$, denoted as σ_8), since they trace comparable scales. Also the shape of the power spectrum, determined by $\Omega_m h$, could be constrained using void statistics as a function of their radius. Here we show how to implement the theoretical method using the observational data. In a forthcoming work, we will use these statistics to derive constraints on the relevant cosmological parameters and explore the sensitivity of the void statistic to other parameters such as ω in the cosmological equation of state.

2. Statistic of voids in the SDSS DR7

We use the NYU Value-Added Galaxy Catalog (NYU-VAGC)¹ associated to the Sloan Digital Sky Survey Data Release 7. See Abazajian et al. (2009) for details of the survey. From the parent catalog, we constructed a volume-limited sample defined by an r -band magnitude threshold $M_r - 5 \log h = -20.3$ and a maximum redshift of $z = 0.13$. Our resulting galaxy sample contains a total of 162076 galaxies.

In this work, we define voids as maximal spheres empty of galaxies brighter than the limiting magnitude of our galaxy sample. To search for voids, we use the *HB* void finder (Patiri et al. 2006). Here, we adopt our *statistic* as the number of voids larger than a given radius, because the sampling errors are smaller than those of other methods (see BPPR09 for a discussion of this topic). In Table 1 we present the resulting statistic of voids obtained in our galaxy sample.

Table 1. Full statistics of voids in the SDSS. N_V^{sdss} denotes the number of voids larger than the radius given in the first column.

Radius ($h^{-1}\text{Mpc}$)	N_V^{sdss}
10	1162
11	829
12	464
13	284
14	141
15	76
16	34
17	20

3. Method and prospective work

The proposed strategy to constrain cosmological parameters from the statistics of voids essentially consists in finding the model predictions (by exploring the relevant parameter space) that reproduces the observed void statistic. To calculate the model predictions for the number of voids, we follow the procedure introduced in BPPR09. In summary, we first obtain the statistic of voids from a large cosmological N -body simulation ($\sim 1h^{-1}\text{Gpc}$ -side box). This provides a robust prediction about the number of voids for a fixed cosmology, i.e. that of the numerical simulation. Then, we use the analytical formalism to *extrapolate* the values found in the mock catalog to different values of σ_8 and $\Omega_m h$. We refer to BPPR09 for details on how to compute all these quantities. In this work, the number density of voids (i.e. number per unit volume) larger than a given radius is given by

¹<http://sdss.physics.nyu.edu/vagc>

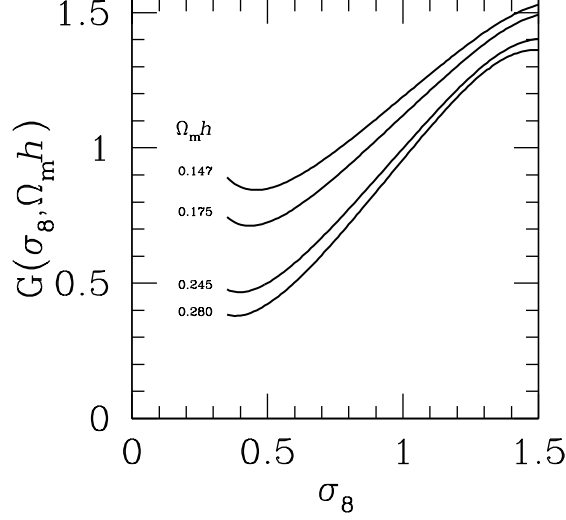


Figure 1. Sensitivity of the void statistics (denoted as G) to σ_8 and $\Omega_m h$. See text for details.

$$\bar{n}_v(r) \simeq \frac{0.68K(r)}{V} e^{-3.5K(r)(1-2.18K(r))} \quad (1)$$

and

$$K(r) = \left(-\frac{1}{3} \frac{d \ln P_0(r)}{d \ln r} \right)^3 P_0(r) \quad ; \quad V = \frac{4}{3} \pi r^3 \quad (2)$$

where $P_0(r)$ is the void probability function (VPF), i.e. the probability that a randomly placed sphere is empty of galaxies. We account for the variations of the void statistics with the values of σ_8 and $\Omega_m h$ using the following expression,

$$\bar{N}_V^{\text{mock}}(\sigma_8, \Omega_m h) = \bar{N}_V^{\text{mock}} G(\sigma_8, \Omega_m h) \quad (3)$$

where \bar{N}_i^{mock} is the mean number of voids obtained from the mock catalogs. $G(\sigma_8, \Omega_m h)$ accounts for the variations of the void statistics with σ_8 , $\Omega_m h$ and is given by:

$$G(\sigma_8, \Omega_m h) = \frac{\bar{n}_v(r, \sigma_8, \Omega_m h)}{\bar{n}_v^{\text{mock}}(r)} \quad (4)$$

where $\bar{n}_v(r, \sigma_8, \Omega_m h)$ is the number density of voids larger than r as a function of σ_8 and $\Omega_m h$, and $\bar{n}_v^{\text{mock}}(r)$ is the number density of voids found in the numerical simulation (for a fixed cosmology). In Fig. 1, we present an explicit example of the sensitivity of the void statistics to the relevant cosmological parameters. In particular, we show the G values computed using the above equations for voids larger than $13h^{-1}\text{Mpc}$ as a function of σ_8 and for four different values of $\Omega_m h$.

Several statistical tests can be constructed to extract cosmological information using void statistics. Here, we propose a χ^2 test since it is reliable and accurate enough for our purposes. The χ^2 statistics is given by

$$\chi_0^2(\sigma_8, \Omega_m h) = \sum_{i=1}^n \frac{[N_i^{\text{sdss}} - \bar{N}_i^{\text{mock}}(\sigma_8, \Omega_m h)]^2}{\bar{N}_i^{\text{mock}}(\sigma_8, \Omega_m h)} \quad (5)$$

where n is the number of bins, N_i^{sdss} is the number of voids found in the observational sample in the i -th bin in radius and $\bar{N}_i^{\text{mock}}(\sigma_8, \Omega_m h)$ is the *mean* number of voids predicted by the theory.

This test quantifies the differences between the observed distribution and the model one. Then the probability of rejecting the corresponding set of parameters is given by:

$$P(\sigma_8, \Omega_m h) = P(\chi^2 \geq \chi_0^2, \nu) \quad (6)$$

where ν is the number of degrees of freedom, which in this case is given by the number of bins. With this equation we can compute a matrix for a wide range of values of σ_8 and $\Omega_m h$. Then, the most probable value for the parameters is given by the minimum of $P(\sigma_8, \Omega_m h)$. Finally, the confidence levels are directly obtained by the iso-probability contours (e.g. the 68% confidence level is given by $P(\sigma_8, \Omega_m h) < 0.68$).

Note that the accuracy of the estimation of the relevant parameters using void statistics scales with the square root of the number of voids. From the number voids obtained in this work (shown in table 1), we estimate that the resulting error in the measurement of both parameters will be $\sim 5\%$.

We have shown that the statistics of voids can be used to develop a method to estimate cosmological parameters, in particular σ_8 and $\Omega_m h$. Moreover, voids might be useful to constrain other parameters such as those of the cosmological equation of state. We will explore this possibility in a future work.

References

- Betancort-Rijo, J. E., Patiri, S. G., Prada, F., et al. 2009, MNRAS, 400, 1835 [BPPR09]
- Hinshaw, G., Weiland, J.L., Hill, R. S., et al. 2009, ApJS, 180, 225
- Komatsu, E., Smith, K. M., Dunkley, J., et al. 2011, ApJS, 192, 18
- Lavaux, G., & Wandelt, B. D. 2010, MNRAS, 403, 1392
- Patiri S. G., Betancort-Rijo J. E., Prada F., et al. 2006, MNRAS, 369, 335
- Plionis M. & Basilakos S. 2002, MNRAS, 330, 399
- Springel, V. et al. 2005, Nature, 435, 629
- Sánchez A. G., Crocce M., Cabré A., et al. 2009, MNRAS, 400, 1643
- Vikhlinin A., et al., 2009, ApJ, 692, 1060

Angular momentum conservation in Λ CDM simulations

S. Pedrosa¹ and M. E. De Rossi^{1,2,3}

¹*IAFE, Argentina*

²*CONICET, Argentina*

³*FCEyN, UBA, Argentina*

Abstract. We study the morphological and dynamical properties of galaxies obtained from high resolution hydrodynamical cosmological simulations. The parameters that regulate the star formation and supernova feedback have been chosen in order to obtain galaxies that present a good agreement with observations. We analyse their angular momentum content and correlate it with the galaxy formation history. We also analyse in detail the properties of the stellar component of galaxies.

1. Introduction

During the complex process of galaxy assembly, both the baryonic and dark matter components affect each other in a very complicated way. We have already analysed extensively the influence of the baryons condensation in the dark matter halo (Pedrosa et al. 2010; Tissera et al. 2010). The correlation between the specific angular momentum of the galaxy disk and the dark matter halo is a consequence of the formation model assumed. For a hierarchical clustering scenario, Fall & Efstathiou (1965) found that the specific angular momentum of the galaxy should be equal to that of the halo, due to the fact that both components are subject to the same external gravitational torques in the protogalactic stage.

Several physical factors are involved in the formation and evolution of the disk, such as mass accretion, mergers, the star formation rate and its regulation due to supernovae (SN) feedback. The evolution of galactic disks with redshift poses important questions. For example, the observational findings from the SINFONI Integral Field Spectroscopy (SINS) survey of an extended disk at $z \sim 2$ seem to be in conflict with the classical model of Mo, Mao & White (1998, MMW98), as this model predicts smaller disks at higher redshifts. Another crucial factor that needs to be considered is the environment: the effects that tidal stripping and mergers have on the evolution of galaxies.

In this work we analyse the angular momentum content of simulated galaxies and its relation to the evolution of these systems. We also investigate the effects of mergers on the survival of disks and on the final morphology of galaxies. Sect. 2 describes the numerical experiments that we have carried out, while Sect. 3 shows our preliminary results.

2. Numerical simulations

We performed cosmological simulations of a typical field region of the Universe, consistent with the concordance model with $\Omega_\Lambda = 0.7$, $\Omega_m = 0.3$, $\Omega_b = 0.04$, a normalization of the power spectrum of $\sigma_8 = 0.9$ and $H_0 = 100 h \text{ km s}^{-1} \text{ Mpc}^{-1}$, with $h = 0.7$. They have been run with 2×230^3 particles. The particle mass is $5.9 \times 10^6 h^{-1} M_\odot$ and $9.1 \times 10^5 h^{-1} M_\odot$ for the dark matter and baryonic particles, respectively.

Simulations were performed using the code GADGET-3, an update of GADGET-2 optimized for massive parallel simulations of highly inhomogeneous systems (Springel 2005). This version of the code includes treatments for metal-dependent radiative cooling, stochastic star formation, chemical enrichment, a multiphase model for the interstellar medium (ISM), and the SN feedback scheme of Scannapieco et al. (2005, 2006). In order to obtain our galaxy catalog, we have identified virialized structures using a friends-of-friends technique, then finding the substructures in each halo using the SUBFIND program by Springel et al. (2001).

3. Results and discussion

We study the morphology of our simulated galaxies and the dynamics of their stellar, gas and baryonic phases. In order to identify the different components of our galaxies we choose a reference system so that the disk plane is perpendicular to the total angular momentum. To discriminate between disk, bulge and halo components we apply a method based on the technique used by Abadi et al (2003). We obtain a variety of different morphologies in our simulations.

In order to be able to perform realistic comparisons with observational results, it is important to define carefully the characteristic radius of the galaxy. We analyse different possible estimators such as the baryonic radius, defined as the one that encloses 83 percent of the total baryonic mass, the radius given by a fixed fraction of the virial one, often used in analytical models, and the half mass and effective radii. We find that although the baryonic radius in some cases slightly overestimates the galactic radii, it gives a good measure of the size of the galaxy.

We analyse the angular momentum content of baryons in our simulated galaxies. In Fig. 1, we show a plot of j_d vs m_d , j_d being the ratio between the angular momentum of the galaxy and that of the dark matter halo measured at the virial radius (defined as the radius that encloses a sphere with a density contrast of 200 times the critical density), and m_d the ratio between the galaxy mass and that of the dark matter halo within the virial radius, at redshift zero. From this plot it can be seen that when galaxies with an important baryonic disk component (i.e., a disk fraction greater than 0.5, the filled circles in the plot) are considered, the relation is closer to that predicted by MMW98. If the spheroidal component is taken into account for the computation of the angular momentum of the galaxy (empty circles), the points fall below the one-to-one relation. It is worth noticing that the maximum stellar disk fraction ranges between 0.35 and 0.4. We acknowledge the fact that these fractions are still too low to represent real disks properly.

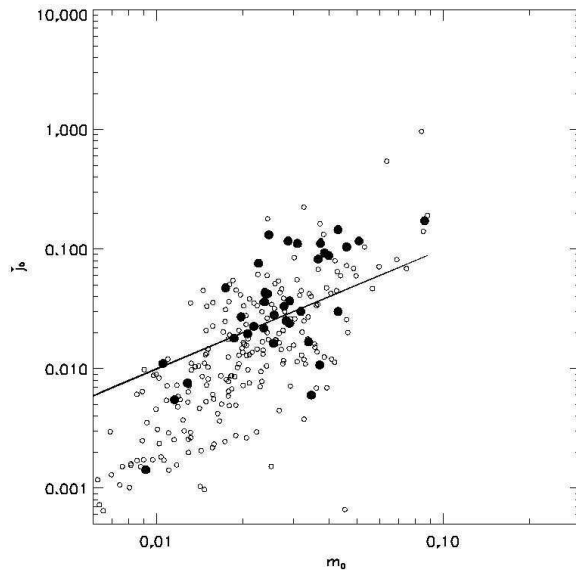


Figure 1. The ratio j_d between the galaxy angular momentum and that of the dark matter halo (measured within the virial radius), as a function of the ratio m_d between their respective masses. Red symbols correspond to galaxies with an important disk component.

We also analyse in detail the stellar component of our simulated galaxies. We study our population of galaxies at $z = 2$ in order to compare it with the observational data from the SINS survey (Bouche et al. 2007; Cresci et al. 2009; Forster-Schreiber et al. 2009) which suggests the existence of a large population of extended disks at $z = 2$. Our more massive objects are in good agreement with the SINS results, but we find an important population of galaxies with much lower rotational velocity at the same radius.

The morphology of our simulated galaxies at $z = 0$ is the result of a complex evolution in which several physical factors participate. Inspecting the star formation profiles with time, we find a trend in the sense that when the star formation is more regular and continues until lower redshifts, the final fraction of stellar mass in the disk component is larger. In the case of the gas component, the disk fraction covers a wide range from 0.2 to 1, and the gas rotation velocity follows closely the potential well of the system, as expected.

We find also that mergers and interactions play an important role in shaping and reshaping the galaxy. We are currently analysing the precise mechanism through which mergers affect central galaxies in halos and to what extent the disks are modified by these mergers and accretion.

Acknowledgments. We acknowledge support from the PICT 32342 (2005), PICT 245-Max Planck (2006) of ANCyT (Argentina), PIP 2009-112-200901-00305 of CONICET (Argentina) and the Loreal-Unesco-Conicet 2010 Prize. Sim-

ulations were run in Fenix and HOPE clusters at IAFE and Cecar cluster at University of Buenos Aires.

References

- Abadi M. G., Navarro J. F., Steinmetz M., et al. 2003, *ApJ*, 591, 499
Bouché N., Cresci G., Davies R., et al. 2007, *ApJ*, 671, 303
Brook C. B., Governato F., Roskar R., et al. 2011, *MNRAS*, 415, 1051
Cresci G., Hicks E. K. S., Genzel R., et al. 2009, *ApJ*, 697, 115
Fall S. M., Efstathiou G. 1980, *MNRAS*, 193, 189
Forster Schreiber N. M., Genzel R., Bouche N., et al. 2009, *ApJ*, 706, 1364
Mo H. J., Mao S., White S. D. M. 1998, *MNRAS*, 295, 319
Pedrosa, S., Tissera, P.B. & Scannapieco, C. 2010, *MNRAS*, 402, 776
Sales, L. V., Navarro, J. F., Theuns, T., et al. 2011, arXiv1112.2220S
Scannapieco C., Tissera P. B., White S. D. M., et al. 2005, *MNRAS*, 364, 552
Scannapieco C., White S. D. M., Springel V., et al. 2006, *MNRAS*, 364, 70
Springel V. 2005, *MNRAS*, 364, 1105
Springel V., Yoshida N., White S. D. M. 2001, *New Astronomy*, 6, 79
Tissera, P. B., White, S. D. M., Pedrosa, S., et al. 2010, *MNRAS*, 406, 922

The distribution of young stars and metals in simulated cosmological disk galaxies

K. Pilkington^{1,2}, B.K. Gibson^{1,2} and D.H. Jones²

¹*Jeremiah Horrocks Institute, UCLan, Preston, UK*

²*Monash Centre for Astrophysics, Clayton, Australia*

Abstract. We examine the distribution of young stars associated with the spiral arms of a simulated L^* cosmological disk galaxy. We find age patterns orthogonal to the arms which are consistent with classical density wave theory, a view further supported by recent observations of Grand Design spirals such as M51. The distribution of metals in a simulated $\sim 0.1 L^*$ disk is also presented, reinforcing the link between star formation, the age-metallicity relation, and metallicity distribution functions.

1. Star formation

We make use of a fiducial L^* simulated disk galaxy (g15784) from the McMaster Unbiased Galaxy Survey (MUGS) (Stinson et al. 2010). Our earlier work with this simulation focused on the temporal evolution of its metallicity gradient (Pilkington et al. 2012a) and metallicity distribution function (Calura et al. 2012). Here, we examine briefly the distribution of recent star formation within the simulation, with an emphasis on the location of the young stars with respect to the simulation's most prominent spiral arm.¹

A detailed description of g15784 can be found in Stinson et al. (2010) and Pilkington et al. (2012a); here, we simply summarise the star formation prescription. The MUGS simulations were run with the gravitational N-Body + SPH code GASOLINE (Wadsley et al. 2004). Stars particles are formed with a user-specified efficiency from gas particles when the latter are sufficiently cool (< 15000 K), dense ($> 1 \text{ cm}^{-3}$), and in a convergent flow ($\nabla \cdot v_i < 0$). Energy feedback from supernovae follows the Stinson et al. (2006) blastwave formalism.

Fig. 1 (left panel) shows the young stellar population (in this case, stars born in the last 300 Myr, at redshift $z=0$) of the g15784 simulation. The prominence of the centrally-concentrated star formation has been commented upon already by Stinson et al. (2010), Pilkington et al. (2012a), and Calura et al. (2012). Three 100 Myr age bins are denoted, with the youngest in blue, the intermediate in green, and the oldest in red. The right panel of Fig. 1 isolates the most prominent spiral feature within the simulation (noted by the box inset to the left panel of Figure 1). *We find that the younger (older) stars tend to lie on the inside/trailing (outside/leading) parts of the arm.* This age 'gradient' in the young stellar populations orthogonal to the arm is consistent with the basic predictions of classical density wave theory (e.g. Dobbs & Pringle 2010), where

¹Space precludes an analysis of the full suite of MUGS disks, but we can state that the results described here for g15784 are *representative*, and not *special*.

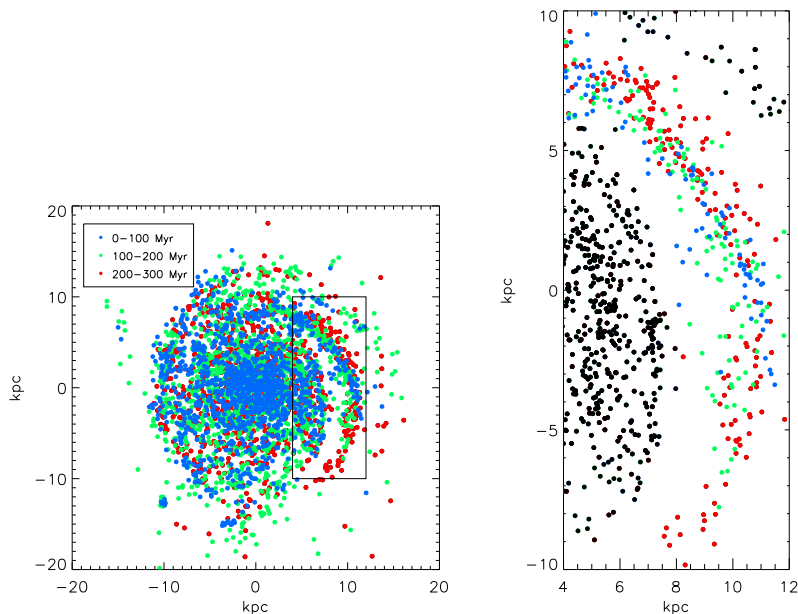


Figure 1. The star particles born in the last 300 Myr (at $z=0$) of the `g15784` simulation. The particles are separated into three age bins: ‘young’ (with ages 0–100 Myr, shown in blue), ‘intermediate’ (100–200 Myr, shown in green), and ‘old’ (200–300 Myr, shown in red). The black box in the left panel identifies the most prominent spiral feature, for which an expanded view is provided in the right panel. The black points in the latter represent the stars born in the last 300 Myr that are not part the spiral arm.

star formation has been triggered by gas shocked by the passage of a spiral density wave.² A more thorough examination of the issues pertaining to spiral arm age gradient/offsets can be found in Grand et al. (2012).

The offsets we see in the populations associated with the spiral arm are most prominent in the ‘upper’ part of the figure, before the arm opens up to its full extent. To achieve a fairer comparison with both the high-resolution models of Dobbs & Pringle (2010) and the observations which show similar trends (e.g. for M51, as in Sánchez-Gil et al. 2011), we would need much finer temporal resolution (where the age ranges probed are 0–10 Myr, rather than 0–300 Myr); having said that, the gross trends in orthogonal age gradients/offsets do appear to extend to ~ 100 Myr old stellar populations (e.g. Calzetti et al. 2005) and so perhaps the result highlighted here is not obviated by the larger age bins.

²At least within co-rotation; we emphasise that we are *not* claiming that this is necessarily what we are witnessing within the simulation, but simply that it is consistent with the predictions of the basic theory.

2. Chemical properties

Finally, we wish to show our most recent work on the distribution of metals in a suite of $\sim 0.1 L^*$ disk simulations³ undertaken with a wide range of feedback prescriptions (including supernovae and thermal energy from OB-stars during their pre-supernovae phase), initial mass functions, and metal diffusion efficiencies. We focus here on our fiducial simulation, **11mKroupa**, which was first introduced in a different context by Brook et al. (2012). This simulation, like **g15784**, was realized with the GASOLINE code, but with an upgraded version which takes into account a broader spectrum of elements beyond just oxygen and iron.

The left-most panel of Fig. 2 shows the age-metallicity relation of the ‘solar neighborhood’ (an annulus ~ 3 disk scalelengths from the center, lying within a kpc of the mid-plane) associated with **11mKroupa**. The middle panel shows the corresponding relationship in the solar neighborhood of the Milky Way, as derived from the Geneva-Copenhagen Survey (GCS) by Holmberg et al. (2009). The right-most panel shows the associated metallicity distribution functions (MDFs) for these respective ‘solar neighborhoods’; the (indistinguishable) overlaid curves on the right-most MDF within the panel correspond to two ‘cuts’ of the GCS (essentially, ‘volume-limited’ and ‘open’, as per Pilkington et al. 2012b), while the left-most MDF is that constructed from **11mKroupa**.⁴

What should be readily apparent from Fig. 2 is that the age-metallicity relation for the solar neighborhood of **11mKroupa** is significantly more correlated than that of the Milky Way’s solar neighborhood and that it is very tight at a given age. The former should not be surprising, in that the star formation and infall histories of the two are not the same. Regardless, this tight correlation has an inexorable effect on the resulting MDF, in the sense that it is more negatively skewed, possesses greater kurtosis, while the MDF’s ‘peak’ component is quite narrow (due to the minimal dispersion in $[\text{Fe}/\text{H}]$ at a given age convolved with the simulation’s star formation history). A deeper analysis is provided by Pilkington et al. (2012b).

Acknowledgments. Without the help of our collaborators, this work would not have been possible; we thank them for their ongoing advice and guidance. We wish to thank both Monash and Saint Mary’s Universities for their generous visitor support. KP acknowledges the STFC studentship: (ST/F007701/1).

References

- Brook, C.B., Stinson, G., Gibson, B.K., et al. 2012, MNRAS, 419, 771
 Calura, F., Gibson, B.K., Michel-Dansac, L., et al. 2012, MNRAS, in press
 Calzetta, D., Kennicutt, R.C., Bianchi, L., et al. 2005, ApJ, 633, 871
 Dobbs, C.L., Pringle, J.E. 2010, MNRAS, 409, 396

³A parallel study of the MDFs associated with the full MUGS suite, including **g15784**, is presented in Calura et al. (2012).

⁴The stellar mass of **11mKroupa** is only $7.1 \times 10^9 M_{\odot}$, an order of magnitude lower than that of **g15784**, or the Milky Way; as such, the ~ 0.7 dex offset in the **11mKroupa** and GCS’ MDF centroids is to be expected.

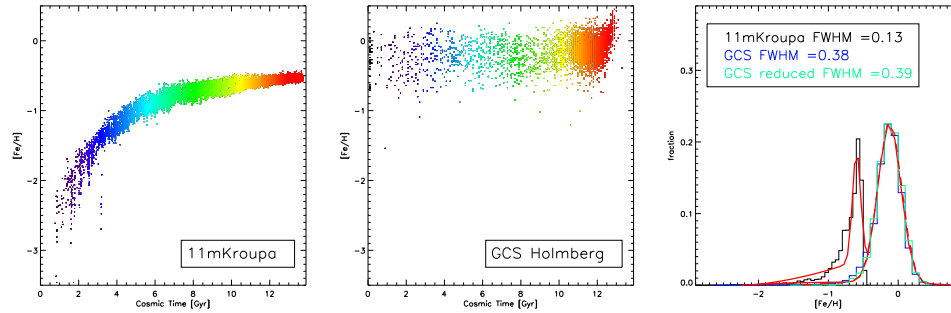


Figure 2. The left-most panel shows the age-metallicity relation for the stars situated in the ‘solar neighborhood’ of the 11mKroupa simulation. The stars are colored by age where red is the youngest and purple is the oldest. The middle panel, for comparison, shows the observed age-metallicity relation for the solar neighborhood of the Milky Way (Holmberg et al. 2009). The right-most panel shows the resulting metallicity distribution functions for these age-metallicity relations, along with simple single Gaussian fits to their respective peak regions.

- Grand, R.J.J., Kawata, D., Cropper, M. 2012, MNRAS, in press
 Holmberg, J., Nordström, B., Andersen, J. 2009, A&A, 501, 941
 Pilkington, K., Few, C.G., Gibson, B.K., et al. 2012a, A&A, 540, A56
 Pilkington, K., Gibson, B.K., Brook, C.B., et al. 2012b, MNRAS, 425, 969
 Sánchez-Gil, M.C., Jones, D.H., Pérez, E., et al. 2011, MNRAS, 415, 753
 Stinson, G.S., Bailin, J., Couchman, H., et al. 2010, MNRAS, 408, 812
 Stinson, G., Seth, A., Katz, N., et al. 2006, MNRAS, 373, 1074
 Wadsley, J.W., Stadel, J., Quinn, T. 2004, New Astron, 9, 137

The contribution of starbursts and normal galaxies to IR luminosity functions and the molecular gas content of the Universe at $z < 2$

M. T. Sargent¹, E. Daddi¹, M. Béthermin¹ and D. Elbaz¹

¹*CEA Saclay, DSM/IRFU/Sérvise d’Astrophysique, France*

Abstract. We present a parameter-less approach capable of predicting the shape of the infrared luminosity function at redshifts $z \leq 2$. It relies on three observables: (1) the redshift evolution of the stellar mass function for star-forming galaxies, (2) the evolution of the specific star formation rate of main-sequence galaxies, and (3) the double-Gaussian decomposition of the specific star formation rate distribution at fixed stellar mass into the contributions (assumed to be redshift- and mass-invariant) from main-sequence and starburst activity.

Using this self-consistent and simple framework, we identify the contributions of main-sequence and starburst activity to the global infrared luminosity function and find a constant or only weakly redshift-dependent contribution (8–14%) of starbursts to the star formation rate density at $z \leq 2$. Over the same redshift range, we also infer the evolution of the cosmic abundance of molecular gas in star-forming galaxies, based on the relations between star formation rate and molecular gas mass followed by normal and starburst galaxies.

1. Introduction

Star-forming galaxies (SFGs) at both high and low redshift are a mixture of (1) “normal” SFGs obeying a tight relation – the “galaxy main sequence” – between star formation rate (SFR) and stellar mass M_\star (e.g. Brinchmann et al. 2004; Daddi et al. 2007), and (2) “starbursts” with a strong excess in specific SFR (sSFR) compared to typical galaxies on the SFR- M_\star main sequence.

Distributions of M_\star and SFR describe galaxy populations at a very basic level. The stellar mass function (MF) of SFGs is well-fitted by a Schechter function (e.g., Ilbert et al. 2010), whereas their infrared (IR) luminosity function (LF, a proxy for the SFR distribution) is generally parameterized as a double exponential or power law function (e.g., Le Floch et al. 2005; Magnelli et al., 2009). A plausible explanation of this difference is the occurrence of burst-like and “normal” star formation (SF) activity among SFGs. The evolving shape of IR LFs hence implicitly contains information on the relative importance of the two modes of SF in the past.

Here we discuss how the contribution of main-sequence and starburst galaxies to IR LFs (and thus to the SFR density) can be disentangled and use this information to reconstruct the molecular gas history of the Universe.

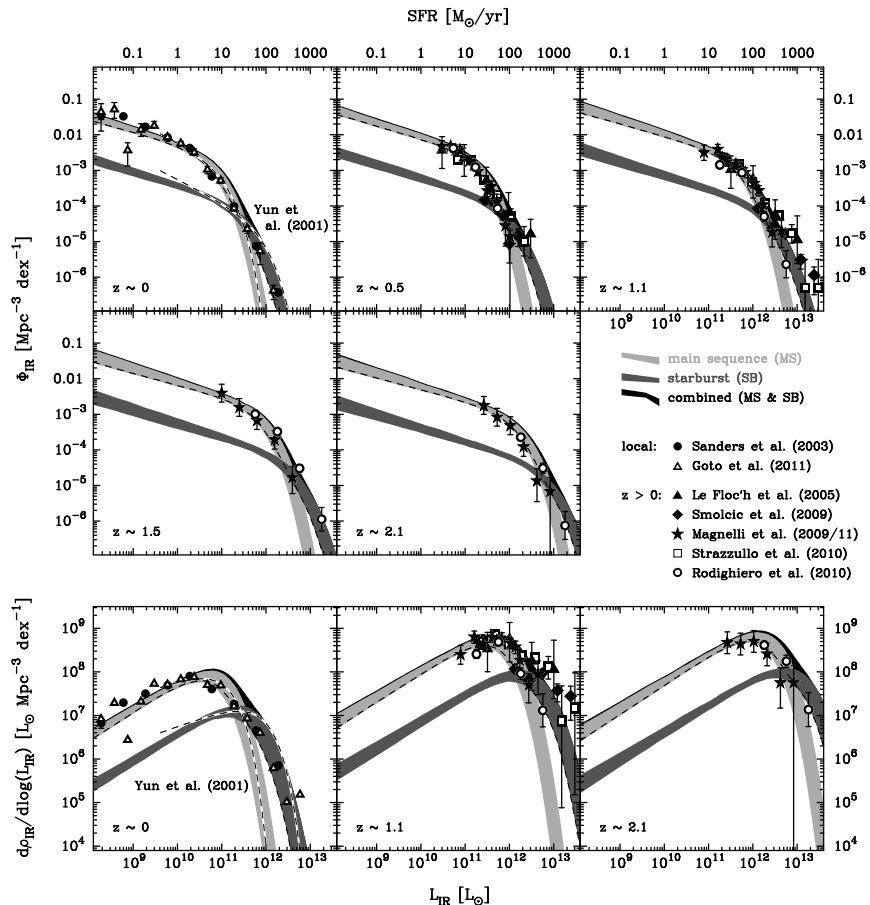


Figure 1. *Top*: Predicted contribution of normal (light grey) and burst-like (dark grey) star formation to IR LFs (SFR distributions; conversion between SFR and L_{IR} following Kennicutt 1998) at $z < 2$. Literature measurements are overlaid (see legend for authorship key). *Bottom*: Predicted IR luminosity density distributions.

2. Method

- *A simple model for the prediction of IR LFs*: The redshift evolution of the average sSFR in main-sequence galaxies out to $z \sim 2$ (e.g., Elbaz et al. 2011; Karim et al. 2011) can be combined with the evolution of the stellar MF of SFGs to predict the shape of the IR LF if the distribution of sSFR at fixed stellar mass is known. Based on the results of Rodighiero et al. (2011) for SFGs at $z \sim 2$, we approximate this distribution by a double-Gaussian function (identified as being due to main-sequence and burst-like SF activity, respectively; see Sargent et al. 2012 for details and a discussion of the underlying assumptions). The mapping of the stellar MF to an IR LF is effectively a convolution of the MF and a variable double-Gaussian kernel with (i) normalization fixed by the shape

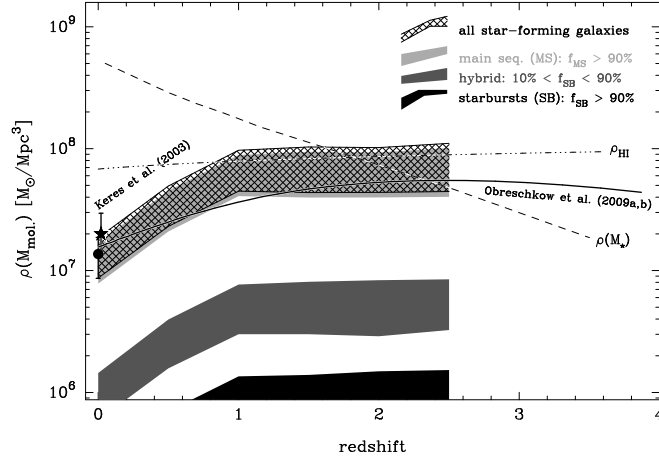


Figure 2. Inferred evolution of the comoving cosmic molecular gas density at $0 < z < 2.5$, contributed by SFGs dominated by normal, by burst-like SF activity or by a mixture of both SF modes (hatched curve – total SFG population). Dashed line: evolution of the stellar mass density (e.g. Fontana et al. 2006); dash-dotted line: evolution of cosmic HI abundance (Bauermeister et al. 2010); black, thin curve: simulation-based predictions (Obreschkow et al. 2009). The $z = 0$ measurements from Obreschkow et al. (2009; dot) and Keres et al. (2003; star) are also shown.

of the MF and (ii) main-sequence peak position that – given the redshift – is uniquely determined by the position of the SF main sequence in the (s)SFR vs. M_{\star} plane. Thanks to our decomposition, we can then also identify the individual contribution of normal and burst-like SF activity to the IR LF (see Fig. 1).

- *The molecular gas history of the Universe:* The well-constrained evolution at $z < 2.5$ of stellar MF and sSFR of SFGs and our decomposition of the SFR distribution at fixed M_{\star} into components due to normal and burst-like SFR activity provides a powerful framework for the prediction of cosmological observables, e.g. the evolution of molecular gas reservoirs in normal and starburst galaxies (Sargent et al. 2012, in prep.). One of the main discoveries that recently gave rise to the notion of “bimodal” SF is that “normal” galaxies at low and high redshift convert their molecular gas into stars with an approximately 10-fold lower efficiency than starburst galaxies (cf. Daddi et al. 2010b; Genzel et al. 2010). The two populations follow parallel, slightly supralinear relations between SFR and molecular mass (M_{mol}). We use these integrated Kennicutt-Schmidt relations to convert the SFR-distributions in Fig. 1 into mass functions for the molecular gas component of SFGs experiencing either normal and burst-like SF activity. The redshift-dependent molecular gas MFs can then be integrated to infer the cosmic abundance of molecular gas (Fig. 2).

3. Results and discussion

In Fig. 1 we show that the evolution of the stellar MF and of the IR LF (i.e. of the SFR distribution) of SFGs at $z < 2$ is self-consistent (see also Bell et al. 2007) and that starburst galaxies are the dominant factor shaping the bright end of the IR LFs. We find (cf. Sargent et al. 2012) that the fractional contribution of starburst activity to the cosmic SFR density (8–14%) is only weakly redshift-dependent at $z < 2$. We also reproduce the well-known fact that most local ULIRGs are starbursts (e.g., Sanders & Mirabel 1996). At $z > 0.9$, the majority of ULIRGs are main-sequence galaxies. Importantly, however, their high SFR ($>100 M_{\odot}$) is not triggered by merging as in most local ULIRGs but is a secular process linked to large gas reservoirs in high- z disks (e.g., Daddi et al. 2010a, Tacconi et al. 2010, Geach et al. 2011). Local and distant ULIRGs are *intrinsically different objects* for which direct comparisons should be avoided.

Fig. 2 illustrates the rapid growth of molecular gas reservoirs in SFGs. We infer that most of this 10-fold increase takes place at $z < 1$ and that it is entirely dominated by the molecular gas fuelling “secular” SF activity in main-sequence galaxies. By $z \sim 2$, the comoving stellar and molecular mass content of the Universe are predicted to become equal, in good agreement with the molecular gas fractions of $\sim 50\%$ measured in $z \sim 2$ disks (e.g., Daddi et al. 2010a; Tacconi et al. 2010).

References

- Bauermeister, A., et al. 2010, ApJ, 717, 323
Bell, E. F., et al. 2007, ApJ, 663, 834
Brinchmann, J., et al. 2004, MNRAS, 351, 1151
Daddi, E., et al. 2007, ApJ, 670, 156
Daddi, E., et al. 2010a, ApJ, 713, 686
Daddi, E., et al. 2010b, ApJ, 714, L118
Elbaz, D., et al. 2011, A&A, 533, A119
Fontana, A., et al. 2006, A&A, 459, 745
Geach, J. E., et al. 2011, ApJ, 730, L19
Genzel, R., et al. 2010, MNRAS, 407, 2091
Ilbert, O., et al. 2010, ApJ, 709, 644
Karim, A., et al. 2011, ApJ, 730, 61
Keres, D., et al. 2003, ApJ, 582, 659
Le Floch, E., et al. 2005, ApJ, 632, 169
Magnelli, B., et al. 2009, A&A, 496, 57
Obreschkow, D., & Rawlings, S. 2009, ApJ, 696, L129
Rodighiero, G., et al. 2011, ApJ, 739, L40
Sanders, D. B., & Mirabel, I. F. 1996, ARA&A, 34, 749
Sargent, M., et al. 2012, ApJ, 747, L31
Tacconi, L. J., et al. 2010, Nature, 463, 781

A first look at galaxy flyby interactions: characterizing the frequency of flybys in a cosmological context

M. Sinha¹ and K. Holley-Bockelmann¹

¹*Department of Physics & Astronomy, Vanderbilt University, Nashville, USA*

Abstract. Hierarchical structure formation theory is based on the notion that mergers drive galaxy evolution, so a considerable framework of semi-analytic models and N-body simulations has been constructed to calculate how mergers transform a growing galaxy. However, galaxy mergers are only one type of major dynamical interaction between halos – another class of encounter, a close flyby, has been largely ignored. We analyze a $50 h^{-1}$ Mpc, 1024^3 collisionless cosmological simulation and find that the number of close flyby interactions is comparable to, or even surpasses, the number of mergers for halo masses $\gtrsim 10^{11} h^{-1} M_{\odot}$ at $z \lesssim 2$. Halo flybys occur so frequently to high mass halos that they are continually perturbed, unable to reach a dynamical equilibrium. We also find tentative evidence that at high redshift, $z \gtrsim 14$, flybys are as frequent as mergers. Our results suggest that close halo flybys can play an important role in the evolution of the earliest dark matter halos and their galaxies, and can still influence galaxy evolution at the present epoch.

1. Introduction

In a Λ CDM Universe, the smallest dark matter halos form first; bigger halos are then formed via successive mergers with smaller halos. Thus, mergers are instrumental in the formation and evolution of halos. Mergers can dramatically change a galaxy – from its morphology (e.g., Holmberg 1941; Toomre & Toomre 1972; Barnes 2002), to its stellar population (e.g., Mihos & Hernquist 1994), to the evolution of the central supermassive black hole (e.g., Hopkins et al. 2006; Micic et al. 2011). Consequently, merger rates have been studied extensively, both theoretically (e.g., Lacey & Cole 1993; Genel et al. 2009) and observationally (e.g., Schweizer 1986). Collisionless cosmological N-body simulations can be used to measure halo merger rates, where a merger is defined to occur when a bound dark matter halo falls into another bound dark matter halo. Galaxy merger rates can then be inferred from the subhalo mergers within a primary halo by assuming a $M_{\text{halo}}-M_{\text{gal}}$ relation (e.g., Guo & White 2008; Wetzel et al. 2009) or directly measured in hydrodynamic simulations (e.g., Maller et al. 2006; Simha et al. 2009). Observationally, galaxy merger rates are typically derived from close-pair counts – i.e. galaxies with small projected separations and relative velocities – and are globalized using an estimate of the lifetime or duration of the observed merger phase (Lotz et al. 2010; Zavala et al. 2012).

Ultimately, galaxy mergers are successful in shaping galaxy properties because they cause a large perturbation within the potential. However, one entire

class of galaxy interactions also capable of causing such perturbations – galaxy flybys – has been largely ignored. Unlike galaxy mergers where two galaxies combine into one remnant, flybys occur when two independent galaxy halos interpenetrate but detach at a later time; this can generate a rapid and large perturbation in each galaxy. We developed and tested a method to identify mergers and flybys between dark matter halos in cosmological simulations and to construct a full ‘interaction network’ that assesses the past interaction history of any given halo. In this work, we present a census of halo flybys and mergers in the Universe determined from cosmological simulations. Please see Sinha & Holley-Bockelmann (2012) for more details.

2. Methods

We use a high-resolution, dark matter simulation with 1024^3 particles in a box of length $50h^{-1}$ Mpc with WMAP-5 cosmological parameters as a testbed to develop our technique. We use a fixed, co-moving softening length of $2.5h^{-1}$ kpc and evolve the particles with GADGET-2 (Springel et al. 2001a; Springel 2005). Since the fundamental mode goes non-linear at $z = 0$, we will only present results up to $z = 1$ where the $50h^{-1}$ Mpc box is still a representative cosmological volume. To begin identifying halos, we first use a Friends-of-Friends (FOF) technique with a canonical linking length $b = 0.2$ ($\sim 10h^{-1}$ kpc). We require at least 20 particles ($\sim 10^8 h^{-1} M_\odot$) to define a halo, but our halo interaction network uses only those halos with greater than 100 particles. Subhalos are identified using the SUBFIND algorithm (Springel et al. 2001b).

We classify a flyby using spatial *and* dynamical information. Conceptually, a grazing flyby occurs when a halo undergoes the transition from a main halo \rightarrow subhalo \rightarrow a main halo and is fundamentally different from mergers. However, using only this main halo \rightarrow subhalo \rightarrow a main halo transition would also capture spurious interactions where one halo just skirts the outer edge of another halo. We eliminate these spurious interactions by only choosing the flybys that have a duration longer than half the crossing time¹. We find that with this definition the rate of flybys converges irrespective of the frequency of snapshot outputs. In a simulation, it is relatively straightforward to identify such chains since the current kinematics and future behavior of a given interaction is fully determined. We note that because flybys imply a population of galaxies that were once well within the virial radius of the main halo but are now outside it, they may be related to the so called ‘backsplash’ galaxies (Gill et al. 2005).

3. Results

In the left panel of Figure 1 we show the number of flybys and mergers on a per halo per Gyr basis, while the ratio of flybys to mergers is seen in the right panel. We see that flybys are more frequent for higher-mass halos at all redshifts, consistent with the Λ CDM framework. From the figure, we can directly see that

¹Since the skirting encounters would necessarily be very short-lived. By imposing this minimum duration, we are capturing the target orbit, i.e., that of a subhalo going through a main halo.

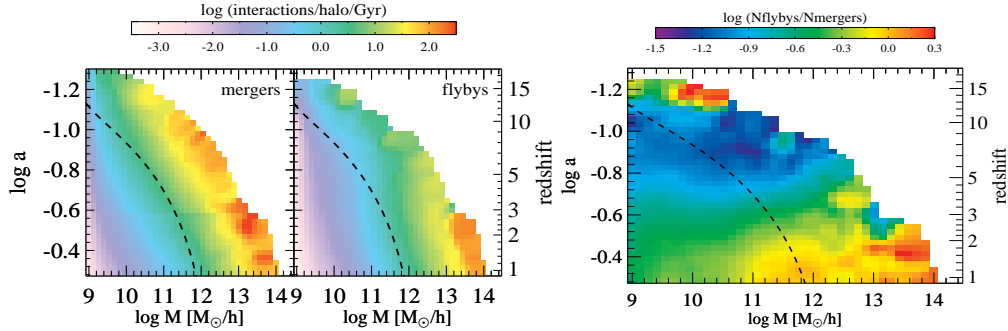


Figure 1. *Left:* This figure shows the number of mergers (left) and flybys (right) per halo per Gyr as a function of primary halo mass and redshift. The dashed line shows the mass accretion history of a typical Milky-Way type obtained from our simulations. The number of flybys increases with the primary halo mass for all redshifts, consistent with Λ CDM. For $z \lesssim 3$, halos above $10^{13} h^{-1} M_\odot$ have flyby rates greater than 100 per Gyr. Such a high flyby rate (in addition to mergers) means these halos are unlikely to be in equilibrium. *Right:* Ratio of number of flybys to mergers as a function of primary halo mass and redshift. Mergers dominate flybys by an order of magnitude for $12 \lesssim z \lesssim 4$. At lower redshifts, however, flybys start becoming more prevalent and by $z \sim 2$, flybys are at comparable or even larger for all halos above $10^{11} h^{-1} M_\odot$.

the number of flybys becomes comparable or larger than the number of mergers for halos $> 10^{11} h^{-1} M_\odot$ for $z \lesssim 2$. Such halos are expected to host galaxies – and the effect of flybys should leave an imprint on the observable properties. We also find tentative evidence that flybys are comparable in number to mergers at the highest redshifts, $z \gtrsim 14$ – however, the numbers are affected by Poisson error and we can not conclusively say that flybys dominate mergers at those redshifts.

We checked to see if there are multiple flybys between the same halo pairs and found that $\sim 70\%$ of the flybys do not recur. About 20% of flybys eventually become a merger and $\sim 6\%$ are repeated flybys. Thus, flybys primarily represent one-off events between two halos. We find that a typical flyby has a relative velocity $\sim 1.5 - 2$ times the circular velocity of the primary and penetrates to $\sim 30\%$ (up to 10%) of the primary virial radius. Such close encounters can create a strong perturbation that potentially transform the galaxy.

4. Conclusions

In this paper we report on a new class of interactions – flybys, that occur frequently. Most of these flybys are one-off events – one halo delves within the virial radius of another main halo and separates at a later time. We find that the number of close flyby interactions is comparable to, or even surpasses, the number of mergers for halo masses $\gtrsim 10^{11} h^{-1} M_\odot$ at $z \lesssim 2$. We find that most flybys are one-off events and about 70% of the flybys do not ever return. In general, slow flybys cause a larger perturbation compared to a fast one, and such features can persist even when the perturbing halo has moved far away (Vesperini & Weinberg 2000). Flybys are then, a largely-ignored type of interaction that

can potentially transform galaxies. Unfortunately, most semi-analytic methods of galaxy formation are designed only to use mergers and thus can not account for the effects of flybys directly.

Although the simulations outlined here pertain strictly to dark matter halo flybys, there are naturally links between these results and galaxy flybys. To better simulate the rate of galaxy flybys, we need to populate these halos with galaxies. This will allow us to constrain the actual galaxy flyby rate and to statistically compare to numerical (e.g., Perez et al. 2006) and observational studies of galaxy-pairs (e.g., Nikolic et al. 2004, Kewley et al. 2006, Driver et al. 2006).

Acknowledgments. MS would like to thank the organizers for a wonderful conference. This work was conducted in part using the resources of the Advanced Computing Center for Research and Education at Vanderbilt University. We also acknowledge support from the NSF Career award AST-0847696.

References

- Barnes, J. E. 2002, MNRAS, 333, 481
Driver, S. P. et al. 2006, MNRAS, 368, 414
Genel, S., et al. 2009, ApJ, 701, 2002
Gill, S. P. D., Knebe, A., & Gibson, B. K. 2005, MNRAS, 356, 1327
Guo, Q., & White, S. D. M. 2008, MNRAS, 384, 2
Holmberg, E. 1941, ApJ, 94, 385
Hopkins, P. F., et al. 2006, ApJS, 163, 1
Kewley, L. J., Geller, M. J., & Barton, E. J. 2006, AJ, 131, 2004
Lacey, C., & Cole, S. 1993, MNRAS, 262, 627
Lotz, J. M., Jonsson, P., Cox, T. J., & Primack, J. R. 2010, MNRAS, 404, 575
Maller, A. H., et al. 2006, ApJ, 647, 763
Micic, M., Holley-Bockelmann, K., & Sigurdsson, S. 2011, MNRAS, 414, 1127
Mihos, J. C., & Hernquist, L. 1994, ApJ, 431, L9
Nikolic, B., Cullen, H., & Alexander, P. 2004, MNRAS, 355, 874
Perez, M. J. et al. 2006, A&A, 449, 23
Schweizer, F. 1986, Science, 231, 227
Simha, V., et al. 2009, MNRAS, 399, 650
Sinha, M., & Holley-Bockelmann, K. 2012, ApJ, 751, 17
Springel, V. 2005, MNRAS, 364, 1105
Springel, V., Yoshida, N., & White, S. D. M. 2001a, New Astronomy, 6, 79
Springel, V., et al. 2001b, MNRAS, 328, 726
Toomre, A., & Toomre, J. 1972, ApJ, 178, 623
Vesperini, E., & Weinberg, M. D. 2000, ApJ, 534, 598
Wetzel, A. R., Cohn, J. D., & White, M. 2009, MNRAS, 395, 1376
Zavala, J., Avila-Reese, V., Firmani, C., & Boylan-Kolchin, M. arXiv:1204.0516

Infant mortality in the hierarchical merging scenario

R. Smith¹, M. Fellhauer¹ and S. Goodwin²

¹*Depto de Astronomia, UdeC, Concepcion, Chile*

²*Department of Physics and Astronomy, University of Sheffield, Sheffield, UK*

Abstract. We examine the effects of gas expulsion on initially sub-structured and out-of-equilibrium star clusters. We perform N -body simulations of the evolution of star clusters in a static background potential before removing the potential to model gas expulsion. We investigate the impact of varying the instant at which gas removal begins. The instant at which gas expulsion occurs is found to have a strong effect on cluster response to gas removal. We find that if gas expulsion occurs prior to one crossing time, cluster response is poorly described by *any* global parameters. Furthermore in real clusters the instant of gas expulsion is poorly constrained. Therefore our results emphasise the highly stochastic and variable response of star clusters to gas expulsion.

1. Introduction

Most stars appear to form in groups of tens to thousands of members embedded in molecular clouds. The initial distribution of stars follows the complex clumpy and filamentary structure of the underlying gas (e.g Bressert et al. 2010; di Francesco et al. 2010). In the hierarchical merging scenario clusters form by mergers of stars and stellar groups from this complex distribution (Allison et al. 2010). Initially the region in which clusters form has a mass that is dominated by the molecular gas. Yet observations show very few young clusters associated with natal gas older than ~ 5 Myr (Lada & Lada 2003; Lada 2010). It is assumed that feedback from massive stars removes residual gas in a gas expulsion phase. This gas expulsion will significantly alter the potential felt by the stars and can result in the destruction of the cluster (e.g. Goodwin & Bastian 2006; Baumgardt & Kroupa 2007; Goodwin 2009). This is often cited as the cause of ‘infant mortality’: the apparently high destruction rate of young clusters.

We examine the impact of gas expulsion when the initial distributions of the stars and gas are not in dynamical equilibrium, causing them to collapse and form a bound cluster within the gas potential (Smith et al. 2011a,b).

2. Method

We present a very simple numerical experiment: a clumpy distribution of equal-mass stars moving in a smooth (Plummer) background potential meant to model the residual gas in young star clusters. We remove the background potential to

model the effects of instantaneous gas expulsion starting at different times. We perform our N -body simulations using the NBODY6 code (Aarseth 2003). We describe our method step-by-step. For parameter values see Table 1:

1. A fractal distribution of stars is placed in a smooth Plummer potential background. The fractal is constructed using the box fractal method (Goodwin & Whitworth 2004; Allison et al. 2010). We conduct 5 realisations of any cluster.
2. We set the initial velocity dispersion of the stars relative to the total potential (gas and stars) including a sub-virial and virial case. The stars are evolved within the gas potential until gas expulsion begins at time t_{exp} .
3. Just before gas expulsion occurs, we measure two key properties of the star cluster; the local stellar fraction (LSF), and the pre-gas expulsion virial ratio Q_{ge} (see Table 1 for a discussion of LSF and Q_{ge}).
4. We use a range of values for the time at which gas expulsion begins¹. In this contribution we shall only consider instantaneous gas expulsion², modelled by the total removal of the gas potential at t_{exp} .
5. Finally, we measure the final bound fraction f_{bound} of each star cluster at $t = 15$ Myr to determine how well the cluster survives.

Number of star particles	$N = 1000$ ($0.5M_{\odot}$ each)
Total stellar mass	$500M_{\odot}$
Fractal Dimension	$D = 1.6$ (very clumpy)
Radial cut-off	1.5 pc
Plummer mass of gas (at $r = \infty$)	$M_{\text{g}} = 2000M_{\odot}$
Plummer scale length of gas	$r_{\text{g}}=1.0$ pc
Crossing-time of the region	$t_{\text{cr}} \sim 1.3$ Myr
Star formation efficiency ($r < 1.5$ pc)	SFE=0.3
Initial virial ratio of stars	$Q_{\text{i}}=0.2$ (subvirial), 0.5 (virial)
Instant of gas expulsion	$t_{\text{exp}}=0.1, 1.0, 5.0, 9.0$ Myr

Table 1. Star forming region parameters for the initial fractal of stars (upper rows), the gas (middle rows), and the complete star forming region (lower rows).

As we have shown previously (Goodwin 2009; Smith et al. 2011a) if the stars can collapse relative to the gas distribution then the effect of gas expulsion is less important. We defined the local stellar fraction (LSF, Smith 2011a) as $\text{LSF} = M_{\text{s}}^{r_{\text{h(s)}}} / (M_{\text{g}}^{r_{\text{h(s)}}} + M_{\text{s}}^{r_{\text{h(s)}}})$ where $M_{\text{s}}^{r_{\text{h(s)}}}$ and $M_{\text{g}}^{r_{\text{h(s)}}}$ are the mass of stars and gas, respectively, *measured at the half-mass radius of the stars*. Thus, the LSF is a measure of the mass of gas in the region where the stars are found, and (unlike the SFE) can evolve as the stars redistribute.

¹The time at which gas removal begins in real clusters is uncertain, and depends on the specific gas loss mechanism at work, e.g. late starts maybe due to the supernovae of low-mass O stars.

²We consider a variable gas expulsion rate in Smith et al. (2013).

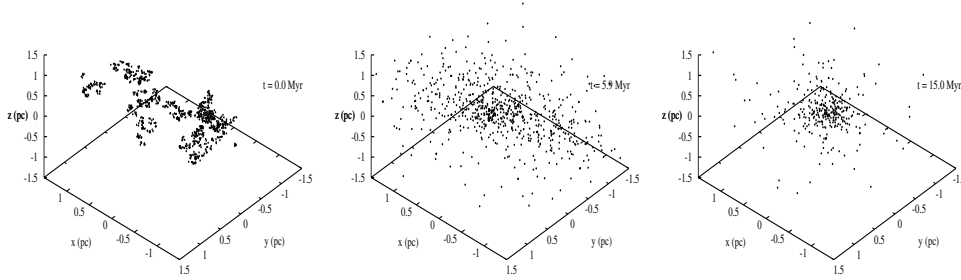


Figure 1. The evolution of the stellar distribution in the gas potential for the initial fractal distribution (left panel), that of the instant of gas expulsion (central panel), and the final distribution (right panel).

The virial ratio of the stars at the moment of gas expulsion Q_{ge} is also important (Goodwin & Bastian 2006). We found the LSF and Q_{ge} to be effective predictors of the response of an initially out-of-equilibrium cluster to instantaneous gas expulsion after a few crossing times (Smith et al. 2011a).

3. Results

Fig. 1 shows a representative example. An initially subvirial fractal distribution of stars (SFE=20%) evolves within the gas potential. Violent relaxation occurs due to the clumpy stellar structure, causing the majority of the substructure to be quickly erased (within 1-2 t_{cr}). The LSF oscillates considerably but when gas expulsion occurs, it is almost twice³ its original value because the stars concentrate within the gas potential, resulting in better survival to gas-loss. The removal of the gas potential results in the loss of unbound stars. We emphasise that this example is always below the critical SFE ($\sim 30\%$, Goodwin & Bastian 2006; Baumgardt & Kroupa 2007) for the survival of a bound core⁴. Yet by $t=15$ Myr a settled bound core remains. The virial ratio when gas expulsion occurs can also affect the cluster survival (Smith et al. 2011a). During violent relaxation, large oscillations in the virial ratio occur around the virial value, but these reduce as the cluster settles. Thus we might predict the influence of the virial ratio to be reduced if gas expulsion is delayed.

The effects of varying the time at which gas expulsion occurs t_{exp} are shown in Fig. 2. If gas expulsion occurs between 1-2 t_{cr} (centre panel), a broad trend of increasing f_{bound} with increasing LSF can be seen. Some of trend's scatter is from the virial state at the time of gas expulsion, with sub-virial star clusters surviving better (blue circles) and super-virial star clusters surviving less well (red circles), as seen in Smith 2011a (faint crosses). However at later times (right panel) the cluster is closer to dynamical equilibrium causing the scatter in the trend to reduce. Even now, some scatter remains due to the *inherent stochasticity introduced by irregular initial distributions of stars*. At early times (left panel), this inherent stochasticity results in a large scatter. In this regime,

³There is considerable scatter in this value between random realisations

⁴From an initially virialised star-gas distribution, with instantaneous gas expulsion

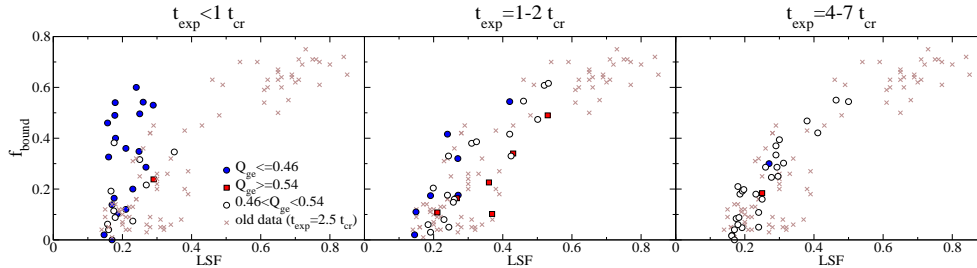


Figure 2. Final bound fraction of stars f_{bound} vs. local stellar fraction (LSF) for clusters with early gas removal ($t_{\text{exp}} \leq 1t_{\text{cr}}$), intermediate gas removal time ($t_{\text{exp}} = 1.5-2.0t_{\text{cr}}$), and late gas removal ($t_{\text{exp}} = 4-7t_{\text{cr}}$). The stellar virial ratio at the onset of gas expulsion Q_{ge} is either low (blue circles, $Q_{\text{ge}} < 0.46$), roughly virialised (open circles, $0.46 < Q_{\text{ge}} < 0.54$), or high (red squares, $Q_{\text{ge}} > 0.54$). Light crosses show the results for $t_{\text{exp}} = 2.5t_{\text{cr}}$ from Smith et al. (2011a).

neither the LSF or Q_{ge} are reliable indicators of cluster survival. *In brief, the cluster response to gas loss is sensitive to the time at which gas expulsion occurs – a poorly constrained parameter in real clusters.*

4. Conclusions

In this contribution we present a simple numerical experiment examining the evolution of non-equilibrium small- N clusters within a smooth background potential which models the gas. Whilst this is clearly not realistic, we wish to examine the stochasticity that complex stellar distributions introduce. As we have demonstrated, statistically identical non-equilibrium clusters can evolve in *very* different ways even in our very simple numerical experiments. By adding more realistic physics (e.g. a stellar mass function) stochasticity will likely increase further. This stochasticity removes the simple correlation between initial conditions and survivability that is so often assumed. In summary, there is no reason to think that if one cluster survives and another did not, they have had very different initial conditions. We urge caution in drawing any conclusions about the initial conditions of a cluster system (e.g., true SFE) from observations of naked clusters and infant mortality rates.

Acknowledgments. RS acknowledges support by FONDECYT grant 3120135.

References

- Aarseth, S. J., 2003, ‘Gravitational N-body Simulations’, Cambridge Univ. Press
- Allison, R. J., Goodwin, S. P., Parker, R. J., et al., 2010, MNRAS, 407, 1098
- Baumgardt, H., Kroupa, P., 2007, MNRAS, 380, 1589
- Bressert, E., Bastian, N. and Gutermuth, et al., 2010, MNRAS, 409, L54
- di Francesco, J., Sadavoy, S., Motte, et al., 2010, A&A, 518, L91
- Gieles, M., Portegies Zwart, S. F., 2011, MNRAS, 410, L6
- Goodwin, S. P. and Whitworth, A. P., 2004, A&A, 413, 929

- Goodwin, S. P., Bastian, N., 2006, MNRAS, 373, 752
Goodwin, S. P., 2009, Ap&SS, 324, 259
Lada, C. J., Lada, E. A., 2003, ARA&A, 41, 57
Lada, C. J., 2010, Philosophical Transactions: MP&ES, 368, 1913
Smith, R., Fellhauer, M., Goodwin, S., et al., 2011a, MNRAS, 414, 3036
Smith, R., Slater, R., Fellhauer, M., et al., 2011b, MNRAS, 416, 383
Smith, R., Fellhauer, M., Goodwin, S., et al., 2013, MNRAS, 428, 1303

The effect of supernovae on galaxy chemical evolution

O. N. Snaith¹, P. B. Tissera¹ and S. Pedrosa¹, M. E. de Rossi¹ and J. M. Vilchez²

¹*IAFE, CONICET-UBA, Ciudad de Buenos Aires, Argentina*

²*CSIC, Apartado 3004, 18080 Granada, Spain*

Abstract. We report preliminary results on a study of the effects of supernova feedback on galaxy chemical enrichment using cosmological hydrodynamical simulations. Our simulated galaxies have disc systems which form inside out, in agreement with current theories of galaxy formation. We acknowledge the fact that the parameters used for the analyzed SN feedback models generated galactic outflows too efficient at driving metals outside the galaxies, and produced abundances lower than those observed in nearby galaxies. We find that the disc components have metallicity gradients in global agreement with observed ones. A trend for galaxies with relatively steep gradients at $z \sim 1$ to have slightly shallow gradients at $z \sim 0$ is detected in agreement with observations.

1. Introduction

Galaxy formation is a complex process involving dark matter, gas and stellar physics (see Cole et al. 2000). For the purposes of this work, the effect of supernova (SN) feedback on the metallicity gradients of galaxies will be explored using cosmological hydrodynamical simulations, and the results will be compared to observational findings. The metallicity gradients in disc galaxies have been also studied by other authors using different codes (e.g. Pilkington et al. 2012).

SN feedback plays an important role in regulating star formation and hence, the chemical evolution of the galaxies. However, this process is not fully understood as yet and there exist different models of SN feedback which are being tested. We explore the effects of SN on the chemical evolution of galaxies, focusing on the metallicity gradients. In this proceeding, we report preliminary results of the analysis of two numerical experiments obtained using different SN parameters.

2. Method

GADGET-3, an optimised version of GADGET-2 (Springel & Hernquist 2003, Springel 2005), was used to simulate a region of the universe $10 \text{ h}^{-1} \text{ Mpc}$ on the side using the WMAP Year 1 cosmology with the cosmological parameters, $\Omega_m=0.3$, $\Omega_\Lambda=0.7$, $\Omega_b=0.04$, $\sigma_8=0.9$, $h=0.7$ (Spergel et al. 2003). This version of GADGET-3 has been modified to include the multiphase ISM approach and the SN feedback implementation of Scannapieco et al. (2005, 2006). The set of simulations analyzed here have been previously studied by de Rossi, Tissera &

Pedrosa (2010). The initial gas mass particle is $9.1 \times 10^5 h^{-1} M_{\odot}$ and the dark matter mass particle is $5.9 \times 10^6 h^{-1} M_{\odot}$.

The simulations used have the same initial conditions, differing only in the amount of energy and metals delivered to the hot and cold phase of the gas. So, any difference between the experiments is due to the SN feedback. The values of the parameters used in simulation A (simulation B) are 7×10^{50} erg (4×10^{50} erg) and 50% (80%) for the SN energy and the fraction of metals ejected into the cold gas, respectively. The SN in simulation A are more energetic and impart over half their metals to the cold phase of the gas, while simulation B imparts 80% of the metals to the cold phase (the remainder goes to the hot gas, see Scannapieco et al. 2009 for a complete explanation of the model). Also, the parameters used in Simulation A were designed to produce a Milky Way type galaxy (Scannapieco et al. 2008). We identify the corresponding objects in both simulations and compare their physical properties.

3. Results

The discs were extracted from each galaxy using the procedure outlined by Tissera, White & Scannapieco (2012). In the following analysis we focus only on the disc components. The galaxy discs tend to have increasingly young stars with increasing radius, in agreement with current galaxy formation theories which predict an inside out formation. The first notable difference between the properties of both experiments is the amount of baryonic mass converted into stars. As expected, simulation B contains almost 50% more mass locked up in stars than simulation A. This has a direct effect on the amount of metals, with simulation B being correspondingly more metal-rich.

We calculate $12+\log(\text{O}/\text{H})$ gradients for the 10 most massive galaxies (resolved with more than 30000 baryonic particles within the galaxy radius), and compare the results with the observations of Dutil & Roy (1999) and Rupke et al. (2010). These authors studied the metallicity gradients of the HI gas in disc galaxies. The left panel of Fig. 1 shows that, for stars, both simulations underestimate the amount of metals when compared to the gas component in observed galaxies by approximately ~ 0.8 dex and ~ 0.5 dex for simulations A and B respectively. The gas metallicity gradients tend to be shallower than those of the simulated stellar components but are within observed values. The abundances of the simulated gas components is still lower than observed.

We also subdivided the stars by age, producing a young sample of stars formed within approximately the SN Ia lifetime, two intermediate age samples and a sample of old stars with ages greater than 8 Gyr. The process of chemical enrichment with time is recovered for some galaxies in both models, although not for all. This implies a complex star formation history, with considerable variation between individual galaxies, which will be explored in a separate paper.

When we look back to $z \sim 1$ (Fig. 2) and follow the ten most massive (selected at $z = 0$) galaxies forwards in time to $z = 0$ we find that the gradients of the galaxies change so they are much steeper at early times. This trend is in agreement with recently reported observations by Yuan et al. (2011) who measured a metallicity gradient of ~ -0.16 dex kpc^{-1} at $z \sim 1.5$. A more detailed study will be presented in an extended paper.

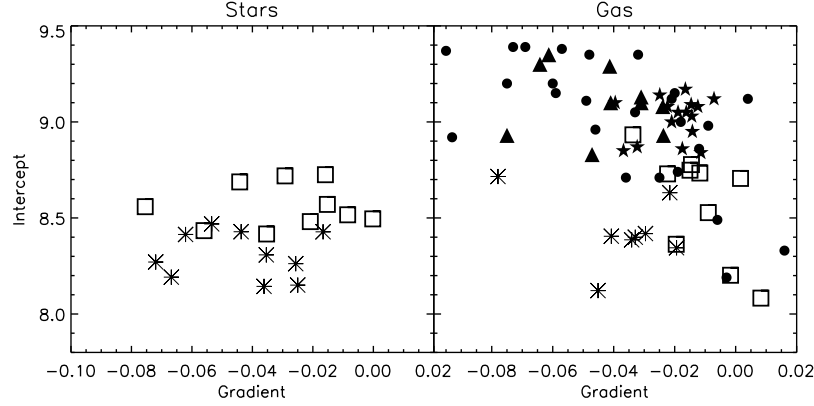


Figure 1. Intercepts and gradients of the $12 + \log(O/H)$ profiles for the stellar (left panel) and the gas (right panel) components of the ten most massive galaxies in simulation *A* (asterisks) and simulation *B* (hollow squares). For comparison, observations from Dutil et al. (1999) (filled circles) and Rupke et al.'s isolated (filled triangles) and interacting (stars) galaxy samples have been included.

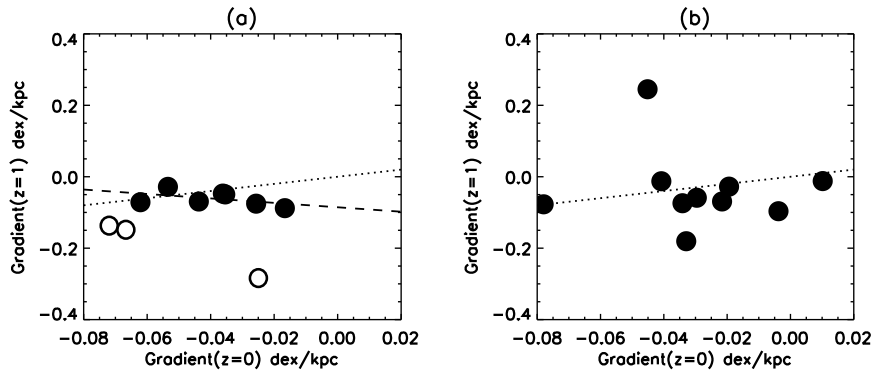


Figure 2. Panel A: Correlation of O/H gradients measured at $z = 0$ and $z = 1$ for stars in simulation *A*. The dotted line shows the 1:1 ratio and the dashed line shows the best fit straight line for simulation *A*, neglecting the three outliers (rings). Panel B is the same as Panel A but for the gas. The redshift evolution of the gradients are in agreement with the trend reported by Yuan et al. (2011) for a galaxy at $z \sim 1.5$.

4. Conclusion

The simulated discs form inside-out as expected from current models for disc formation. The total metallicities of the gas and stars in both simulations are too low, indicating that our SF feedback model has been too efficient at transporting chemical elements outside the galaxies. However, new detailed observations may provide improved information on the metallicity content of HII regions and consequently better constrain our models, e.g. Sanchez et al. (2012). The gas metallicity gradients are within observed range values. An analysis of the metallicity gradients according to stellar age shows the expected evolution of an inside-out formation for some of the galaxies, however, others exhibit a more complex chemical structure history suggesting the actions of other physical mechanisms along the evolutionary history.

Acknowledgments. ONS wishes to thank a fellowship from the European Commissions Framework Programme 7, through the Marie Curie Initial Training Network CosmoComp (PITN-GA-2009-238356). PBT thanks the PICT 32343 (2005) and PICT Max Planck 245 (2006) of the Ministry of Science and Technology (Argentina). We also thank the referee for their helpful comments.

References

- de Rossi, M. E., et al. 2010, *A&A*, 519, A89
Dutil Y. & Roy J. 1999, *ApJ*, 516, 62
Rupke, D. S. N., et al. 2010, *ApJ*, 723, 1255
Sanchez, S.F., et al. 2012, *A&A*, 546, A2
Scannapieco, C., et al. 2005, *MNRAS*, 364, 552
Scannapieco, C., et al. 2006, *MNRAS*, 371, 1125
Scannapieco, C., et al. 2008, *MNRAS*, 389, 1137
Scannapieco, C., et al. 2009, *MNRAS*, 396, 696
Spergel, D. N, et al. 2003, *ApJS*, 148, 175
Springel, V, Hernquist, L. 2003, *MNRAS*, 339, 289
Springel, V. 2005, *MNRAS*, 364, 1105
Tissera, P. B., et al. 2012, *MNRAS*, 420, 255
Yuan, T.T, et al. 2011, *ApJL*, 732, L14

Massive galaxies in most dense environments at $z \sim 1.4$

V. Strazzullo¹, P. Rosati², M. Pannella¹, R. Gobat¹ and J. Santos³

¹*CEA Saclay, Service d'Astrophysique, France*

²*ESO, Garching, Germany*

³*ESAC/ESA, Madrid, Spain*

Abstract. At a cosmic time when galaxy clusters start showing evidence of a still active galaxy population, the X-ray luminous cluster XMMU J2235-2557 at $z = 1.39$ already hosts massive early-type galaxies on a tight red sequence. The bulk of their stars formed at $z \sim 3$, with star formation already effectively terminated in the cluster core. Overall, the high-mass end galaxy populations in the central regions of this cluster appear to be in a very advanced evolutionary stage, not only in terms of the formation of the stellar populations, but also of the assembly of their stellar mass. On the other hand, the sizes of the massive red-sequence early-type galaxies suggest that these galaxies are smaller (on average, by a factor up to ~ 2) than similarly massive early-type galaxies in the nearby Universe. While the interpretation of this result is still affected by possible biases, this might indicate that these sources will still undergo later evolution which will shape the structural properties of these objects to resemble typical early-type galaxies today.

1. Introduction

Galaxy clusters at high redshift allow galaxy evolution to be studied at early cosmic times in the archetypal biased environment. Thanks to considerable efforts with dedicated surveys using a variety of approaches, the number of high-redshift clusters is increasing, although spectroscopically confirmed systems beyond $z \sim 1.3$ still make just a small sample. In contrast with lower redshift clusters, where massive galaxy populations in the core generally appear already well evolved, several studies claimed the presence of still actively forming galaxies in many of these highest redshift structures. In fact, from observations of clusters at low/intermediate redshifts, it is expected that around redshift 2 we are approaching the formation epoch of massive cluster galaxies. This is particularly important for the study of galaxy evolution in the most dense environments, since the closer we get to their major formation epoch, the tighter are the constraints we can set on their evolution, as well as on the relevance of the cluster environment in shaping their physical properties.

In this work we resume results from a multi-wavelength study of the X-ray luminous galaxy cluster XMMU J2235-2557 (hereafter XMMU J2235, Mullis et al. 2005) at $z = 1.39$, one of the most massive among the highest redshift clusters discovered thus far ($r_{500} \sim 750$ kpc, $M_{200} \sim 6 \times 10^{14} M_{\odot}$, Rosati et al. 2009), spectroscopically confirmed with more than 30 members at $1.37 < z < 1.41$. In

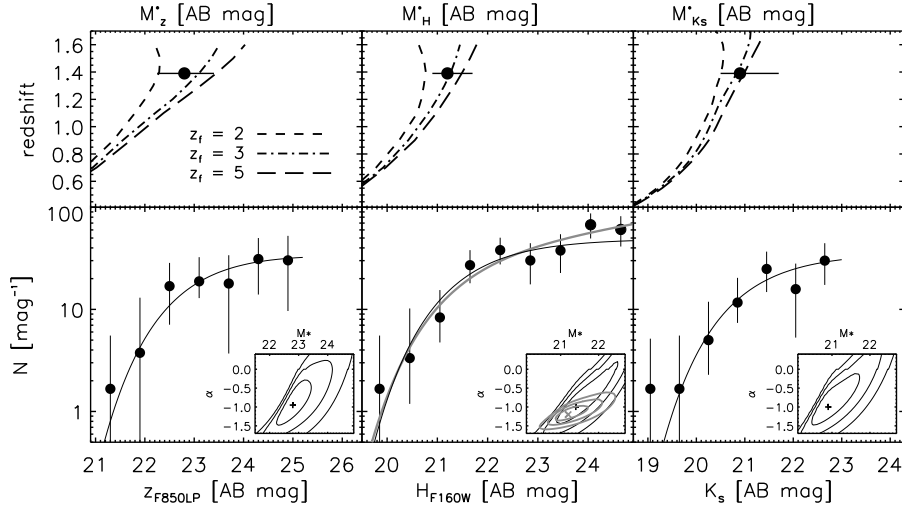


Figure 1. The LF of galaxies in the central region of XMMU J2235, as measured in the z , H and K_s bands (adapted from Strazzullo et al. 2010). *Bottom panels*: binned counts with the best-fit Schechter function determined for magnitudes brighter than $\sim M^* + 2$ ($\sim M^* + 4$, gray lines, only for the H -band LF). *Top panels*: the redshift evolution of M^* in the z , H and K_s band, according to Kodama & Arimoto (1997) models, for different formation redshifts. Solid symbols show M^* as determined from the LFs in the lower panels.

the following, we adopt $H_0 = 70 \text{ km s}^{-1} \text{ Mpc}^{-1}$, $\Omega_M = 0.3$, $\Omega_\Lambda = 0.7$ cosmology, and the AB magnitude system. Most results briefly discussed here have been presented in detail in Strazzullo et al. (2010).

2. Massive cluster galaxies already in place at $z \sim 1.4$

The luminosity function (LF) of galaxies in the central region of XMMU J2235 (within a cluster-centric distance ~ 700 kpc, about r_{500}) was determined in the z (HST/ACS F850LP), H (HST/NICMOS F160W) and K_s (VLT/HAWKI K_s) bands (Fig. 1), roughly corresponding to restframe U , R , and z bands at the cluster redshift.

The K_s band samples the restframe near-infrared light, which can be considered as a probe of the stellar mass, while the H and particularly z bands sample wavelengths more affected by recent star formation activity. Nonetheless, all three LFs show a roughly flat faint-end slope, and a characteristic magnitude close to passive evolution predictions of the local M^* with the bulk of the stars formed at $z > 2$ (Fig. 1). This suggests that the LF bright end is similar in shape to that of local cluster galaxies, besides evolution due to aging of the stellar populations. This extends previous findings on the early assembly of massive galaxies in cluster core regions (e.g., among many others, De Propris et al. 1999;

Andreon 2006; Mancone et al. 2010) to a spectroscopically confirmed $z \sim 1.4$ cluster. On the other hand, we also recall recent results showing that semi-analytic (hierarchical) model predictions are also consistent with the measured M^* of high redshift clusters (Capozzi et al. 2012), and indeed consistent within the (large) errors with the M^* measured here in the K_s band, $20.9^{+0.8}_{-0.4}$.

The shape of the galaxy stellar mass function within r_{500} , as determined from the K -band LF as well as from SED-derived stellar masses (Strazzullo et al. 2010), appears to be in very good agreement with previous measurements in lower redshift clusters up to $z \sim 1$, once again suggesting an early assembly of the high-mass population, essentially in place at one third of the Hubble time.

On the other hand we note that, even in the central regions, the galaxy populations observed at $z = 1.39$ may be not representative of the descendant populations at $z = 0$. An halo occupation analysis of XMMU J2235 based on the K -band LF within r_{500} suggests that the number of galaxies is consistent with what expected for a nearby cluster of similar mass (Lin et al. 2004). However, considering the likely mass growth of XMMU J2235 down to $z = 0$, the observed number of galaxies might be just 20% of the final $z = 0$ population – this would be consistent with theoretical simulation results from Berrier et al. (2009).

3. Red-sequence cluster galaxies

Fig. 2 shows the $z-H$ vs H and $z-J$ vs J color-magnitude diagrams (CMDs), the colors corresponding approximately to restframe $U-B$, $U-V$ and $U-R$. While the observed $z-J$ color best samples the 4000\AA break, the $z-H$ CMD benefits from the excellent accuracy and depth of HST imaging. A tight red sequence is clearly observed in both CMDs, with zero-point and slope in agreement with passive evolution predictions for a formation redshift of ~ 3 . Fig. 2 also shows the stellar mass against (circularised) effective radius as measured through surface brightness fitting on the ACS F850LP imaging, for the sample of bright red-sequence early-type galaxies (within the gray shaded area in left panel). The comparison with the most commonly used determination by Shen et al. (2003) of the local mass-size relation, suggests that these galaxies are smaller than their local counterparts of similar stellar mass, on average by a factor of ~ 2 . However, systematics and biases affecting both mass and size measurements prevent us from drawing definite conclusions. As an example, using the local relation from Valentinuzzi et al. (2010) rather than Shen et al. (2003), and estimating stellar masses with Maraston (2005) rather than Bruzual & Charlot (2003) stellar population models, would already reduce the size evolution factor to $\sim 30\%$, which – by the way – might be largely accounted for by the effect of progenitor bias when comparing the $z = 1.4$ sample of already quiescent early-type galaxies with the reference sample in the nearby Universe (e.g. van der Wel et al. 2009, Valentinuzzi et al. 2010). These and other uncertainties contribute to making the evolution of the mass-size relation, and especially the relevance of size evolution of individual cluster galaxies, still an entirely open issue (see Strazzullo et al. 2010 for a detailed description of the determination of the mass-size relation in XMMU J2235, and a more extensive discussion of the results).

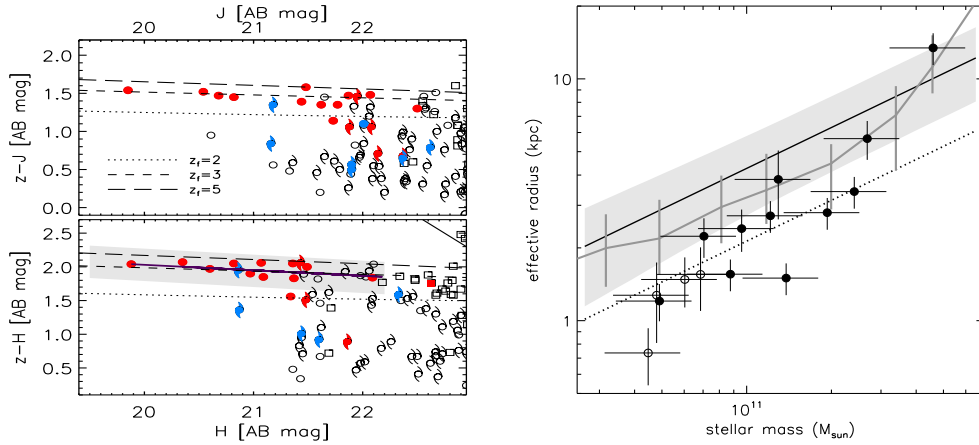


Figure 2. *Left:* CMDs in the cluster central area. Blue/red symbols are spectroscopic members with/without detectable [OII] emission. Circle and spiral symbols show early and late-type galaxies, respectively. Dotted and dashed lines show the red sequence predicted by Kodama & Arimoto (1997) models for different formation redshifts. The purple line is a fit to the red sequence within the gray shaded area. *Right:* The stellar mass vs. size relation for massive red-sequence early-type galaxies. Filled/empty symbols are spectroscopic/photometric- z members, respectively. The black line is the Shen et al. (2003) local determination for early-type galaxies (dotted line is shifted by a factor 2 in size). The gray line is the determination by Valentinuzzi et al. (2010) for a sample of nearby cluster galaxies. Adapted from Strazzullo et al. (2010).

References

- Andreon, 2006, *A&A*, 448, 447
 Berrier et al., 2009, *ApJ*, 690, 1292
 Bruzual & Charlot, 2003, *MNRAS*, 344, 1000
 Capozzi et al., 2012, *MNRAS*, 419, 2821
 De Propris et al., 1999, *AJ*, 118, 719
 Kodama & Arimoto, 1997, *A&A*, 320, 41
 Lin et al., 2004, *ApJ*, 610, 745
 Mancone et al., 2010, *ApJ*, 720, 284
 Maraston, 2005, *MNRAS*, 362, 799
 Mullis et al., 2005, *ApJ*, 623, L85
 Rosati et al., 2009, *A&A*, 508, 583
 Shen et al., 2003, *MNRAS*, 343, 978
 Strazzullo et al., 2010, *A&A*, 524A, 17
 Valentinuzzi et al., 2010, *ApJ*, 712, 226
 van der Wel et al., 2009, *ApJ*, 698, 1232

Contributed posters

Counter-rotating bar in a simulation of a disk galaxy

D. G. Algorry^{1,2} and M. G. Abadi^{1,2}

¹*IATE, CONICET, Córdoba, Argentina*

²*OAC, CONICET, Córdoba, Argentina*

Abstract. We present a dynamical analysis of a simulated disk galaxy which has a counter-rotating stellar component. By using different dynamical parameters, such as energy or circularity, we identify an internal bar which rotates in an opposite direction to the main galactic disk.

1. Procedure and results

In the last few years, the presence of counter-rotating stars and/or gas has been detected in several disk galaxies. The origin of the stellar counter-rotation has been extensively studied, and in general it is interpreted as the result of the accretion of a small satellite galaxy or the gradual acquisition of gas in a retrograde orbit (see Merrifield & Kuijken 1994; Thakar & Ryden 1996). In this work, we show that it is possible to find counter-rotating components in simulated disk galaxies within a Λ CDM cosmology model, enabling a detailed study of its formation and evolution.

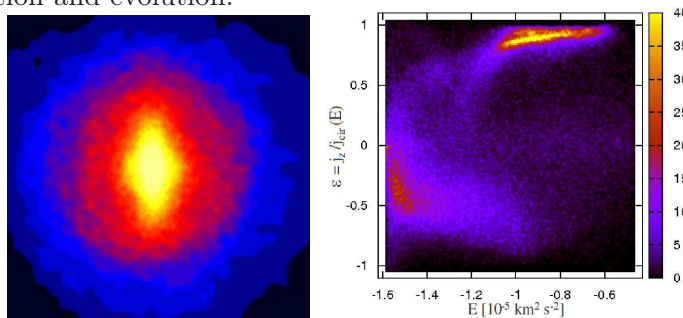


Figure 1. Face-on distribution of stellar particles of the simulated galaxy (left). Energy vs circularity diagram of stellar particles (right).

The left panel of Fig. 1 shows the face-on distribution of stellar particles of a disk galaxy with an appreciable counter-rotating component. The energy (E) vs circularity (ε) diagram is shown in the right panel of Fig. 1. Two well defined structures (the regions with higher number density) can be seen: stars with $\varepsilon \sim 1$ and high energy values, the co-rotating disk; and stellar particles mostly with $\varepsilon < 0$ and low energy values, the counter-rotating bar.

References

- Merrifield, M.R., Kuijken, K. 1994, ApJ, 432, 575
 Thakar, A.R., Ryden, B.S. 1996, ApJ, 461, 55

Determination of the Galactic star formation rate by means of dynamical simulations of open clusters

L. A. Bignone¹, L. J. Pellizza^{1,2}, A. E. Piatti^{1,2} and T. E. Tecce^{1,2}

¹*IAFE, CONICET-UBA, Buenos Aires, Argentina*

²*CONICET, Argentina*

Abstract. We study the history of the star formation rate and the evolution of the Galactic disk by means of dynamical simulations of open clusters. We have included in our simulation dissolution effects due to stellar evolution, tidal stripping and the effect of passages through the spiral arms. We compare the simulated age distribution with the observed distribution of open clusters in the Solar neighborhood.

1. Galactic open cluster system simulations

A useful approach to study the star formation rate (SFR) and the evolution of the Galactic disk is the use of open clusters (OCs) to trace back the history of star formation. OCs constitute an intrinsically abundant sample with well determined properties (age, metallicity, and position) which makes them excellent tracers of the Galactic disk properties. Moreover, as most of the disk stars are formed in OCs, a strong correlation between the SFR and the age distribution function (ADF) of OCs is expected.

Improving upon the method introduced by Tecce et al. (2006), we generate a simulated OC system starting with a trial SFR. We calculate the orbit of each simulated cluster and the mass loss due to dissolution effects in a self-consistent way, using semi-analytical descriptions of disruption effects (Lamers et al. 2005; Gieles et al. 2007), but taking into account the path of the cluster. Finally, we extract from our simulation an ADF that can be compared to observations. This in turn allows us to improve upon the original trial SFR.

We find that our simulation reproduces the qualitative properties of the spatial distribution of OCs in the Galaxy. We also find that a constant SFR explains the observed ADF in the solar neighborhood, except for some age ranges around $\log(\text{age}/\text{yr}) < 7$ and $\log(\text{age}/\text{yr}) \sim 8.5$ at which bumps in the ADF are observed.

References

- Tecce, T. E., Pellizza, L. J., Piatti, A. E. 2006, BAAA, 26, 86
Lamers, H. J. G. L. M., Gieles, M., Bastian, N., et al., 2005, A&A, 441, 117
Gieles, M., Zwart, S. F. P., Baumgardt, H., et al., 2006, MNRAS, 371, 793

Ultra compact dwarf galaxies in the Antlia cluster

J. P. Caso^{1,2}, L. Bassino^{1,2}, T. Richtler³ and A. Smith Castelli^{1,2}

¹ *FCAG, UNLP, La Plata, Argentina*

² *IALP, CONICET - UNLP, Argentina*

³ *Depto de Astronomía, Univ. de Concepción, Concepción, Chile*

Abstract. A summary of the results achieved so far in the study of ultra compact dwarf galaxies and bright globular clusters in the nearby Antlia cluster is presented.

1. New results in the study of Antlia ultra compact dwarfs

Ultra compact dwarf galaxies (UCDs) are known as globular-cluster-like objects, but with higher brightness. A review of this issue was written by Hilker (2009). The Antlia cluster is one of the nearest galaxy clusters ($d \approx 35$ Mpc). It presents a complex structure, consisting mainly of two groups, each one dominated by a giant elliptical galaxy (NGC 3258 and NGC 3268). As a first step in the search of Antlia UCDs, a catalogue of candidates was built considering their colours and magnitudes in the Washington photometric system (Caso et al. 2010). Radial velocities were measured from Gemini-GMOS spectra, confirming several Antlia members (Caso et al. 2011, Caso et al. 2013). Almost half of the confirmed objects present radial velocities in the range $2550 - 2850 \text{ km s}^{-1}$, which is consistent with NGC 3258 and NGC 3268 values (2792 km s^{-1} and 2800 km s^{-1} respectively, NASA Extragalactic Database). Two Advanced Camera for Surveys fields, observed with the F814 filter, were obtained from the Hubble Space Telescope Data Archive (programme 9427, PI: W. E. Harris). For confirmed objects located in these fields, the effective radii (R_{eff}) were estimated, obtaining a maximum value of $R_{\text{eff}} \approx 12$ pc. A correlation between luminosity and R_{eff} seems to exist. The location of the confirmed objects in the color-magnitude diagram is consistent with that of the nuclei of dwarf elliptical galaxies and UCDs in other clusters (Caso et al. 2013). To test the reliability of NGC 3268 UCDs being bright globular clusters (GCs), a Monte-Carlo method was used to generate a thousand GC systems with richness equal to that of NGC 3268. Our results indicate that the brightness range of the majority of the UCDs around NGC 3268 is consistent with the brightest GCs generated (Caso et al. 2011).

References

- Hilker, M., 2009, arXiv: 0906.0776
Caso, J.P., Bassino, L.P., Smith Castelli, A.V. 2010, BAAA, 53, 59
Caso, J.P., et al. 2011, Actas de la Segunda Jornada de Astrofísica Estelar, 75
Caso J.P., Bassino L.P., Richtler T., et al. 2013, MNRAS, in press

The Tully-Fisher relation and the formation histories of galaxies

M. E. De Rossi^{1,2,3} and S. E. Pedrosa^{1,2}

¹*IAFE, derossi@iafe.uba.ar*

²*CONICET, Argentina*

³*FCEyN, UBA, Argentina*

Abstract. We studied the Tully-Fisher relation from $z \sim 3$ up to the present by performing cosmological hydrodynamical simulations. We paid particular attention to the role of supernova feedback and merger histories on the evolution of the kinematical and dynamical properties of galaxies.

1. Main results and conclusions

We found that the more efficient action of supernova feedback in shallower potential wells generates a bend in the Tully-Fisher Relation (TFR) at its low-mass end, which is consistent with observations (De Rossi et al. 2010). In particular, by analysing the gas kinematics of the surviving disc components of our whole sample, we determined that the rotation velocity (V_{rot}) evaluated at the maximum of the rotation curve is the best proxy for the circular velocity (V_{circ}), regardless of the galaxy morphology.

Our results also indicate that the scatter of the simulated TFR is strongly modulated by galaxy interactions and mergers, which affect the gas kinematics and produce TFR outliers. It is interesting that mergers exhibit a weak trend to generate negative variations of $\log(V_{\text{rot}}/V_{\text{circ}})$, while interactions can lead to negative or positive variations with similar frequency. Moreover, we obtained that kinematical indicators which combine velocity dispersion (σ) and V_{rot} in their definition lead to a tighter TFR. In particular, in these simulations, $s_{1.0} = (V_{\text{rot}}^2 + \sigma^2)^{1/2}$ seems to be a good proxy for V_{circ} at radii $r > 0.5R_{\text{bar}}$, with R_{bar} defined as the radius which encloses 83 per cent of the baryonic mass of the system. For more details about this work, see De Rossi et al. (2012).

Acknowledgments. We acknowledge support from the PICT 32342 (2005), PICT 245-Max Planck (2006) of ANCyT (Argentina), PIP 2009-112-200901-00305 of CONICET (Argentina) and the L’Oreal-UNESCO-CONICET 2010 Prize. Simulations were run in Fenix and HOPE clusters at IAFE and CeCAR cluster at University of Buenos Aires.

References

- De Rossi, M. E., Tissera, P. B., Pedrosa, S. E. 2010, *A&A*, 519, A89
De Rossi, M. E., Tissera, P. B., Pedrosa, S. E. 2012, *A&A*, 546A, 52

Extragalactic globular clusters in the Milky Way?

B. Dias^{1,2}, B. Barbuy¹, I. Saviane², E. Held³, S. Ortolani⁴, G. Da Costa⁵, M. Gullieuszik⁶, L. Rizzi⁷, Y. Momany^{2,3} and D. Katz⁸

¹*Univ. of Sao Paulo*; ²*ESO/Chile*; ³*Osserv. Astronomico di Padova*;
⁴*Univ. of Padova*; ⁵*Australian National Univ.*; ⁶*Royal Observ. of Belgium*;
⁷*Joint Astronomy Centre*; ⁸*Observ. de Paris*
e-mail: *bdias@astro.iag.usp.br; bdias@eso.org*

A few dwarf galaxies have been identified as merging with the Milky Way since the discovery of Sagittarius (Ibata et al. 1994), which includes a few globular clusters such as its possible core M 54 (NGC 6715). Many other globular clusters of the Milky Way were found to have a clear distribution in metallicity (iron abundance) and are now considered to be nuclei of dwarf galaxies, for example ω Centauri (NGC 5139), M 22 (NGC 6656), NGC 1851, NGC 2419 and Terzan 5. NGC 5824 appears as a new candidate to be the core of a dwarf galaxy. We obtained mid-resolution ($\Delta\lambda = 2.5\text{\AA}$) spectra of about 10–20 red giants per cluster with FORS2@VLT/ESO in the range 4600–6000 \AA , for a sample of 31 Milky Way globular clusters. The main goal of this project is to identify medium-resolution indicators of their alpha enhancement. The same stars were observed also in the CaII triplet region (Da Costa et al. 2009, Saviane et al. 2012).

We used the code ETOILE (Katz et al. 2011) to derive [Fe/H], T_{eff} , and $\log g$ for each star. This code compares an observed spectrum with a grid of 1959 stars of the ELODIE library (Prugniel & Soubiran 2001) and finds the best fit by using a modified least squares method. In order to determine the alpha-enhancement dependence on metallicity, the Lick indices Mg2 and Fe5270 (Worthey et al. 1994) were measured. The results of the best ETOILE fits are in agreement with the curve expected from the ELODIE red giants.

We found a larger metallicity spread for NGC 5824, confirming that its origin is distinct from a typical globular cluster, probably as the core of a dwarf galaxy (or at least related to a dwarf galaxy). In addition, this cluster is located in the orbit of the Cetus Polar Stream recently discovered in SDSS/SEGUE data (Newberg et al. 2009), which corroborates our findings. Besides, we also confirmed the metallicity spread of M 22.

References

- Ibata et al. 1994, *Nature*, 370, 194
- Da Costa et al. 2009, *ApJ*, 705, 1481
- Saviane et al. 2012, *A&A* (in press)
- Katz et al. 2011, *A&A*, 525, 90
- Prugniel & Soubiran 2001, *A&A*, 369, 1048
- Worthey et al. 1994, *ApJS*, 94, 687
- Newberg et al. 2009, *ApJL*, 700, 61

Differential CCD photometry of globular clusters

R. Figuera Jaimes¹, A. Arellano Ferro¹, D. M. Bramich² and S. Giridhar³

¹*Instituto de Astronomía, UNAM, Mexico.*

²*ESO, Garching bei München, Germany.*

³*IIA, Bangalore, India.*

Since 2003 we have been carrying a program of time series CCD photometry of globular clusters with the 2.0 m telescope in Hanle, in the Indian Himalayas at 4500 m above sea level. The analysis is made via Differential Imaging Approach (DIA). The goal has been to estimate physical parameters of stars from specific empirical calibrations. With the aim of highlighting the usefulness of the program, we summarize some of the major results encountered for numerous globular clusters and point to representative publications by our team.

The DIA approach allows precise measurements of star fluxes even in highly crowded central regions of a globular cluster, and allows to fully complete the variable star census of a given cluster. This has led to the discovery of 22 RR Lyrae, 18 semi-regular red giants, 1 anomalous cepheid, 1 eclipsing binary and 27 SX Phe in the clusters M53, M72, NGC 5053, NGC 6366, NGC 5466, M2, and NGC 4147 (e.g., Arellano Ferro et al. 2011, and references therein). The program also allowed to produce good colour-magnitude and colour-colour diagrams to estimate the reddening and age of the clusters. The Fourier decomposition of the light curves of RR Lyrae stars allows to obtain good estimates of the mean value of the cluster $[Fe/H]$, the mean distance and the structure of the horizontal branch. The accuracy of the photometry produces high quality light curves, which has allowed the discovery of numerous RR Lyrae stars with the Blazhko effect, in particular the largest population known of 22 Blazhko RR1 stars in a given cluster (M53; Arellano Ferro et al. 2012). These results suggest that stellar evolution in the horizontal branch takes place towards the red and that the Blazhko modulations may be associated with a change of pulsating mode.

The numerous SX Phe stars have led to an empirical calculation of the P-L relation, and a general discussion of these short-period pulsators as distance indicators (Arellano Ferro et al. 2012). A new statistical index was given that helps the detection of stars with amplitude and phase modulations. The program continues on numerous clusters in both hemispheres, and expects to significantly extend our knowledge of the variable stars in globular clusters.

References

- Arellano Ferro, A., Bramich, D. M., Figuera Jaimes, et al. 2012, MNRAS, 420, 1333
Arellano Ferro, A., Figuera Jaimes, R., Giridhar, S., et al. 2011, MNRAS, 416, 2265

Revisiting the colour–magnitude relation of early-type galaxies in the Virgo cluster

N. González¹, A. Smith Castelli^{1,2}, F. Faifer^{1,2} and J. C. Forte^{1,3}

¹*FCAG, UNLP, Argentina*

²*IALP (CCT La Plata, CONICET - UNLP), Argentina*

³*CONICET, Argentina*

Abstract. In this contribution, we revisit the colour–magnitude relation of the Virgo cluster by performing our own photometry and analysis on the images of 100 early-type galaxies observed as part of the Virgo Cluster Survey of the Advanced Camera for Surveys of the Hubble Space Telescope. We aim at disentangling whether the alleged non-linearity of the relation may be associated with an improper morphological classification of some galaxies of the sample.

1. Context and results

The colour–magnitude relation (CMR) is a well known photometric relation that has been studied for a long time. In the colour–magnitude diagram, early-type galaxies define a sequence in the sense that bright galaxies are redder than fainter ones. Spectroscopic studies of bright and dwarf early-type galaxies have shown that this relation is mainly driven by differences in metal abundances.

It is widely accepted that the CMR is linear along its extension, and that it shows no perceptible change of slope from the bright galaxies to the dwarf regime except, perhaps, at the very bright end. In addition, there is strong evidence for the universality of this relation in clusters of galaxies which led several authors to suggest its use as a reliable distance indicator (see, for example, Smith Castelli et al. 2008, 2012, and references therein).

Despite all the evidence about the existence of a common linear colour–magnitude relation in groups and clusters, non–linear trends for the CMR of the Virgo cluster have been reported: Janz & Lisker (2009) have obtained an S-shaped CMR that seems to be consistent with the quadratic relation found by Ferrarese et al. (2006) for the same cluster.

From our analysis, we have found that when the very bright end of the relation, the zone populated by compact elliptical galaxies, and that of dwarf irregular/dwarf elliptical transition objects are excluded from the colour–magnitude diagram of the Virgo cluster, a linear trend seems to arise, in agreement with what is found in other groups and clusters of galaxies (Fig. 1; Smith Castelli et al. in preparation).

References

Ferrarese, L. et al. 2006, ApJS, 164, 334

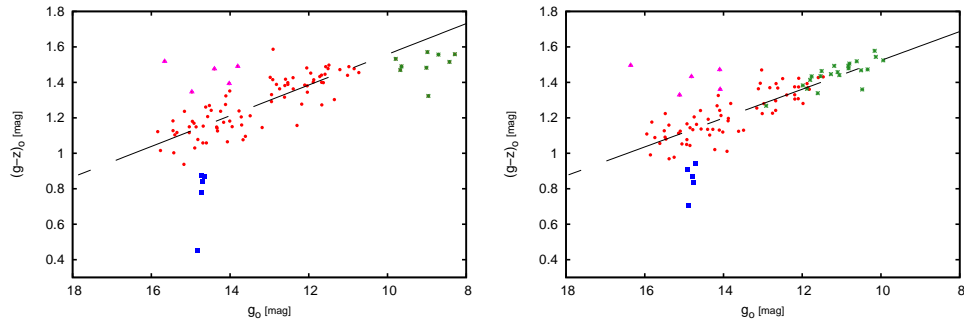


Figure 1. Reddening and extinction corrected CMR of early-type galaxies in the Virgo cluster built from the data published by Ferrarese et al. (2006, left panel) and from our photometry (right panel). The black dashed lines represent the linear fits performed to the relation excluding galaxies displaying cE morphologies (magenta triangles) and systems showing evidence of star formation (blue squares). In the left panel, we also excluded from the fit the very bright galaxies that define a break in the relation, and in the right panel, the galaxies that are not fully contained in the ACS field of view, which have underestimated integrated magnitudes and colours (green asterisks).

- Janz, J., Lisker, T. 2009, ApJ, 696, L102
 Smith Castelli, A. et al. 2008, MNRAS, 386, 2311
 Smith Castelli, A. et al. 2012, MNRAS, 419, 2472

Kinematics and morphological properties of southern interacting galaxies: the minor merger AM 1219-430

J. A. Hernandez-Jimenez¹, M. Pastoriza¹, I. Rodrigues², A. Krabbe²,
C. Winge³ and C. Bonatto¹.

¹*UFRGS, Porto Alegre - Rio Grande do Sul, Brazil*

²*UniVap, São Jose dos campos, Brazil*

³*Gemini Observatory, La Serena, Chile*

Abstract.

We present an observational study of the effects of the interaction on the kinematics and morphology of the components in the minor merger AM 1219-430. The main galaxy shows strong perturbations in its structure, with asymmetric tidal arms. It has also conspicuous HII-region complexes at the nucleus and at a strong tidal arm. These HII regions show important radial velocity deviations ($V > 100$ km/s) with respect to the average velocity field. On the other hand, the secondary galaxy shows prominent symmetric tidal tails.

This work is based on g' and r' images and long slit spectra obtained with Gemini Multi-Object Spectrograph at the Gemini South Telescope. The image field of view ($5.5' \times 5.5'$) includes the whole system and its neighbourhood. Long slit spectra at two different position angles were taken: $PA=162^\circ$ and $PA=341^\circ$ fall along the apparent major axis and the tidal arm of the main galaxy (AM 1219A). We separated the two-fold symmetric and the non-symmetric parts of the galaxies by performing successive image rotations and subtractions. The symmetric images, obtained by subtracting the asymmetric one from the observed image, show the “primordial” disk and the non-perturbed spiral pattern. The overall geometrical parameters of the galaxies, such as inclination and position angle of the line-of-nodes, were obtained from the photometric analysis of the symmetrized g' and r' images. Structural decomposition of the brightness profiles into bulge (Sérsic profile) and disk (Freeman profile) components were also derived for the main and secondary galaxies. The rotation curve of AM 1219A was obtained from the long slit spectra. The mass-to-light ratio inside r_{25} is $3.91 \pm 0.1 M_\odot L_\odot^{-1}$ and $3.03 \pm 0.1 M_\odot L_\odot^{-1}$ in g' and r' , respectively. These values are comparable with the mass-to-light ratio of normal (isolated) galaxies of the same Hubble type (Faber & Gallagher 1979).

References

Faber, S. M., & Gallagher, J. S. 1979, ARA&A, 17, 135

Simulations of galaxy cluster mergers: the dynamics of Abell 3376

Rubens E. G. Machado and Gastão B. Lima Neto

IAG-USP, Universidade de São Paulo, São Paulo, Brazil

Abstract. In large scale structure formation, massive systems assemble through the hierarchical merging of less massive ones. Galaxy clusters, being the most massive and thus the most recent collapsed structures, still grow by accreting smaller clusters and groups. In order to investigate the dynamical evolution of the intracluster medium, we perform a set of adiabatic hydrodynamical simulations of binary cluster mergers.

Abell 3376 is a nearby ($z=0.046$) rich galaxy cluster whose bullet-shaped X-ray emission suggests that it is undergoing a major collision, approximately on the plane of the sky. It has an estimated virial mass of $5.2 \times 10^{14} M_{\odot}$. This is the closest galaxy cluster with such morphology, to our knowledge. The brightest cluster galaxy lies far from the region of the largest X-ray emission, a feature which must be accounted for by the reconstruction of its dynamical history. Additionally, this cluster presents diffuse radio emission (due to the acceleration of relativistic electrons), whose morphology and intensity are compatible with a recent merger scenario (Bagchi et al. 2006).

With our simulations, run using the parallel SPH code Gadget-2 (Springel 2005), we are able to obtain gas emissivity maps comparable to those derived from X-ray observations. In particular, we attempt to model the intracluster gas morphology. Exploring the parameter space of initial conditions (specially mass ratios, impact parameters and relative velocity) allows us to put constraints on the original masses (baryonic and non-baryonic) of the colliding clusters, and their dynamical history.

Our set of preliminary simulations suggests an approximately head-on collision with mass ratio of about 3:1. Simulated X-ray emission presents a morphology roughly comparable to that of Abell 3376 at approximately 0.2 Gyr after the instant of central passage. Projections angles larger than 10° appear to give poorer results, indicating that the collision axis must lie close to the plane of the sky.

Acknowledgments. This work was partially supported by FAPESP (2010/12277-9) and by the CAPES/COFECUB cooperation.

References

- Bagchi, J., Durret, F., Lima Neto, G.B., et al. 2006, *Science*, 314, 791
Springel, V. 2005, *MNRAS*, 364, 1105

Characterizing the magnetic field in the intracluster medium

M. S. Nakwacki¹, E. M. de Gouveia Dal Pino¹, G. Kowal¹ and R. Santos-Lima¹

¹*IAG-USP, Cidade Universitária, São Paulo, Brazil*

Abstract. During structure formation, energetic events and random motions of the hot gas residing inside galaxy clusters (the intracluster medium) generate turbulent motions. Radio diffuse emission probes the presence of magnetic fields and relativistic particles in the intracluster medium, being a key ingredient for understanding the physical processes at work in clusters of galaxies. In this work, we present results from numerical simulations of magnetic field turbulence in standard and kinetic magnetohydrodynamics frameworks. We characterize magnetic field structures through the imprints left on polarization maps.

1. Results and conclusions

We simulated magnetohydrodynamic (MHD) and kinetic MHD (KMHD) turbulence in a 3D periodic box of 1 Mpc³ employing a modified Godunov-MHD code (Falceta-Gonçalves et al. 2008; Kowal et al. 2011) with periodic boundaries, a resolution of 128³ grid points, different ICM conditions (subsonic and super-alfvénic), a gravity center mimicking the distribution of galaxies in a cluster, and a variable parallel to perpendicular pressure ratio (a_{\parallel}/a_{\perp}). We constructed polarization maps using the simulated magnetic field and density. The KMHD model predicts a more granulated plasma density and magnetic field intensity, due to mirror instability that accumulates energy in the smaller structures. As $a_{\parallel}/a_{\perp} \rightarrow 1$ the gravity center leads to a more homogeneous density and magnetic field, probably due to an enhancement of particle mobility favoring their redistribution, the mixing of magnetic field, and pressure isotropization. The correlation between two different points can be measured by the structure function $S(r)$ (see e.g., Kowal et al. 2011, for further details). From $S(r)$ we obtained a coherence length for the magnetic field of ~ 100 kpc for KMHD (lower than the one obtained without a gravity center, e.g. ~ 200 kpc, Nakwacki et al. 2012).

The gravity center decreases the magnetic field coherence length, indicating that its presence is needed to explain more accurately observational results.

Acknowledgments. We thank the Brazilian agencies FAPESP and CNPq.

References

- Falceta-Gonçalves, D., Lazarian, A., Kowal, G. 2008, ApJ, 679, 537
Kowal, G., Falceta-Gonçalves, D. A., Lazarian, A. 2011, New J. Phys., 13, 053001
Nakwacki, M. S., de Gouveia dal Pino, E. M., Kowal, G., et al. 2012, in prep.

Survival of galaxy disks in a Λ CDM cosmology

L.F. Quiroga¹, J.C. Muñoz-Cuartas², S. Sanes¹, J.E. Forero-Romero³,
 S. Gottlöber² and J. Zuluaga¹

¹Universidad de Antioquia, Medellín, Colombia

²Leibniz-Institut für Astrophysik Potsdam, Potsdam, Germany

³University of California, Berkeley, EEUU

Abstract. We use numerical simulations to study the dynamical evolution of disk galaxies in a cosmological context. Using Constrained Simulations of the Local Universe (CLUES, Gottlöber et al. 2010), we identify Milky Way (MW) galaxy candidates, extract merger trees of halos, and model the properties of the galaxies hosted in the halos at different points in the tree. Galactic disks and spheroids are modelled according to the properties of their host halos. Using this information, we simulate the process of merging of galaxies at specific points in the merger tree, at larger resolution, from redshift 2.0 to 0 and evaluate several quantities that characterise the structure of the galaxy: density profiles, mass distribution of components, and the structure of orbits in the disk and halo. With our simulations, that reproduce the most heavy mergers in the history of one of the MW candidates, we see that the galactic disk can survive at $z = 0$ without requiring special isolation or environment conditions.

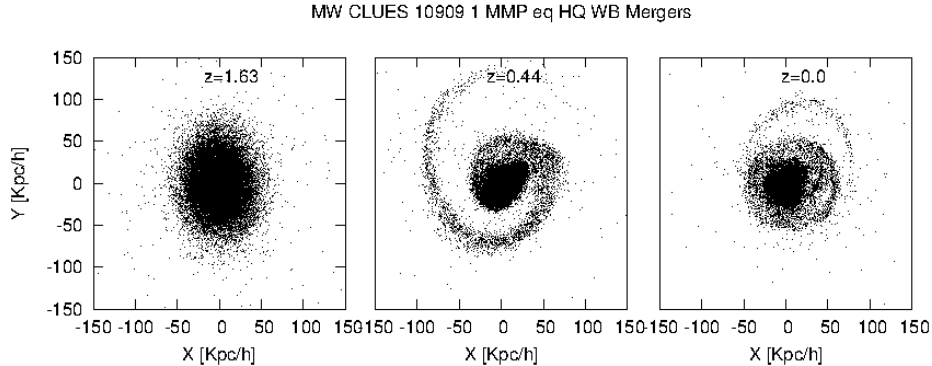


Figure 1. Projection of the stellar disk at three different redshifts, showing its evolution during the merger with three satellites of mass ratio $M_{\text{disk}}/M_{\text{sat}} = 0.4, 0.6$ and 0.7 , respectively. The mergers generated streams that resemble those observed in the MW and other galaxies.

Acknowledgments. This project has been funded by the German-Colombian program PROCOL DAAD-COLCIENCIAS and by CODI.

References

- Gottlöber, S., Hoffman, Y., Yepes, G. 2010 arxiv:1005.2687
 Mo, H.J., Mao, S., & White, S.D.M. 1998, MNRAS, 295, 319

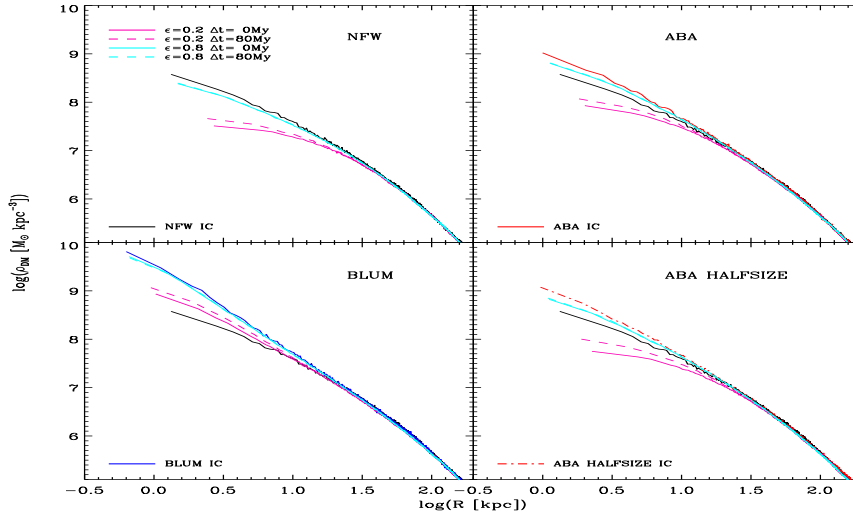
Effects of baryon mass loss on profiles of large galactic dark matter halos

Cinthia Ragone-Figueroa¹, Gian Luigi Granato², and Mario G. Abadi¹

¹*IATE, CONICET-OAC, Córdoba, Argentina*

²*INAF, OATS, Trieste, Italy*

We study the effect of baryon mass loss in the inner structure of large galactic dark matter haloes by means of numerical experiments, designed to study active galactic nuclei (AGN) feedback in precursors of massive early-type galaxies (ETG). This process has been proposed to remove a substantial fraction of their baryons in a few dynamical times.



The figure (for more details see Ragone-Figueroa et al. 2012) shows that the inner region of the dark matter (DM) halo expands and its density profile flattens by a large amount, with little dependence on the expulsion timescale (Δt). The ratio between the final and initial baryon mass is dubbed ϵ . Besides the standard NFW profile found in gravity-only simulations (plotted in all panels for reference), we use profiles contracted according to the findings from cosmological hydrodynamical simulations (ABA), as well as profiles in which the contraction is estimated using an analytical treatment (BLUM). Cuspy density profiles in DM halos of ETGs could be difficult to reconcile with an effective AGN (or stellar) feedback during the evolution of these systems.

References

Ragone-Figueroa C., Granato G. L., Abadi M. G., 2012, MNRAS, 423, 3243R

A photometric and spectroscopic study of the Hickson Compact Group 44

A. Smith Castelli^{1,2}, F. Faifer^{1,2}, C. Escudero², J. M. Gomes³,
L. Vega Neme⁴ and N. González²

¹*IALP (CCT La Plata, CONICET - UNLP), La Plata, Argentina*

²*FCAG, UNLP, La Plata, Argentina*

³*Centro de Astrofísica, Universidade do Porto, Portugal*

⁴*IATE, Córdoba, Argentina*

Abstract. We present a photometric and spectroscopic study of the galaxies originally considered as members of HCG 44, based on Gemini-GMOS images and Sloan Digital Sky Survey and NASA/IPAC Extragalactic Database archival spectra. We analyze the globular cluster systems, show the colour maps of the galaxies, and present results obtained from the stellar population synthesis code STARLIGHT.

1. Galaxy content of HCG 44 and results

HCG 44, at a distance of ~ 19 Mpc, was classified by Hickson (1982) as a compact group with four galaxy members: an Sa galaxy (NGC 3189/3190 or HCG44a), an E2 galaxy (NGC 3193 or HCG44b), an SBc galaxy (NGC 3185 or HCG44c) and an Sd galaxy (NGC 3187 or HCG44d). Williams et al. (1991) identified a dwarf-like galaxy ([WMv91]1015+2203) at the same redshift of the group, increasing to five the number of confirmed members. However, Tonry et al. (2001) obtained a surface brightness fluctuation distance of ~ 35 Mpc for NGC 3193, reducing the number of group members to four (see also Aguerri et al. 2006).

From our photometric analysis, we have identified a globular cluster population belonging to HCG 44 that seems to trace the interactions among the bright members. Our results are consistent with those of previous studies about NGC 3193 which revealed that it is a background galaxy. We have detected a new early-type galaxy candidate in our fields, as well as several ultra compact dwarf candidates. From our spectroscopic analysis of the three brightest members of the group, we have found that NGC 3185 displays active galactic nucleus / low-ionization nuclear emission-line region features, NGC 3187 is a star-forming galaxy, and NGC 3189/3190 shows a typical spectrum of an early-type, passive galaxy.

References

- Aguerri J. et al., 2006, A&A, 457, 771
Hickson P., 1982, ApJ, 255, 382
Tonry J. et al., 2001, ApJ, 546, 68
Williams B., McMahon P., van Gorkom J., 1991, AJ, 101, 1957

Environment and properties of obscured and unobscured active galactic nuclei

M. Taormina¹ and C. Bornancini¹

¹IATE, Córdoba, Argentina.

Abstract. We analyze the properties of obscured and unobscured active galactic nuclei selected using mid-infrared colors in the redshift range $1 < z < 3$. We find that obscured objects are located in a denser local galaxy environment compared to the unobscured sample.

1. Procedure and conclusions

Observational data were obtained from the MUSYC survey (Cardamone et al., 2010), in the ECDF-S field. We selected a sample of active galactic nuclei (AGNs) in the redshift range $1 < z < 3$ using a color-color diagram in the mid-infrared (Stern et al., 2005), as shown in Fig. 1 (left panel, dashed line). We use a color-luminosity criterion (see Hickox et al., 2007) in order to separate the obscured and unobscured AGN samples. Fig. 1 (right panel) shows the distributions of the $N_{0.5}$ density parameter, defined as the number of galaxies with $\Delta z < 0.5$ and within 0.5 Mpc, for the two samples. We find a tendency for obscured AGNs to be located in rich galaxy environments, compared to the environment of unobscured AGNs.

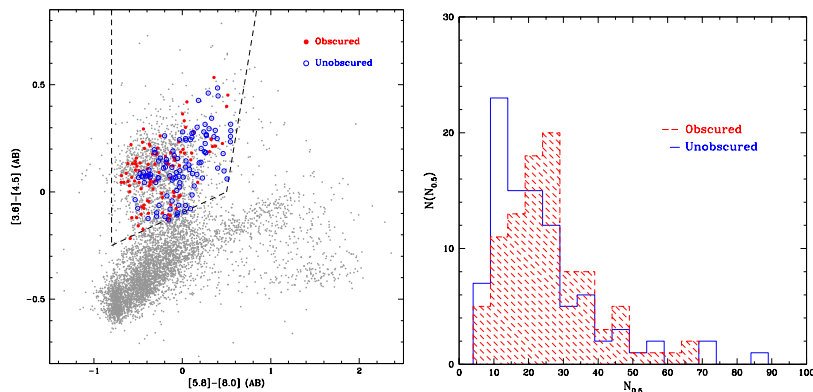


Figure 1. Left: Color-color diagram showing the selection of the obscured (filled circles) and unobscured (open circles) AGN samples (within dashed lines). Right: Distribution of the $N_{0.5}$ density parameter for the two samples.

References

- Cardamone, C. N., et al., 2010, ApJS, 189, 270
 Hickox, R. C., et al., 2007, ApJ, 671, 1365
 Stern, D., et al., 2005, ApJ, 631, 163

Formation of first structures in a Λ CDM Universe

C. Villalón¹ and M. Domínguez Romero¹

¹*IATE - OAC, CONICET, Córdoba - Argentina*

Abstract. We developed simulations of the formation and evolution of the first structures using an AMR, grid-based code: Enzo. Our simulations are aimed to follow the complex physics of the joint evolution of super massive black holes and galaxies in the reionization epoch.

1. Introduction

The existence of massive black holes ($\sim 10^9 M_\odot$) in galaxies at only a billion years after the Big Bang is one of the unsolved problems in cosmology. One of the formation mechanisms suggests that these objects may be the remnants of population III stars. New technologies are being developed that will make possible the analysis of the first stars and thus making them an interesting target of study. The purpose of the present study is to evaluate the performance of Enzo by running a series of tests and cosmological simulations, including hydrodynamical and gravitational processes. This work is the first step of a bigger project that attempts to study and explain the growth mechanisms of SMBHs.

2. Procedure and results

Enzo is a 3D MPI-parallel Eulerian block-structured adaptive mesh refinement cosmological code designed for hydrodynamical astrophysical calculations. For further details, see <http://enzo-project.org/>, and O'Shea et al. (2004).

In order to get a better understanding of Enzo, we have run several tests, such as a *binary collapse* and a *Zel'dovich pancake*. The results of the latter test are in good agreement with analytical solutions (Zel'dovich 1970). On the other hand, we have run a cosmological simulation from $z = 30$ to $z = 1$ in a 63^3 grid using an AMR version, assuming the equilibrium model and a precomputed cooling function. We have followed the evolution of a $16h^{-1}$ Mpc comoving side box adopting a Λ CDM cosmology. The ρ - T plot shows the progressive shock heating experienced by the gas, produced by the gravitational collapse into dark matter haloes. Using this kind of diagrams, it is possible to separate and understand the complex multiphase medium where the first stars and black holes co-evolve.

3. Conclusions

This work presents preliminary results of our simulations. Nevertheless, it is important to notice that we need to include further physical processes such as chemical evolution, star formation, and radiative feedback in order to get a more realistic representation of the systems under study.

References

O'Shea et al, 2004, Springer Lecture Notes in Comp. Science and Engineering.

Participant institutions

- Campus of International Excellence UAM+CSIC, Universidad Autónoma de Madrid, E-28049 Madrid, Spain
- Cavendish Laboratory, University of Cambridge, 19 J.J. Thomson Ave., Cambridge CB3 0HE, UK
- CEA-Saclay, IRFU, Institute of Research into the Fundamental Laws of the Universe, DSM, Direction des Sciences de la Matière, Service d'Astrophysique, 91191 Gif-sur-Yvette Cedex, France
- Centro de Astrofísica, Universidade do Porto, Portugal
- CONICET, Consejo Nacional de Investigaciones Científicas y Técnicas, Argentina
- Departamento de Astronomía, UdeC, Universidad de Concepción, Casilla 160-C, Concepción, Chile
- Departamento de Investigación Básica, CIEMAT, Centro de Investigaciones Energéticas, Medioambientales y Tecnológicas, Madrid, E28040, Spain
- Department of Astronomy, UCA, University of California, Berkeley, CA 94720-3411, USA
- Department of Physics & Astronomy, Saint Mary's University, Halifax, B3H 3C3, Canada
- Department of Physics and Astronomy, University of Sheffield, Hicks Building, Hounsfield Road, Sheffield, S3 7RH, UK
- Department of Physics & Astronomy, Vanderbilt University, Nashville, USA
- European Southern Observatory, Karl-Schwarzschild-Str. 2, 85748 Garching bei München, Germany
- European Space Astronomy Centre (ESAC)/ESA, Madrid, Spain
- FCAG, Facultad de Ciencias Astronómicas y Geofísicas, UNLP, Universidad Nacional de La Plata, Paseo del Bosque S/N, 1900, La Plata, Argentina
- FCEN, Facultad de Ciencias Exactas y Naturales, Universidad de Buenos Aires, Intendente Güiraldes 2160, C1428EGA, Ciudad Universitaria, Buenos Aires, Argentina
- Gemini Observatory, La Serena, Chile
- Grupo de Astrofísica, Universidad Autónoma de Madrid, Madrid, E-28049, Spain
- IAFE, Instituto de Astronomía y Física del Espacio, CONICET-UBA, CC 67, Suc. 28, 1428, Buenos Aires, Argentina
- IAG-USP, Instituto de Astronomia, Geofísica e Ciências Atmosféricas, Universidade de São Paulo, Rua do Matão, 1226, São Paulo, Brazil 05508-090
- IALP, Instituto de Astrofísica de La Plata, CCT La Plata, CONICET, UNLP, La Plata, Argentina
- IANIGLA, Instituto Argentino de Nivología, Glaciología y Ciencias Ambientales, Apartado Postal 330, Mendoza, Argentina
- IATE, Instituto de Astronomía Teórica y Experimental, CONICET, Laprida 922, Córdoba, Argentina

- INAF, Istituto Nazionale di Astrofisica, Osservatorio Astronomico di Trieste, Via Tiepolo 11, I-34131, Trieste, Italy
- Institute of Computational Mathematics and Mathematical Geophysics SB RAS, prospect Akademika Lavrentjeva 6, 630090 Novosibirsk, Russia
- Instituto de Astrofísica de Andalucía (CSIC), Glorieta de la Astronomía, E-18008 Granada, Spain
- Instituto de Astrofísica de Andalucía (CSIC), Apartado 3004, 18080 Granada, Spain
- Instituto de Astronomía, UNAM, Universidad Nacional Autónoma de México, Apartado Postal 70-264, 04510 México, D.F., México
- Instituto de Física Teórica, (UAM/CSIC), Universidad Autónoma de Madrid, Cantoblanco, E-28049 Madrid, Spain
- Jeremiah Horrocks Institute, UCLan, University of Central Lancashire, Preston PR1 2HE, UK
- Kavli Institute for Cosmology, Madingley Road, Cambridge CB3 0HA, UK
- Leibniz-Institut für Astrophysik Potsdam (AIP), An der Sternwarte 16, 14482 Potsdam, Germany
- MoCA, Monash Centre for Astrophysics, Clayton, 3800, Australia
- OAC, Observatorio Astronómico de Córdoba (CONICET), Laprida 854, Córdoba, X5000BGR, Argentina
- Physics Department, University of the Western Cape, Cape Town, South Africa
IIA, Indian Institute of Astrophysics, II Block, Koramangala, Bangalore 560 034, India
- PUC, Universidad Católica de Chile, Avda. Libertador Bernardo O'Higgins 340, Santiago, Chile
- UFRGS, Universidade Federal do Rio Grande do Sul, Av. Paulo Gama, 110 - Bairro Farroupilha - Porto Alegre - Rio Grande do Sul, Brazil
- UniVap, Universidade do Vale do Paraíba, Av. Shishima Hifumi, 2911 - Urbanova, São José dos Campos, Brazil
- Universidad de Antioquia, calle 67 No. 53 - 108, Medellín, Colombia
- Université Lyon 1, F-69230, France
- University of California, Berkeley, CA 94720-5800, USA
- University of Texas, Department of Astronomy, Austin, TX 78712, USA
- UNLP, Universidad Nacional de La Plata, La Plata, Argentina

From the First Structures to the Universe Today

Our knowledge of how cosmic structures formed and evolved has improved in the last decades as new and more precise observations are being achieved. Moreover, the development of more sophisticated theoretical models and the advent of high-resolution numerical simulations have contributed a great deal to the comprehension of the physical universe. Therefore, the confrontation of observations and theoretical models is crucial to improve our understanding of galaxy formation within the hierarchical clustering scenario.

In November 2011, the “Second Workshop on Numerical and Observational Astrophysics: From the First Structures to the Universe Today” was held in the Institute for Astronomy and Space Physics (IAFE), Ciudad Autónoma de Buenos Aires, Argentina. This international workshop brought together about seventy active scientists working in both areas to discuss about new results and future challenges. This book contains the proceedings arising from this fruitful meeting.

ISBN 978-987-24948-1-0